Multicomponent AM–FM Energy Demodulation with Applications to Signal Processing and Communications

A THESIS

Presented to

The Academic Faculty

By

Balasubramaniam Santhanam

In Partial Fulfillment

of the Requirements for the Degree of

Doctor of Philosophy in Electrical Engineering

Georgia Institute of Technology

November, 1997

Multicomponent AM–FM Energy Demodulation with Applications to Signal Processing and Communications

Approved:

____
Petros Maragos, Chairman

____
James H. McClellan

____
Douglas B. Williams

Date approved by Chairman ______________

Dedicated to my parents for their love, support and patience in regards to this endeavour.

ACKNOWLEDGEMENTS

CONTENTS

LIST OF FIGURES

GLOSSARY

ALP Adaptive Linear Prediction

AM–FM Amplitude and frequency modulated

APLL Analog Phase–Locked Loop

AR Autoregressive random signal

AWGN Additive White Gaussian Noise

BB–DPLL Baseband Digital Phase–Locked Loop

CC–DPLL Cross–Coupled Digital Phase–Locked Loop

DDF Double Difference Function

DESA Discrete Energy Separation Algorithm

DPLL Digital Phase–Locked Loop

ECG Electrocardiogram

EDM Energy Demodulation of Mixtures

ESA Energy Separation Algorithm

EKF Extended Kalman Filtering

FFT Fast Fourier Transform

FIM Fisher Information Matrix

FIR Finite Impulse Response

GDE Generating Differential/Difference Equation

HRR Hankel Rank Reduction

IA , IF Instantaneous Amplitude and Frequency

ITD Instantaneous Toeplitz Determinant

LMS Least Mean–Square

MA Moving Average

MAP Maximum Aposteriori Estimation

MAS Matrix Algebraic Separation

MEDM Multiband Energy Demodulation of Mixtures

MESA Multiband Energy Separation Algorithm

MLMS Multiband Least Mean–Square

MPR Mean Power Ratio

NCS Normalized Carrier Separation

NLMS Normalized Least Mean–Square

NMAE Normalized Mean Absolute Error

NRMSE Normalized Root Mean–Square Error

PASED Periodic Algebraic Separation Energy Demodulation

PLL Phase–Locked Loop

RLS Recursive Least–Squares

SESA Smoothed Energy Separation Algorithm

SPM Separation of Periodic Mixtures

SNR Signal to Noise Ratio

SVD Singular Value Decomposition

SX Algorithm X with post smoothing

VCO Voltage–Controlled Oscillator

SUMMARY

The goal of this thesis is to study the problem of energy–based demodulation of multicomponent AM–FM signals (components contain both amplitude and frequency modulation) and its applications to signal processing and communications. Specific attention is given to the case where the component signals have overlapping spectra (co–channel problem). Existing multicomponent AM–FM demodulation approaches either assume that the components are distinct or that they can be separated by linear filtering techniques. These assumptions produce singularity problems in the algorithms when the components overlap spectrally or when one of the components is much stronger than the other. To illustrate these shortcomings the existing approaches are briefly discussed and simulated.

This goal of multicomponent AM–FM demodulation is actually a two part task that first involves component separation followed by demodulation of the separated components into frequency and amplitude information signals. The underlying concepts behind the energy–based demodulation approaches are the tracking of the source energy or higher–order energy measures using the second-order (Teager–Kaiser) energy operator or its higher–order extensions and separation of these energies into amplitude and frequency components via instantaneous nonlinear algorithms. The first algorithm, the *energy demodulation of mixtures* (EDM), uses higher–order energy signatures of the composite signal to perform both tasks simultaneously. The second approach embodied in the *periodic algebraic separation energy demodulation* (PASED) algorithm performs these tasks separately using algebraic separation techniques to separate the components and monocomponent energy demodulation (the *energy separation algorithm*) (ESA) to demodulate each component. This enables the PASED algorithm to deal with the difficult cases where the components overlap spectrally or when the component frequency tracks cross over. Both these algorithms are evaluated by applying them to the problem of separation and demodulation of voice–modulated two–component co–channel FM signals (message signals are human voice signals). The *matrix algebraic separation* (MAS) algorithm which is the separation section of the PASED algorithm is independently analyzed in the frequency domain and the insight obtained from this analysis is used to improve the performance of the MAS algorithm via harmonic restoration techniques. The improved MAS algorithm is then applied to the problem of separating the components of a mixture of both synthetic and natural vowels.

CHAPTER 1

INTRODUCTION

1.1 Multicomponent AM–FM Signal Model

Monocomponent continuous–time AM–FM signals are defined as signals of the form

$$x(t) \;\triangleq\; A(t)\cos\left[\int_0^t \omega(\tau)d\tau + \theta\right] \tag{1.1}$$

that contain both *amplitude modulation* (AM) and *frequency modulation* (FM). These signals find extensive use in: (a) human-made communication systems [21] for the transmission of information over communication channels; (b) radar systems for modeling target information; (c) speech–processing applications for modeling speech resonances. They are also often present in signals created and processed by some biological systems. The signal processing task that is of interest is the extraction of the information bearing instantaneous frequency (IF) signal $\omega(t)$ and instantaneous amplitude (IA) signal $A(t)$ from the modulated signal $x(t)$. Discrete–time monocomponent AM–FM signals (over finite time intervals) are defined as signals of the form

$$x[n] \;\triangleq\; A[n]\cos\left(\phi[n]\right) \;=\; A[n]\cos\left(\int_0^n \Omega[k]dk + \theta\right),\ \Omega[n] \;=\; \frac{d\phi}{dn}[n] \tag{1.2}$$

where $A[n]$ and $\Omega[n]$ are the discrete [1] instantaneous amplitude (IA) and instantaneous frequency (IF) information signals and $\phi[n]$ is the instantaneous phase signal. Discrete–time multicomponent AM–FM signals are superpositions of these discrete–time monocomponent AM–FM signals [10]

$$x[n] \triangleq \sum_{i=1}^{M} \underbrace{A_i[n]\cos\left(\int_0^n \Omega_i[k]dk + \theta_i\right)}_{x_i[n]}, \; M \geq 2, \tag{1.3}$$

where $\{A_i[n], \Omega_i[n]\}$ are the IF and IA information signals corresponding to the i^{th} component $x_i[n]$. Each component IF and IA signal is typically of the form

$$\begin{aligned} \Omega_i[n] &= \Omega_{ci} + \Omega_{mi} q_{fi}[n] \\ A_i[n] &= A_{ci}\left(1 + \kappa_i q_{ai}[n]\right), \end{aligned} \tag{1.4}$$

where Ω_{ci} is the carrier frequency, Ω_{mi} is the maximum frequency deviation, κ_i is the AM modulation index, $q_{fi}[n]$ and $q_{ai}[n]$ are the normalized IF and IA message signals corresponding to the i^{th} component.

These multicomponent AM–FM signals find numerous applications in the general modeling of non–stationary signals as superpositions of modulated sines, where each component signal occupies a narrow spectral band around its carrier frequency and in particular find applications: (a) for modeling co–channel and adjacent channel interferences over communication channels, where one of the components models the desired signal and the other models the dominant interference [19]; (b) in speech processing where speech signals are modeled as a superposition of resonances and each AM–FM component of the signal models a speech resonance [52]; (c) where they

[1] In the definition of the discrete–time IF it is assumed that both signals $\phi[n]$ and $\Omega[n]$ can be expressed as known mathematical functions that can be differenciated or integrated yielding known computable functions. This is not a restrictive assumption because as shown in [38] any finite length discrete–time signal $\Omega[n]$ can be expressed as a linear combination of cosines via the DFT.

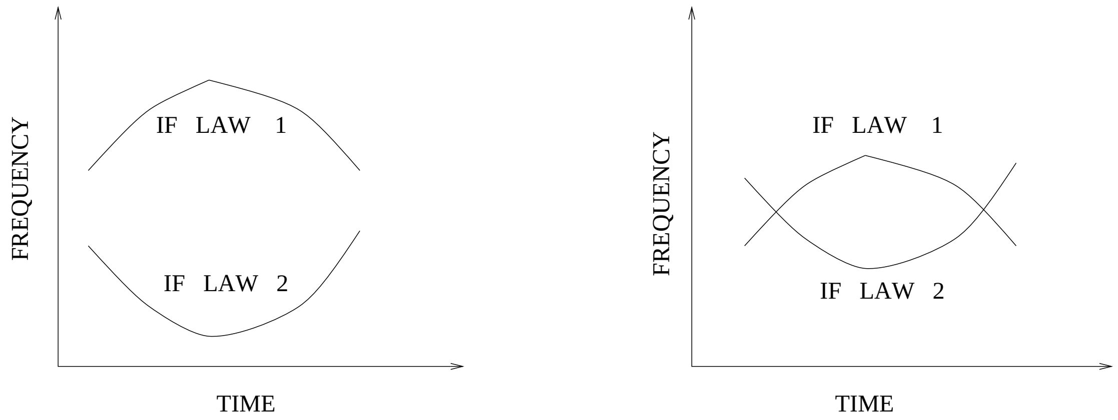

Figure 1.1: Examples of multicomponent signals where the components are well separated and distinct in the time–frequency plane or overlap spectrally. The IF law in the case of a AM–FM component is just the instantaneous frequency (IF) signal of the component [10]. IF law overlap indicates significant spectral overlap between the components.

are used to model clutter in high frequency radar [49] or in multiple target tracking applications [33]; and (d) in the modeling of different image textures via the use of 2D spatial AM–FM signals [47].

For the demodulation of monocomponent AM–FM signals, many successful demodulation approaches exist, ranging from standard methods such as Gabor's analytic signal and Hilbert transform (which is a global linear integral approach) or phase-locked Loops (PLL's) [16, 18, 34] to the recent energy separation algorithm (ESA) [38, 39] that tracks and demodulates the energy of the source producing the AM–FM signal using instantaneous nonlinear differential operators. While each of these monocomponent algorithms may have its relative advantage or disadvantage, they more or less offer a solution to the monocomponent AM–FM demodulation problem. This, however, is not the case for multicomponent AM–FM demodulation. The existing methods for multicomponent AM–FM demodulation either assume that the components are distinct in the time–frequency plane or assume that the components can be separated using linear filtering techniques.

Due to these assumptions, the existing algorithms only work in restricted ranges of spectral separation or relative power separation between the components. They are specifically unable to handle the case where the components overlap spectrally and are no longer distinct in the time–frequency plane (co–channel problem) [10]. This co–channel problem is especially prevalent in communication systems that support a large number of users and require frequency or bandwidth reuse [19]. This problem becomes more acute when the IF tracks of the components cross–over as described in Fig. 1.1 where the existing algorithms develop singularity problems. The separation and demodulation of co–channel voice–modulated FM signals is in particular an important problem in this category that one encounters both in military and civilian communication bands, where the signal of interest encounters co–channel interference from other terrestrial sources [43].

Another related and important problem is the problem of separating an additive mixture of periodic or quasi-periodic signals into its constituent components, where one or both of the components may contain useful information. This is an important signal processing and detection task that one encounters: (a) when dealing with the problem of recovery of multiple sinusoidal signals in noise [62]; (b) in biomedical signal processing problems such as separating a fetal *electrocardiogram* (ECG) signal from the composite ECG signal obtained from the abdominal lead of an expectant mother which contains the dominant and omnipresent maternal ECG signal superimposed on a weaker fetal ECG signal [66]; (c) in other ECG applications requiring the removal of periodic interference from powerlines from the recorded ECG signal [66]; (d) when dealing with the problem of interference rejection in communication systems that employ narrowband bandpass signals for transmission [19]; (e) or when dealing with concurrent vowel or periodic sound separation and in the process of separating a speech signal from an interfering speech signal [1, 64].

1.2 Thesis Goal and Contributions

The major goal of this thesis is multicomponent AM-FM signal separation and demodulation. Towards this goal the thesis has three objectives: (a) *multicomponent AM–FM signal demodulation via the use of energy demodulation techniques with specific attention given to the case where the components overlap spectrally* (co–channel problem)*;* (b) *separation of the constituent components of a mixture of periodic signals, i.e., periodic mixture separation where attention is again given to the case where the components overlap spectrally and* (c) *a combination of both* (a) *and* (b) *in cases where just* (a) *is not sufficient.*

Other existing techniques for multicomponent AM–FM separation and demodulation either make assumptions regarding the distinctness of the components or assume that the components are separable via linear filtering which are not valid in this co–channel case and consequently fail. The existing approaches for multicomponent AM–FM signal demodulation are reviewed and simulated and the problems that arise when either the spectral separation between the components is small or when one of the components is much stronger than the other are pointed out. This goal of multicomponent AM–FM signal demodulation is actually a two part task that involves: (a) the separation of the signal components from the composite signal and (b) the demodulation of the separated components for extraction of the information bearing IF and IA signals for each component. To accomplish this goal the *energy demodulation of mixtures* (EDM) algorithm and the *periodic algebraic separation energy demodulation* (PASED) are developed.

The first algorithm, the EDM, performs both component separation and demodulation tasks simultaneously and provides a computationally simple and physically meaningful alternative to the existing techniques. The EDM algorithm makes use of the *generating differential/difference equation* (GDE) of the composite signal and higher–order energy measurements of the composite signal to accomplish this purpose. The PASED algorithm, on the other hand, separates the component separation and demodulation tasks. The separation task of the PASED involves the use of the *matrix algebraic separation* (MAS) algorithm [44, 45]. In this part, the components are modeled as periodic signals and the knowledge regarding the spectrally additive nature of the mixture is combined with the periodic model in a matrix framework [5, 57, 58]. The component demodulation task is accomplished via the use of the *energy separation algorithm* (ESA) [37, 38, 39, 41] that uses the Teager–Kaiser energy operator to demodulate the separated component into IF and IA signals [26, 27]. The PASED algorithm is then evaluated by applying it to the problem of separating spectrally overlapping voice modulated FM signals. The PASED algorithm is also compared with the existing techniques in terms of computational complexity, robustness to the presence of noise and in terms of the effect of component spectral separation and relative power ratio on performance.

On route to solving the multicomponent AM–FM separation and demodulation problem, the MAS algorithm, which is the separation section of the PASED algorithm, is independently analyzed in the frequency domain in relation to the *separation of periodic mixtures* (SPM) problem. The insight obtained in this analysis is used to develop harmonic restoration methods for the MAS algorithm to improve its performance so that it can accomplish the separation of the constituent components of a mixture of discrete periodic signals. The modified MAS algorithm is then evaluated by applying it to the problem of separating a mixture of vowels, using both synthetic and real vowels.

1.3 Parameters and Performance Measures

The definition of the multicomponent AM–FM model assumes that the components in the superposition are distinct entities in the time–frequency plane [10]. This assumption is not valid when the components are spectrally close (adjacent channel problem) or overlap (co–channel problem). Although they are a subclass of the multicomponent AM–FM separation demodulation algorithms, two–component AM–FM demodulation algorithms are particularly important because they reveal the problems and the shortcomings of the existing multicomponent AM–FM separation and demodulation algorithms in terms of their inability to handle the interaction between just two of the components and hence are a clear indicator of the problems that one can expect when dealing with multicomponent AM–FM signals that contain more than two AM–FM components. For the evaluation of the algorithms and techniques presented in this thesis, some performance–related parameters need to be defined for two–component sinusoidally modulated AM–FM signals of the form

$$x[n] = \sum_{i\,=\,1}^{2} A_i[n] \cos\left(\int_0^n \Omega_i[m]dm + \theta_i\right), \tag{1.5}$$

where the IF and IA information signals are sinusoidal and given by

$$\begin{aligned} \Omega_i[n] &= \Omega_{ci} + \Omega_{mi} \cos\left(\Omega_{fi} n + \alpha_i\right) \\ A_i[n] &= A_{ci}[1 + \kappa_i \cos\left(\Omega_{ai} n + \gamma_i\right)] \quad \text{with} \quad i = 1\ ,\ 2\ . \end{aligned} \tag{1.6}$$

A measure of the spectral separation between the components is the *normalized carrier separation* (NCS) parameter of the mixture defined by

$$\mathrm{NCS} \quad = \quad \frac{|\Omega_{c2} - \Omega_{c1}|}{\sum\limits_{i\,=\,1\,,\,2} (\Omega_{mi} + \Omega_{fi} + \Omega_{ai})}. \tag{1.7}$$

Note that the denominator of the NCS measure is the average Carson bandwidth[2]. of the signal, which is a conservative estimate of the actual bandwidth [21]. The *mean power ratio* (MPR) parameter of the mixture is defined as

$$\mathrm{MPR(dB)} \quad = \quad 20 \log \left(\frac{\sigma_{x1}}{\sigma_{x2}} \right), \tag{1.8}$$

where σ_{xi} is the RMS value of component x_i, measures the strength of the first component relative to the second. The strength of the amplitude modulations with respect to the carrier are measured by the AM depth κ_i and the strength of the frequency modulations relative to the carrier are measured by quantity $\left(\frac{\Omega_{mi}}{\Omega_{ci}}\right)$ or equivalently through the *carrier-to-frequency-deviation-ratio* $(\mathrm{CR/FD})_i \;=\; \frac{\Omega_{ci}}{\Omega_{mi}}$. The *carrier-to-information-bandwidth-ratio* (CR/IB) of each component is defined as

$$(\mathrm{CR/IB})_i = \frac{\Omega_{ci}}{\max(\Omega_{fi}, \Omega_{ai})}, \tag{1.9}$$

and is a measure of how fast the signal modulations vary with respect to the carrier. This ratio is typically in the O(10) for speech resonances, $\mathrm{O}(10^2)$ for AM radio applications and $\mathrm{O}(10^3 \;-\; 10^4)$ for FM communication applications.

The *modulation index* of an FM signal is defined as the the ratio of the frequency deviation to the message bandwidth $\beta \;=\; \left(\frac{\Omega_m}{\Omega_f}\right)$. The FM signal is said to be narrowband for $\beta \;<<\; 1$ and broadband if $\beta \;>\; 1$ [21]. The normalized carrier

[2]The Carson bandwidth of an FM signal is defined as the difference between the frequencies where the spectrum of the modulated signal attains 1 % of the peak spectral amplitude of the unmodulated carrier [21]

biased RMS (NRMS) error and mean absolute estimation error (NMAE) associated with the time varying parameter $\Theta_i[n]$ and its estimated value $\hat{\Theta}_i[n]$ are defined by

$$(\mathrm{NRMS})_i \;=\; \frac{||\Theta_i[n]-\hat{\Theta}_i[n]||_2}{||\Theta_i||_2} \quad , \quad (\mathrm{NMAE})_i \;=\; \frac{||\Theta_i[n]-\hat{\Theta}_i[n]||_1}{||\Theta_i||_1}. \tag{1.10}$$

The unbiased frequency and amplitude demodulation errors of the algorithms are defined similarly but with the carrier frequency and amplitude subtracted off from the IF and IA estimates. These measure the capability of the algorithms to track the frequency and amplitude signal modulations.

1.4 Second- and Higher-Order Energy Operators

The *energy demodulation of mixtures* (EDM) algorithm developed in [4, 56] and the demodulation section of the PASED algorithm [5, 58] use energy separation and demodulation concepts. This requires a good understanding of the Teager–Kaiser energy operator [26, 27] and its higher–order extensions. The nonlinear differential Teager–Kasier energy operator introduced in [26, 27] for tracking the energy (second–order) of a signal forms the basis for the *energy separation algorithm* (ESA) [37, 38]. Higher–order extensions of the operator were later proposed in [40] for tracking the higher–order energies. These operators are attractive because of their computational simplicity, their excellent time resolution, and because they track physically meaningful quantities.

1.4.1 Continuous-Time Energy Operators

The continuous-time, nonlinear, and differential, Teager-Kaiser energy operator

$$\Psi(x) \quad = \quad (\dot{x})^2 - x\ddot{x}, \tag{1.11}$$

was introduced in [26, 27] for tracking the energy of the source that produced the signal x. This operator is a very essential ingredient of the *energy separation algorithm* (ESA) [37, 38] which has been used for the demodulation of monocomponent AM–FM signals and finds applications in speech formant and bandwidth tracking [52]. Specifically in the case of a harmonic oscillator excited by a sinusoidal disturbance, this operator tracks the energy of the oscillator normalized by half unit mass [38, 39].

The energy-like quantity

$$C(x, \dot{y}) = \dot{x}\dot{y} - x\ddot{y}, \tag{1.12}$$

which is a measure of the cross–energy between the signals x and $\dot{y}$, was used in [27, 28] to analyze the output $\Psi(x+y)$ of the energy operator applied to a sum of two signals. In [40] the cross–energy between a signal x and its higher-order derivatives was used to develop higher-order energy measurements. Specifically, the k^{th}-order *differential energy operator* (DEO) is defined as [40]

$$\begin{aligned} \Upsilon_k(x) &= C\left(x, x^{(k-1)}\right), \quad k = 0, \pm 1, \pm 2, \ldots \\ &\triangleq \dot{x}x^{(k-1)} - xx^{(k)}, \quad k = 0, \pm 1, \pm 2, \ldots, \end{aligned} \tag{1.13}$$

and yields the cross–energy between a signal $x(t)$ and its $(k-1)^{\text{th}}$ derivative (or integral), where

$$x^{(k)}(t) \triangleq \begin{cases} d^k x(t)/dt^k, & k \geq 1 \\ x(t), & k = 0 \\ \int_{-\infty}^{t} x^{(k+1)}(\tau)d\tau, & k \leq -1 \end{cases} \tag{1.14}$$

Of specific interest are the DEOs of positive orders. The second-order DEO Υ_2, that measures the energy of a harmonic oscillator that produced the signal x, gives to Υ_k the name 'energy' since it is identical to the standard energy operator Ψ. The higher–

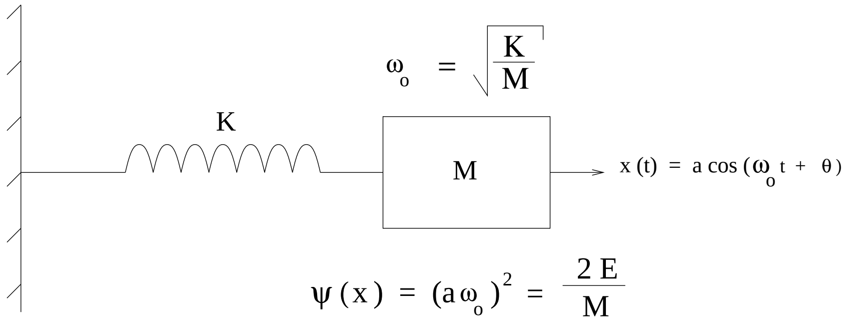

Figure 1.2: The Teager–Kaiser energy operator tracks the energy of the sinusoidal source (normalized by half unit mass) that produces the signal x.

order energy operators track the higher–order energy measurements of the signals x. The third–order DEO Υ_3 is an *energy velocity* operator, whereas the fourth-order DEO Υ_4 has dimensions of *energy acceleration*. When these higher–order energy operators are applied to a sine wave, they yield products of powers of the amplitude and frequency [40]:

$$\Upsilon_k[A\cos(\omega t+\theta)] \quad = \quad \begin{cases} 0, & k=\pm1,\pm3,\pm5,... \\ (-1)^{1+\frac{k}{2}}A^2\omega^k, & k=0,\pm2,\pm4,... \quad . \end{cases} \tag{1.15}$$

These are the called the basic **energy equations**. If the amplitude or the frequency of $x(t)$ are slowly time-varying, i.e., if x is an AM–FM signal, then these energy equations are approximately valid provided that the IF and IA information signals do not vary too fast or too much with respect to the carrier frequency. The excellent time resolution of these operators enables robust estimation of the IF and IA information signals in modulated sinusoids.

1.4.2 Discrete-Time Operators

Application of the energy operators to sampled signals requires replacing the derivatives in continuous operators with finite differences. Replacing continuous-time signals $x(t)$ with sequences $x[n] = x(nT)$ of their samples, also denoted as $x[n]$, and first-order derivatives $\dot{x}(t)$ with backward differences $\Delta_b x[n] = (x[n] - x[n-1])/T$ converts the continuous-time operators into discrete–time ones [40]

$$C(x[n], y[n]) \quad \stackrel{\triangle}{=} \quad x[n]y[n-1] \quad - \quad x[n-1]y[n], \tag{1.16}$$

where the sampling period in this case is $T = 1$. With $y[n] = x[n+1]$, the C operator becomes identical to the discrete Teager-Kaiser energy operator [26]

$$\Psi(x[n]) \quad \stackrel{\triangle}{=} \quad x^2[n] \quad - \quad x[n-1]x[n+1] \; = \; C(x[n], x[n+1]). \tag{1.17}$$

Generalizing this operator with $y[n] = x[n+k]$ in C leads to discrete-time higher-order energy measurements for a signal $x[n]$. For example, we define the k^{th}-order discrete[3] energy operator [40]

$$\begin{aligned} \Upsilon_k(x[n]) \quad &\stackrel{\triangle}{=} \quad C(x[n], x[n+k-1]) \quad , \quad k = 0, 1, 2, 3, ... \\ &= \quad x[n]x[n+k-2] \quad - \quad x[n-1]x[n+k-1]. \end{aligned} \tag{1.18}$$

For $k = 2$, one obtains the discrete–time Teager–Kaiser energy operator $\Upsilon_2 \equiv \Psi$. For $k = 3$, one obtains an *asymmetric discrete–time energy velocity operator*

$$\Upsilon_3(x[n]) \quad \stackrel{\triangle}{=} \quad x[n]x[n+1] \quad - \quad x[n-1]x[n+2].$$

Applying the operators Υ_k to discrete (possibly damped) cosines yields *discrete–time energy equations* [40]

$$\Upsilon_k[Ar^n \cos(\Omega n + \theta)] \quad = \quad A^2 r^{2n+k-2} \sin(\Omega) \sin[(k-1)\Omega], \tag{1.19}$$

[3]For notational simplicity the same symbol is used for both the continuous- and discrete-time higher-order operators Υ_k and the Teager-Kaiser energy operator Ψ, since the input signal can reveal this aspect of the operator.

which are useful for parameter estimation in sinusoids. In addition, these energy equations also hold approximately when the signal is of the AM–FM type and the IF signal does not vary too fast or too much with respect to the carrier. Different discrete AM–FM energy demodulation algorithms can be obtained by combining the above energy equations of various orders. The excellent time resolution of these operators enables the tracking of instantaneous variations in the component IF and IA signals.

Organization of the Thesis

Existing aproaches to multicomponent AM–FM signal separation and demodulation are reviewed and simulated in Chapter 2. Simultaneous component separation and demodulation via the use of the Teager–Kaiser energy operator and its higher–order extensions is explored in Chapter 3 via the EDM algorithm which was a preliminary attempt at solving the two–component AM–FM separation and demodulation problem. The EDM algorithm is then applied to the problem of separating and demodulating two–component voice–modulated FM signals. Chapter 4 contains the heart of the thesis, i.e., the PASED algorithm for the separation and demodulation of spectrally close multicomponent AM–FM signals. The PASED algorithm is then applied to the FM–voice problem to demonstrate its superior performance. It is also compared to the existing techniques in terms of its complexity, robustness to noise, and in terms of the effect of NCS and MPR parameters on algorithm performance. In Chapter 5, the separation section of the PASED algorithm, i.e., the MAS algorithm is independently analyzed, modified, and applied to the problem of separating the components of a mixture of synthetic and natural vowels. Finally, in Chapter 6 conclusions for the thesis and suggestions for future work are presented.

CHAPTER 2

MULTICOMPONENT AM–FM DEMODULATION: AN OVERVIEW OF EXISTING METHODS WITH SIMULATIONS

2.1 Introduction

The basic problem in the processing of AM–FM signals is *demodulation*, i.e., estimation of the information stored in the IF and IA signals given the composite signal. For monocomponent AM–FM signals many successful demodulation approaches exist, ranging from standard methods such as Gabor's analytic signal and Hilbert transform (which is a global linear integral approach) or phase-locked Loops (PLL's) [18, 34, 16] to the recent energy separation algorithm (ESA) [39, 38] that tracks and demodulates the energy of the source producing the AM–FM signal using instantaneous nonlinear differential operators.

For multicomponent AM–FM signals, the additional task of separating the components from the composite signal exists. Of course, the simple case when the

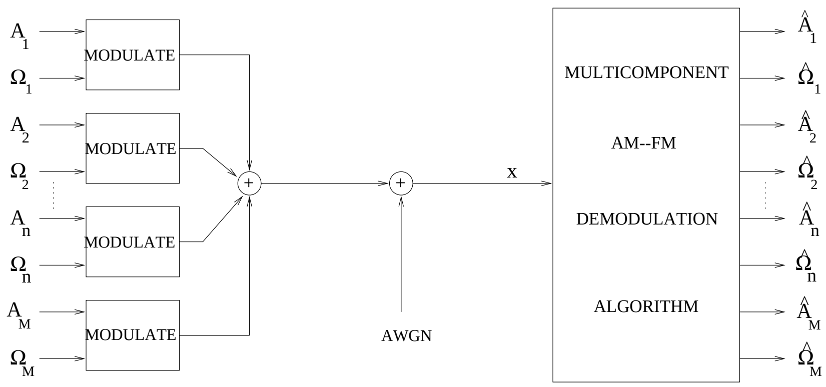

Figure 2.1: The goal of the multicomponent AM–FM demodulation algorithms is to extract the IF and IA signals for each component from the composite signal x.

components have approximately disjoint spectra can be solved successfully via bandpass filtering and monocomponent demodulation. The challenging case, however, is when the the signal components overlap spectrally and are no longer disjoint, as in the case of the co–channel problem [19]. Existing multicomponent AM–FM demodulation approaches include the following classes of algorithms: 1) State space estimation: (a) cross-coupled digital phase-locked loop (CC–DPLL) algorithms [63, 6, 8], and (b) extended Kalman filtering (EKF) [9, 35, 36]; 2) Techniques based on Hankel and Toeplitz matrices: (a) the Hankel rank reduction (HRR) algorithm [13], and (b) the instantaneous Toeplitz determinant (ITD) algorithm [30]; 3) adaptive linear prediction using: (a) exponentially weighted RLS algorithm [20], and (b) the normalized LMS algorithm [22]; 4) Energy demodulation: (a) Multiband–ESA (MESA) [7] that consists of bandpass filtering followed by monocomponent energy separation, and (b) the energy demodulation of mixtures (EDM) algorithm [56] that uses instantaneous nonlinear operators measuring cross-energies between components. (5) Maximum likelihood estimation [15]: that uses the discrete–time polynomial phase transform to initialize an iterative approach based on Newton's algorithm.

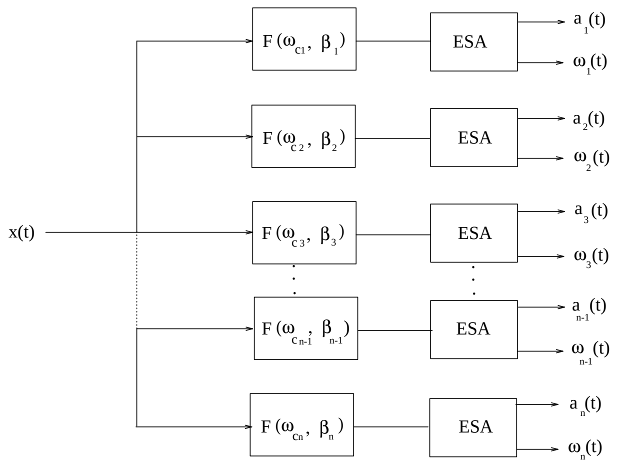

Figure 2.2: Block diagram of the multiband–ESA, depicting multiband filtering followed by energy separation. $\{\omega_{ci}, i = 1, 2, \ldots, n\}$ are the center frequencies and $\{\beta_i, i = 1, 2, \ldots, n\}$ are the bandwidths of the multiband filters.

These multicomponent AM–FM demodulation techniques, however, differ in terms of their complexity, noise suppression capabilities and in terms of their demodulation philosophy. In this chapter, a brief overview of the existing multicomponent AM–FM demodulation techniques is presented. These methods are then applied to the demodulation of a two–component AM–FM signal with parameters: NCS $= 2.12$, MPR $= 0$ dB, where the component IF and IA signals are sinusoidal with 0.5 , 1 % FM and 8 % AM. The problems encountered in this two–component example are a clear indicator of the problems that one has to contend with when dealing with signal with more than two components.

2.2 Multiband Demodulation Algorithms

If the components of the multicomponent AM–FM signal are spectrally well separated then they can be isolated by using the multiband filtering approach proposed in [7]. The multicomponent AM–FM signal is first filtered through a parallel bank of linear

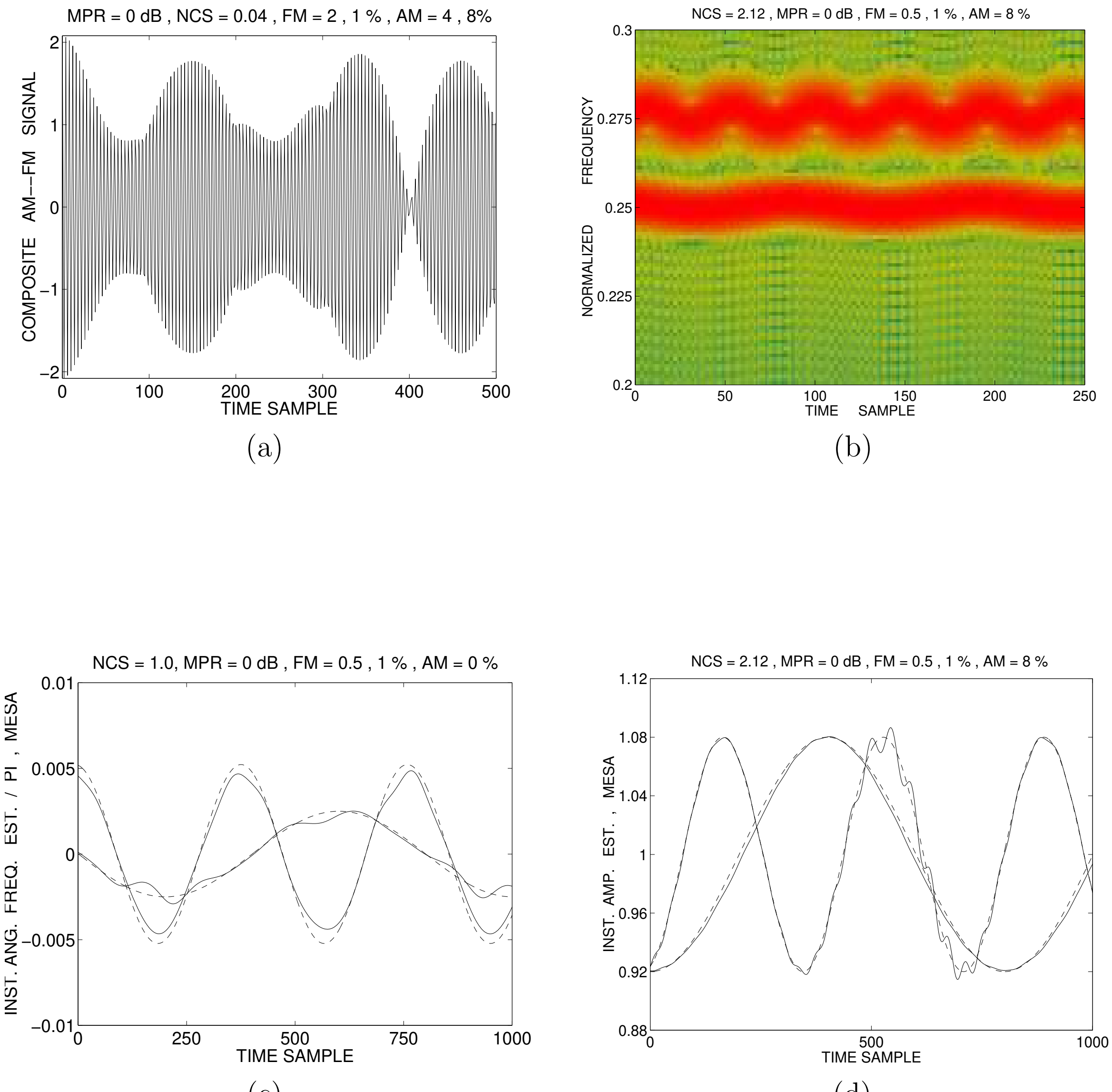

Figure 2.3: Sinusoidal AM–FM example: (a) composite FM signal, (b) spectrogram of composite signal with a Hamming window of 256 samples, FFT length of 1024 samples and time–increment of 8 samples, (c) angular frequency estimates of the *multiband ESA* (MESA) as fractions of π and (d) IA estimates of the MESA. Estimates are solid lines, actual quantities are dashed lines and carrier frequency estimates are dashed–dotted lines. Multiband FIR linear phase filters designed using the kaiser window method with design parameters of $L = 225$ (order of the filter) and $\beta = 6.65$ (controls the passband tolerance of the filter) [46]. Due to the spectral proximity of the components, long filters are needed to separate the components.

phase FIR or Gabor filters that sample the frequency domain densely, where the center frequencies are spaced uniformly in frequency and the bandwidths of the filters have been optimized for minimum distortion of the components. Once the components have been isolated, monocomponent demodulation algorithms like the *energy separation algorithm* (ESA) [38, 39] can be used to demodulate the components into IF and IA signals:

$$\begin{aligned} \omega(t) &\approx \sqrt{\frac{\Psi(\dot{x})}{\Psi(x)}} \\ |a(t)| &\approx \frac{\Psi(x)}{\sqrt{\Psi(\dot{x})}}, \end{aligned} \tag{2.1}$$

where

$$\Psi(x) \quad \triangleq \quad (\dot{x})^2 - x\ddot{x}$$

is the Teager–Kaiser energy operator [26, 27] and dots denote time derivatives. A block diagram of the multiband–ESA is shown in Fig. 2.2. The multiband–ESA has found applications in speech processing, for formant tracking, speech bandwidth estimation [52] and in the development of the AM–FM vocoder [50]. Both noise removal and component separation in these algorithms is accomplished by multiband filtering. For a M component AM–FM signal, the M most active channels (channels with the largest short–time averaged energy operator output) are selected and the other less active channels are rejected. The time resolution and noise rejection capabilities of these algorithms are controlled by the bandwidth of the filters used in the multiband filtering process.

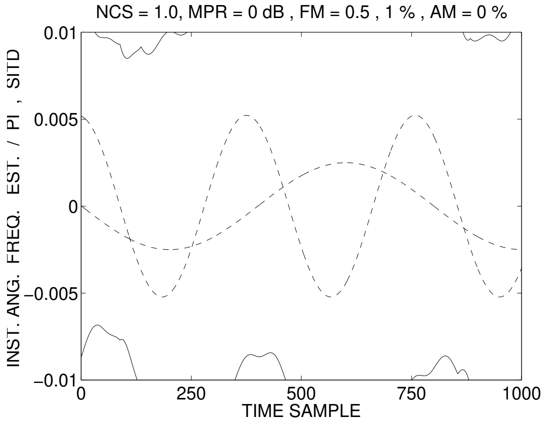

(a)

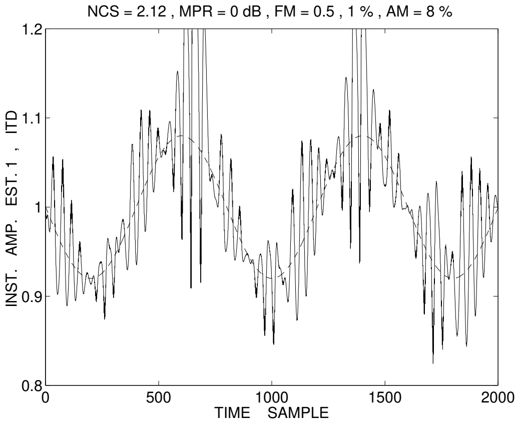

(b)

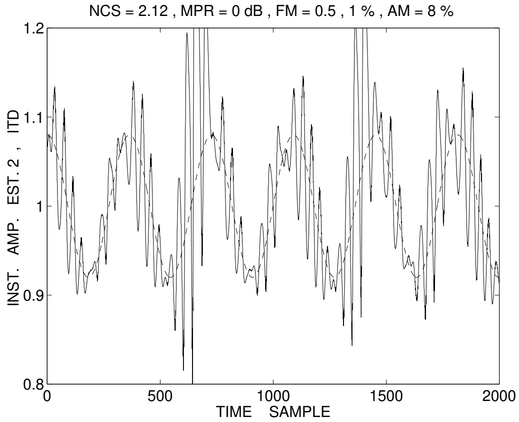

(c)

Figure 2.4: ITD Algorithm: (a) angular frequency estimates of the ITD algorithm (as fractions of π) and (b,c) IA estimates of the ITD algorithms using $L = 20$ rows in the least–squares system of Eq. 2.4. The beating in the amplitude estimates reflects the inability of the ITD algorithm to cope with the spectral proximity of the components.

2.3 Toeplitz and Hankel Matrix based Techniques

2.3.1 Instantaneous Toeplitz Determinant (ITD) Algorithm

Instantaneous operators obtained as the determinant of Toeplitz matrices are the ingredients of the *instantaneous Toeplitz determinant* (ITD) algorithm proposed in [29, 30] for the separation and demodulation of multicomponent AM–FM signals. The two–component algorithm in particular involves the computation of determinants of instantaneous 4×4 Toeplitz matrices. The determinant of the instantaneous Toeplitz matrix corresponding to the signal $x[n]$ is denoted as $\mathbf{D}_x = \mathbf{D}(x[n])$. The modified[4] algorithm (ITD) can be summarized as:

$$\begin{aligned}
\mathbf{D}_{y_1} &= \mathbf{D}(x[n] + x[n-1]) \quad , \quad \mathbf{D}_{y_2} = \mathbf{D}(x[n] - x[n-1]) \\
c_1 &= \frac{1}{8}\left(\frac{\mathbf{D}_{y_1}}{\mathbf{D}_x} - \frac{\mathbf{D}_{y_2}}{\mathbf{D}_x}\right) \quad , \quad c_2 = \frac{1}{8}\left(\frac{\mathbf{D}_{y_1}}{\mathbf{D}_x} + \frac{\mathbf{D}_{y_2}}{\mathbf{D}_x}\right) - 1.
\end{aligned} \tag{2.2}$$

The IF signals are then estimated from the coefficients as :

$$\Omega_{1,2} = \cos^{-1}\left(\frac{c_1 \pm \sqrt{c_1^2 - 4c_2}}{2}\right). \tag{2.3}$$

The instantaneous determinants involved in the ITD algorithm form generalized energy–like operators, that are time–invariant quantities for sinusoidal signals and lowpass quantities for AM–FM signals.

The corresponding linear amplitude estimation algorithm for the component IA signals involves the integration of the component IF signal estimates and the least–squares solution to a system of linear equations in the amplitudes and the phase offsets [60]. Upon defining the quantities: $c_{1,2}[n] = \cos(\Omega_{1,2}n)$, $s_{1,2}[n] = \sin(\Omega_{1,2}n)$, the

[4] The original two–component algorithm proposed in [30, 29] had mistakes of the kind $\sqrt{\cos^2(\Omega)} = \cos(\Omega)$. The modification was to solve for $\cos(\Omega_1)$ and $\cos(\Omega_2)$ instead of $\cos(\Omega_1 \pm \Omega_2)$

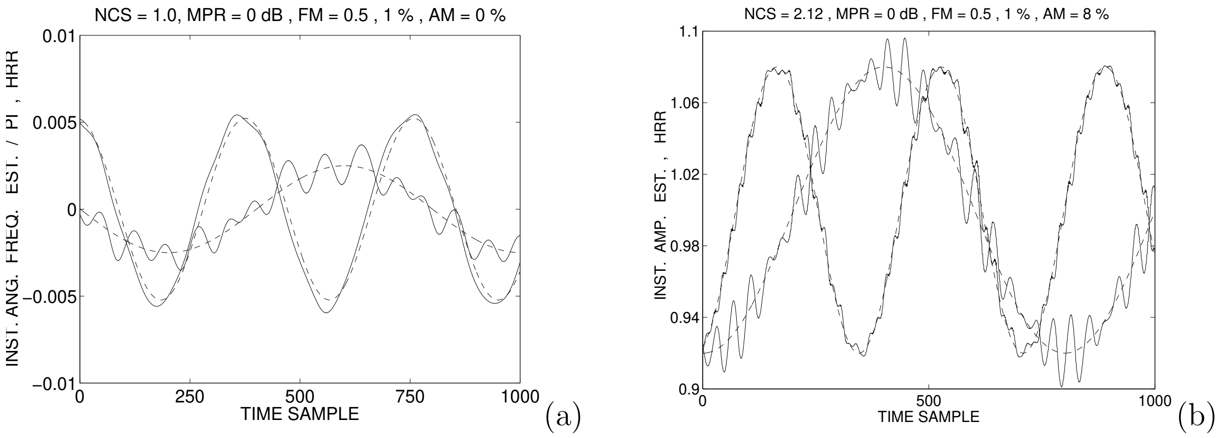

Figure 2.5: Hankel rank reduction: (a) angular frequency estimates of the HRR algorithm, (b) IA estimates of the HRR algorithm using the least–squares system in Eq. 2.4 with $L = 20$ rows. Estimates are shown as solid lines, dashed lines are actual quantities and dashed–dotted lines correspond to the carrier frequency estimates. The Hankel system used for frequency estimation in the HRR algorithm is of order $c = 20$.

---

linear amplitude estimation algorithm is obtained as :

$$\begin{pmatrix} c_1[n] & -s_1[n] & c_2[n] & -s_2[n] \\ c_1[n+1] & -s_1[n+1] & c_2[n+1] & -s_2[n+1] \\ c_1[n+2] & -s_1[n+2] & c_2[n+2] & -s_2[n+2] \\ c_1[n+3] & -s_1[n+3] & c_2[n+3] & -s_2[n+3] \end{pmatrix} \begin{pmatrix} a_1 \cos(\theta_1) \\ a_1 \sin(\theta_1) \\ a_2 \cos(\theta_2) \\ a_2 \sin(\theta_2) \end{pmatrix} = \begin{pmatrix} x[n] \\ x[n+1] \\ x[n+2] \\ x[n+3] \end{pmatrix}. \tag{2.4}$$

The component IA estimates are obtained by eliminating the phase offsets from the equations. The order of the least–squares system needs to be optimized so that noise accumulated during the integration process is smoothed out, while maintaining sufficient instantaneous behavior for the tracking of the component IA signals.

2.3.2 Hankel Rank Reduction (HRR) Algorithm

Component IF signal estimation from superimposed time–varying harmonics has also been approached by using Hankel matrices containing signal samples via the *Han-*

kel rank reduction (HRR) algorithm as described in [49, 13]. The Hankel matrix containing samples of the signal $x[n]$ is denoted $\mathbf{H}_x = \mathbf{H}(x[n])$. The signal of interest

$$y[n] \quad = \quad \sum_{i\,=\,1}^{i\,=\,M} a_i \cos\left(\phi_i[n]\right) \quad , \quad \Omega_i[n] = \phi_i[n] - \phi_i[n-1]$$

is modeled as the output of an oscillator, a marginally stable system with zero input described by the state equations:

$$\begin{aligned} \mathbf{x}[n+1] \quad &= \quad \mathbf{F}[n]\mathbf{x}[n] \\ y[n] \quad &= \quad \mathbf{h}\mathbf{x}[n], \end{aligned} \tag{2.5}$$

where the parameters of the state model are given by

$$\begin{aligned} \mathbf{h} \quad &= \quad [a_1, a_1, a_2, a_2 \ldots, a_M, a_M] \\ \mathbf{F}[n] \quad &= \quad \mathrm{diag}[e^{j\Omega_1[n+1]}, e^{-j\Omega_1[n+1]}, \ldots, e^{j\Omega_M[n+1]}, e^{-j\Omega_M[n+1]}] \\ \mathbf{x}[n] \quad &= \quad [e^{j\phi_1[n]}, e^{-j\phi_1[n]}, \ldots, e^{j\phi_M[n]}, e^{-j\phi_M[n]}]^T. \end{aligned}$$

Under the assumption that the frequencies are slowly time–varying, the Hankel matrix $\mathbf{H}_x$ can be approximated as $\mathbf{H}_x \approx \Theta X$, via a singular value decomposition (SVD) of the form

$$\mathbf{H}_x \quad \approx \quad \mathbf{U}\mathbf{S}\mathbf{V}^T \quad = \quad \sum_{i\,=\,1}^{i\,=\,2M} \sigma_i \mathbf{u}_i \mathbf{v}_i^T, \tag{2.6}$$

where only the $2M$ largest singular values have been retained and $\hat{\Theta} = \mathbf{U}\mathbf{S}$ serves as an estimate of Θ, while $\mathbf{V}^T$ serves as an estimate of X [13, 49]. The k–th to $(k+d)$–th rows of the matrix $\hat{\Theta}$, where $d = \mathrm{floor}(\frac{c+1}{2})$ and c is of the order of $3M$, are then retained in $\hat{\Theta}_k$ to solve the following system of linear equations for the estimate of the state transition matrix in the least–squares sense [13, 49]:

$$\hat{\Theta}_{k+1} \quad = \quad \hat{\Theta}_k \hat{\mathbf{F}}[d+k] \ , \ k \ = \ 1, 2, 3, \ldots \quad . \tag{2.7}$$

The component IF signals are then obtained as phase angles of the eigenvalues of this estimated state matrix. The HRR algorithm proposed in [13] uses the entire data record to perform the SVD of the Hankel matrix retaining only the significant singular values to provide noise rejection. The order of the Hankel system involved is chosen to balance the task of noise rejection with the task of tracking instantaneous variations in the IF and IA signals. For high SNR scenarios, smaller orders will suffice (a minimum order of $c = 2M$ is needed for the M–component problem), while for lower SNR scenarios larger orders are needed.

As in the case of the ITD algorithm, the component IA signals are obtained by integrating the component IF signal estimates and solving the least–squares system in Eq. 2.4 for the amplitudes by elimination of the phase offsets. The order of the least–squares system is chosen so that the frequency demodulation error and the noise accumulated in the process of integration of the component IF estimates are smoothed out.

2.4 Adaptive Linear Predictive Methods

2.4.1 LMS Algorithm

The least mean squared (LMS) algorithm [22, 66] can be used as an adaptive linear predictor for the purpose of separation and demodulation of two–component FM signals [17]. The algorithm is based on the technique of mean–square estimation as applied to linear prediction or autoregressive modeling and makes use of statistical normal equations [20] described by

$$\mathbf{R}_x \mathbf{w} = \mathbf{p}, \tag{2.8}$$

where $\mathbf{R}_x$ is the autocorrelation matrix of $x[n]$, $\mathbf{p}$ is the usual cross–correlation vector and $\mathbf{w}$ is the tap weight vector whose elements are the prediction or AR coefficients $\{a_i\}$. Once the coefficients have been solved for, the roots of the polynomial

$$\mathbf{A}(z) \;=\; 1 \;-\; \sum_{i\,=\,1}^{i\,=\,P} a_i z^{-i} \tag{2.9}$$

are computed. The phase angles of the roots of the polynomial $\mathbf{A}(z)$ are the required frequencies. The LMS algorithm is a steepest descent solution to the normal equations. The normalized version of the LMS algorithm uses a tap weight vector update normalized by the energy in the input and can be summarized as follows [22]:

$$\begin{aligned} e[n] &= d[n] \;-\; \mathbf{w}^T[n]\mathbf{u}[n] \\ \mathbf{w}[n+1] &= \mathbf{w}[n] \;+\; \left(\frac{\mu}{||\mathbf{u}[n]||^2 \;+\; \beta}\right) e[n]\mathbf{u}[n], \end{aligned} \tag{2.10}$$

where

- $d[n] = x[n]$ is the desired process and $u[n] = x[n-1]$ is the input observation process and the vector $\mathbf{u}[n] \;=\; \{x[n-1]\;,\; x[n-2]\ldots, x[n-P]\}$ contains P past samples of the composite signal;
- $\mathbf{w}[n]$ is the P-component tap–weight process containing estimates of the prediction coefficients a_i;
- μ is the step size parameter and β is the offset parameter;
- P is the order of the predictor and the LMS algorithm is guaranteed to converge if $0 < \mu < 2$.

The roots of the predictor polynomial are computed at each instant from the tap weight coefficients of the LMS algorithm. The component IF signal estimates are, therefore, obtained from the mean squared error trajectory of the predictor polynomial roots. The variance of the LMS solution about the solution to the normal equations depends on the step size parameter. For small stepsizes, the LMS algorithm converges slower, but with smaller excess mean squared error. For large step size parameters, the LMS algorithm converges faster but with larger excess mean squared error.

The time resolution and the noise suppression capabilities of the LMS algorithm are controlled by the step size and the filter order parameter. Greater noise suppression can be achieved by using longer filters and smaller stepsizes at the expense of time resolution and longer transients in the estimates. The convergence of the tap weight coefficients in the LMS algorithm is dependent on the eigenvalue spread of the autocorrelation matrix $\mathbf{R}_x$. For components with close spectral proximity, this matrix becomes ill–conditioned [31] and convergence of the tap weight error vector modes is slow [22]. The conditioning of this autocorrelation matrix also becomes poor when one of the components is stronger than the other. As in the case of the ITD and the HRR algorithms, the component IA estimates of the LMS algorithm are obtained from the least–squares system for the amplitudes in Eq. 2.4. The order of this system in this case has to be chosen to smooth out accumulated gradient noise from the component IF estimates, remove interference and still maintain sufficient time–resolution to provide satisfactory tracking of the component IA signals.

2.4.2 Exponentially Weighted RLS Algorithm

The separation and demodulation of the components of a multicomponent AM–FM signal using the adaptive linear prediction can also accomplished via the use of the exponentially weighted version of the *recursive least–squares* (RLS) algorithm. The ex-

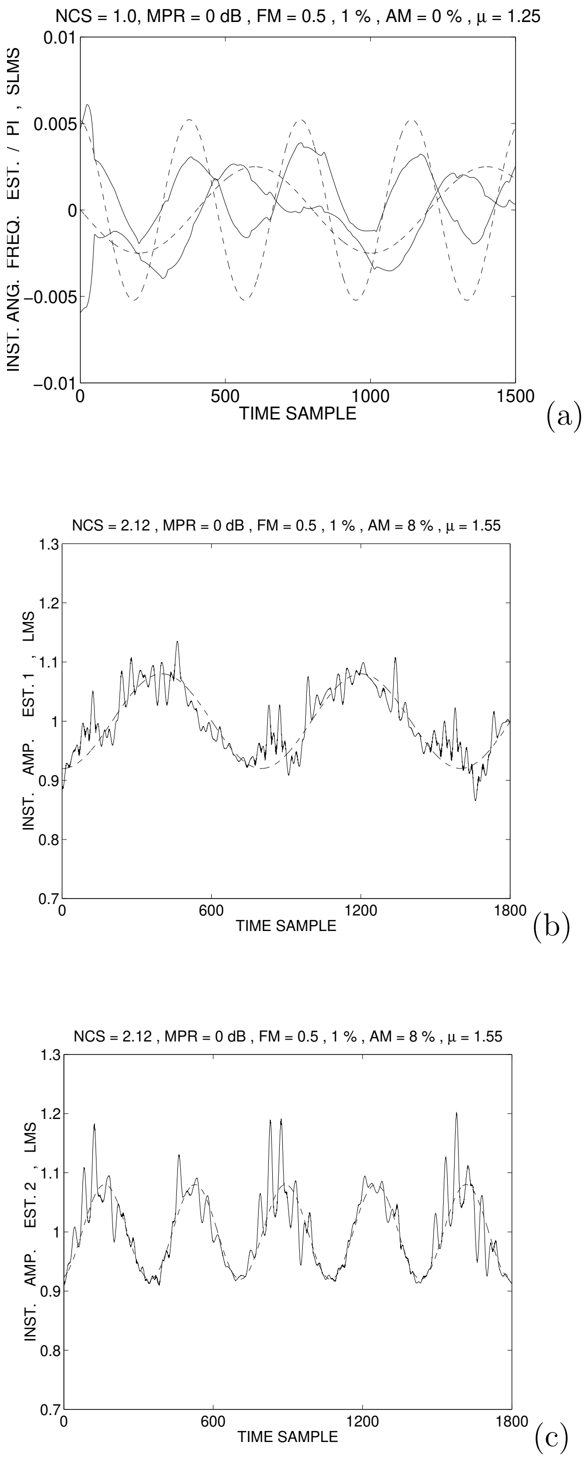

Figure 2.6: LMS algorithm: (a) angular frequency estimates of the LMS algorithm (as fractions of π) and (b,c) IA estimates of the LMS algorithm using the least–squares system in Eq. 2.4 with $L = 20$ rows. Note that the frequency estimates of the LMS exhibit a significant amount of interference (beating) due to the spectral proximity of the components. Solid lines are estimates, dashed lines are actual quantities and dashed–dotted lines correspond to the carrier frequency estimates.

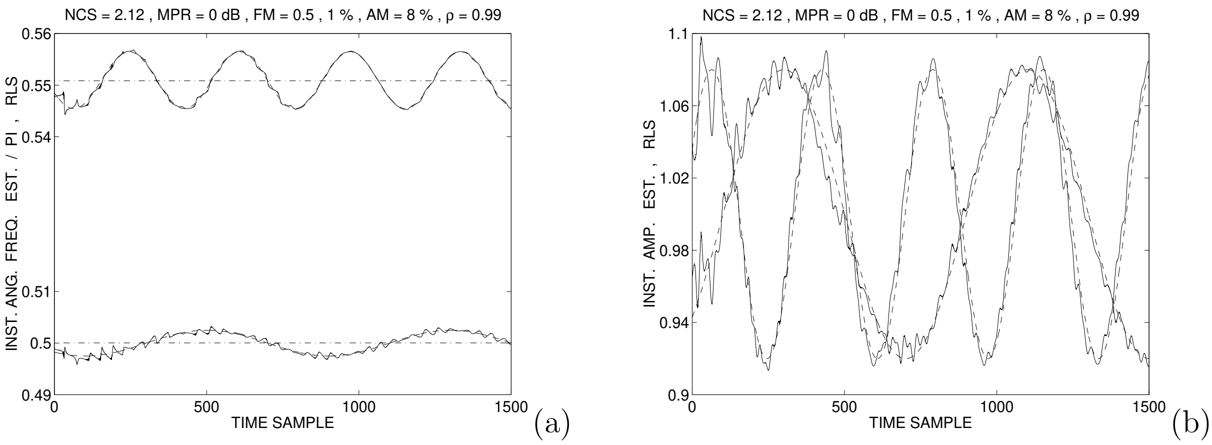

Figure 2.7: Exponentially weighted RLS algorithm: (a) angular IF estimates (as fractions of π) and (b) IA estimates of the RLS algorithm using a $L = 20$ rows in the least–squares system of Eq. 2.4. Actual quantities are dashed lines, carrier frequency estimates are dashed–dotted lines.

---

ponentially weighted RLS algorithm is based on the following exponentially weighted rank–one update of both the autocorrelation matrix $\mathbf{R}_x$ and the cross–correlation vector $\mathbf{p}$:

$$\begin{aligned} \mathbf{R}_x[n] &= \rho\mathbf{R}_x[n-1] + (1 - \rho)\,\mathbf{u}^*\mathbf{u}^T[n] \\ \mathbf{p}[n] &= \rho\mathbf{p}[n-1] + (1 - \rho)\,d[n]\mathbf{u}^*[n]. \end{aligned} \tag{2.11}$$

The update for the tap–weight vector that contains the predictor polynomial coefficients can be summarized as [20]:

$$\begin{aligned} \mathbf{z}[n] &= (1 - \rho)\,\mathbf{P}[n-1]\mathbf{u}^*[n] \\ \mathbf{g}[n] &= \left(\frac{1}{\rho + \mathbf{u}^T[n]\mathbf{z}[n]}\right)\mathbf{z}[n] \\ \alpha[n] &= d[n] - \mathbf{w}^T[n-1]\mathbf{u}[n] \\ \mathbf{w}[n] &= \mathbf{w}[n-1] + \alpha[n]\mathbf{g}[n] \\ \mathbf{P}[n] &= \frac{1}{\rho}\left[\mathbf{P}[n-1] - \mathbf{g}[n]\mathbf{u}^H[n]\right], \end{aligned} \tag{2.12}$$

where $\mathbf{g}[n]$ is the RLS gain vector, $\mathbf{P}[n]$ is the estimate of the inverse of the autocorrelation matrix $\mathbf{R}_x$ at the time instant n and $\alpha[n]$ is the innovations process. The RLS algorithm is initialized by $\mathbf{w}[0] = \mathbf{0}$ and $\mathbf{P}[0] = \delta\mathbf{I}$ for some small $\delta > 0$.

As in the case of the LMS algorithm, the IF estimates are obtained from the phase angles of the roots of the instantaneous prediction polynomial. The component IA estimates are obtained in a similar manner from the least–squares system for the amplitudes in Eq. 2.4. This exponential parameter ρ serves as a memory factor that deemphasizes old data and weighs new data appropriately. The exponential parameter ρ has to be chosen so that the tasks of noise suppression and instantaneous tracking of the component IF signals are balanced. Other variations of the adaptive linear predictive tracking philosophy such as rank reduction and rank–one updating of the eigenvalue decomposition of the autocorrelation matrix to incorporate new data have been studied in [12, 11].

2.5 Cross–coupled Phase–locked Loops

The cross–coupled phase–locked loop (CCPLL) was introduced in [63, 6] for the separation and demodulation of two–component AM–FM signal of the form

$$x(t) = A_1(t)\cos\left(\int_0^t \omega_1(\tau)d\tau\right) + A_2(t)\cos\left(\int_0^t \omega_2(\tau)d\tau\right).$$

The CCPLL algorithm is based on the maximum aposteriori (MAP) estimation technique as described in [63] and consists of two phase–locked loops interconnected in a manner so as to permit one PLL to lock onto and track the stronger component (capture effect), while the other loop tracks the weaker of the two components. A brief overview of the PLL, its design and its tracking capabilities is given in the appendix A. The CCPLL with closed loop amplitude control was proposed in [63],

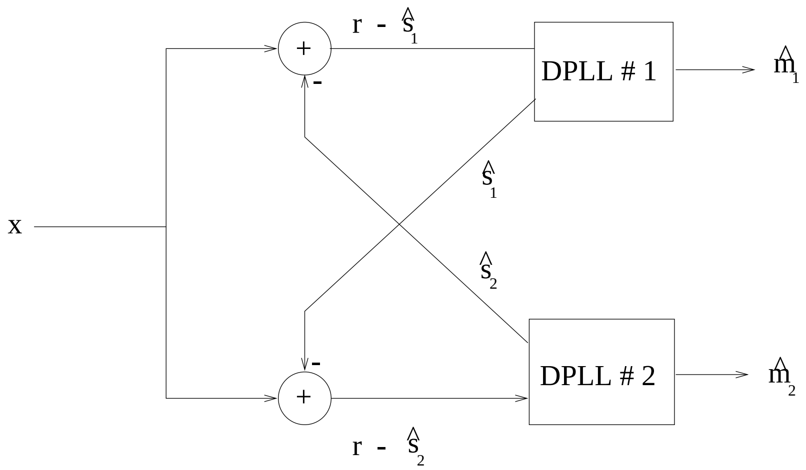

Figure 2.8: Block diagram of the CC-DPLL

---

where amplitude estimation is achieved by using steepest descent techniques. Each PLL is capable of tracking the phase of its corresponding input signal (transparency) provided that the IF laws of the components do not overlap [67]. Experimental results pertaining to the CCPLL and guidelines for their design are presented in [59]. Application of the CCPLL for separating and demodulating co–channel voice–modulated signals which overlap spectrally has been studied in [43].

The discrete-time version of the CCPLL (CC–DPLL) was recently investigated in [24, 23, 8]. The block diagram of the CC–DPLL is shown in Fig. 2.8. The CC–DPLL algorithm for the separation and demodulation of two–component cochannel signals of the form

$$x[n] \;=\; a_1 \cos(\Omega_{c1} n + \phi_1[n]) \;+\; a_2 \cos(\Omega_{c2} n + \phi_2[n])$$

involves the use of inphase and quadrature versions of the output of each DPLL that generate estimates of the components as.

$$\begin{aligned}\hat{s}_2[n] &= x[n] - \hat{a}_{1r}[n] \cos\left(\Omega_{c1} n + \hat{\phi}_1[n]\right) - \hat{a}_{1q}[n] \sin\left(\Omega_{c1} n + \hat{\phi}_1[n]\right) \\ \hat{s}_1[n] &= x[n] - \hat{a}_{2r}[n] \cos\left(\Omega_{c2} n + \hat{\phi}_2[n]\right) - \hat{a}_{2q}[n] \sin\left(\Omega_{c2} n + \hat{\phi}_2[n]\right).\end{aligned}$$

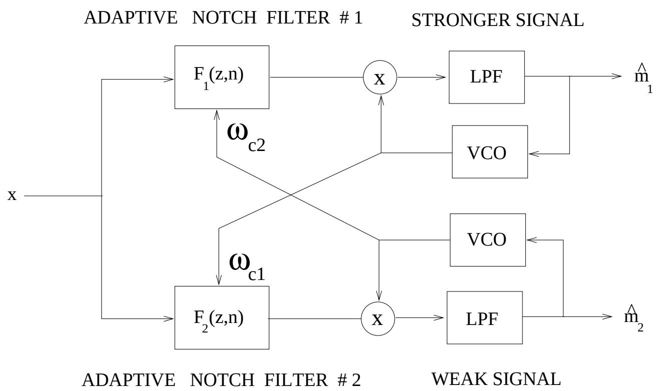

Figure 2.9: Block diagram of the interference suppressor using adaptive notch filters

The first stage involves the estimation of the amplitudes using the component estimates and adaptive filtering techniques [22]. The component estimates are modulated with the corresponding quadrature versions of PLL outputs and integrated to yield recursive formulas of the form

$$\begin{aligned} \hat{a}_{1r}[n+1] &= \hat{a}_{1r}[n] \; + \; g_1[n] * \hat{s}_2[n] \cos\left(\Omega_{c1} n + \hat{\phi}_1\right) \\ \hat{a}_{1q}[n+1] &= \hat{a}_{1q}[n] \; + \; g_2[n] * \hat{s}_2[n] \sin\left(\Omega_{c1} n + \hat{\phi}_1\right) \\ \hat{a}_{2r}[n+1] &= \hat{a}_{2r}[n] \; + \; g_3[n] * \hat{s}_1[n] \cos\left(\Omega_{c2} n + \hat{\phi}_2\right) \\ \hat{a}_{2q}[n+1] &= \hat{a}_{2q}[n] \; + \; g_4[n] * \hat{s}_1[n] \sin\left(\Omega_{c2} n + \hat{\phi}_2\right), \end{aligned} \tag{2.13}$$

where * denotes the convolution operation and $g_k[n]$, $k = 1, 2, 3, 4$ are the impulse responses of the lowpass filters used to combat beating in amplitude estimates [8]. The amplitude estimates are then given by

$$\hat{a}_1 = \sqrt{\hat{a}_{1r}^2 + \hat{a}_{1q}^2} \quad , \quad \hat{a}_2 = \sqrt{\hat{a}_{2r}^2 + \hat{a}_{2q}^2}. \tag{2.14}$$

The second stage involves phase estimation using the component estimates

$$\begin{aligned} \hat{\phi}_1[n+1] &= \hat{\phi}_1[n] + \left[a_1 \sin(\phi_1[n] - \hat{\phi}_1[n]) \; + \; \text{cross terms}\right] * f_1[n] \\ \hat{\phi}_2[n+1] &= \hat{\phi}_2[n] + \left[a_2 \sin(\phi_2[n] - \hat{\phi}_2[n]) \; + \; \text{cross terms}\right] * f_2[n], \end{aligned} \tag{2.15}$$

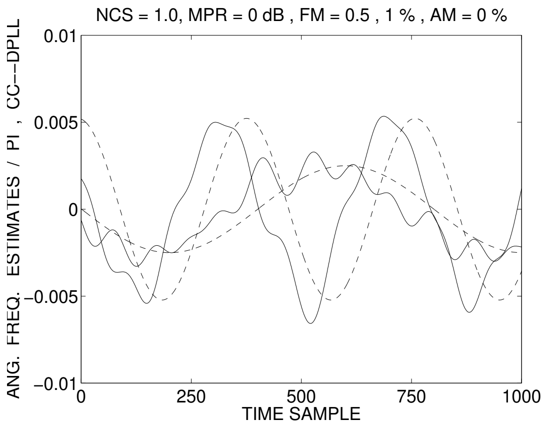

(a)

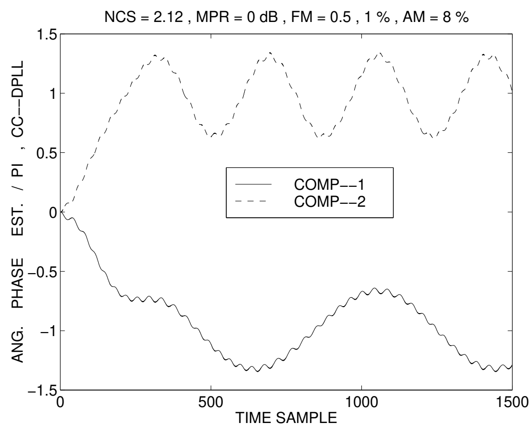

(b)

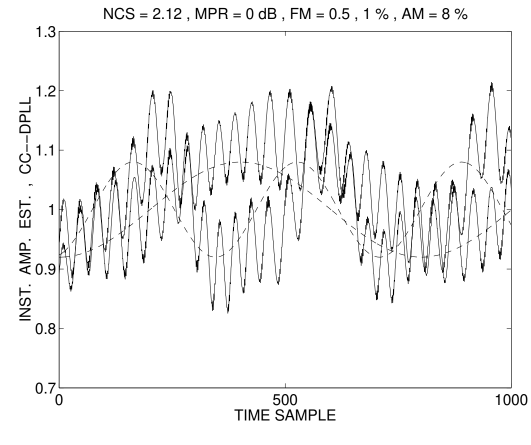

(c)

Figure 2.10: CC–DPLL algorithm: (a) baseband IF estimates of the CC–DPLL (as fractions of π) and (b) baseband phase estimates of the CC–DPLL and (c) IA estimates of the CC–DPLL. Solid lines are for the first component and dashed lines are for the second. There is significant amount of interference in the IA estimates of the CC–DPLL due to the spectral proximity of the components. First order loop filters are used in the implementation of the CC–DPLL. The closed loop transfer function of the linearized system has a damping ratio of $\zeta = 0.707$.

where $f_1[n]$ and $f_2[n]$ are the impulse responses of the two loop filters, $\phi_1[n]$ and $\phi_2[n]$ are the phase inputs to the DPLL's, $\hat{\phi}_1[n]$ and $\hat{\phi}_2[n]$ are the phase estimates of the components and * denotes the convolution operation. The design of the loop however, requires prior knowledge about the carrier frequencies and bandwidths of the signals.

Some guidelines for the design of the loops are

- Parameters of the loops need to be adjusted so that the loops are in their linear region of operation [34].
- The DPLL's are typically second order loops, designed for a damping ratio of 0.707 and the loop filters used are of the constant–integrator type [34].
- The natural bandwidth of the loop's should be optimized so that cross terms, high frequency modulation products and noise are rejected, while minimizing the harmonic distortion induced.

2.5.1 Notch Filter Version of the CC–DPLL

Modified versions of the basic CC–DPLL structure involving adaptive notch filters were studied in [54]. An adaptive notch filter is used to eliminate one of the components instead of subtraction, while the corresponding DPLL locks onto the phase of the filtered signal. The center frequency of each notch filter is at the carrier of the other signal. As in the CC–DPLL, one of the DPLL units locks onto the phase of the stronger signal, while the other one locks onto the phase of the weaker signal. The filter parameters need to be designed for stability of the closed loop. The bandwidth of the filters however, needs to be optimized to balance interference and noise rejection with the harmonic distortion induced. A block diagram of the modified interference suppression algorithm is described in Fig. 2.9.

2.5.2 Performance Measures and Separation Criteria

Performance measures for CC-DPLL's for the separation of co–channel signals have been investigated in [24, 23, 3] and criteria were proposed for the separation of the components which include distinctness of the components and the observability of the state model corresponding to the two–component signal. Observability is defined in terms of the eigenvalue spread of the observability gramian of the state model.

Eventual loss of observability occurs when the coefficients of the state model for the component phases are identical and the components are not distinct. In situations where one of components is stronger than the others, the lower–powered signal becomes less observable, resulting in larger error variance for the corresponding estimates. Loss of obervability occurs when: (a) IF tracks of the components cross or (b) when the components are completely in phase or out of phase with respect to each other. A consequence of this lack of observability is the flipping of state estimates. The singularity of the observability gramian has been proposed in [24, 23] as a means for enumerating and characterizing the number of signals present in the multicomponent signal.

2.6 Extended Kalman Filters

Multicomponent AM–FM demodulation can be accomplished via the use of the *extended Kalman filters* (EKF) in conjunction with the multicomponent AM–FM signal model. The measurement model for the EKF is nonlinear in the phase parameters and is linearized by retaining only the first term in the Taylor series expansion of the nonlinearity [2].

$$y[n] \;=\; \sum_{i\,=\,1}^{M} a_i[n]\cos\left(\phi_i[n]\right) \;+\; rv[n],$$

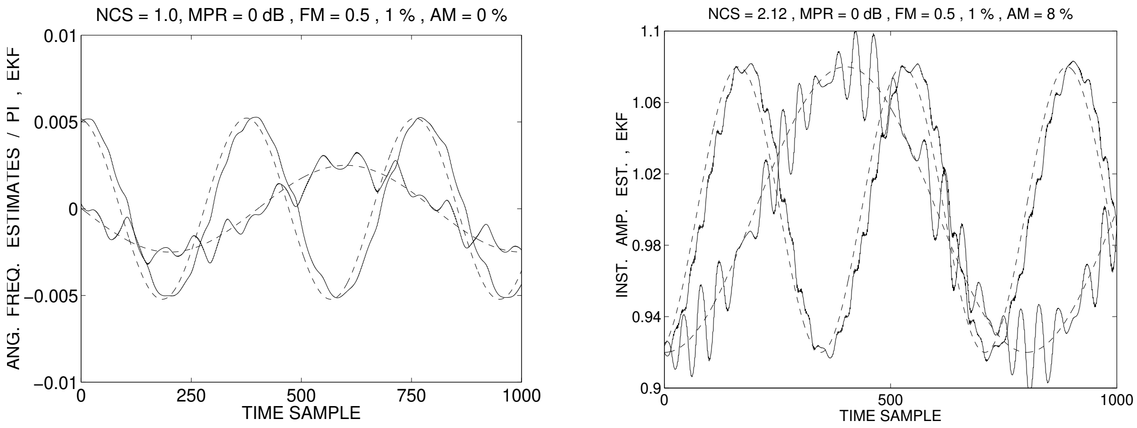

(a) (b)

Figure 2.11: EKF algorithm: (a) angular frequency estimates of the EKF (as fractions of π) and (b) IA estimates of the EKF. Estimates are in solid lines, actual quantities are in dashed lines and carrier frequency estimates are in dashed–dotted lines. α_{a_i} , α_{γ_i} = 0.995, $r = 10^{-7}$ and $T = 1$. Model noise covariance parameters are: q_{γ_i} = 0.09 , 0.05 , q_{f_i} = 0.08 , 0.05 , $q_{a_{1,2}}$ = 20

where $a_i[n]$, $\phi_i[n]$ are the IA and phase signals corresponding to the i^{th} component and v[n] is unit variance, zero mean *additive white gaussian noise* (AWGN). Although different state model definitions are possible, we use the state model defined in [36]. Each IA signal $a_i[n]$ and baseband IF signal $\gamma_i[n]$ is modeled as a first–order *auto regressive* (AR) process. The center frequency of each AM–FM component $f_i[n]$ is modeled as a random walk.

$$\begin{aligned} a_i[n+1] &= \alpha_{a_i} a_i[n] \;+\; q_{ai} w_{ai}[n] \;,\; \gamma_i[n+1] \;=\; \alpha_{\gamma_i}\gamma_i[n] \;+\; q_{\gamma_i} w_{\gamma_i}[n] \qquad (2.16) \\ f_i[n+1] &= f_i[n] \;+\; q_{f_i} w_{f_i}[n] \;,\; \phi_i[n+1] \;=\; \phi_i[n] \;+\; (2\pi T)\,(f_i[n] \;+\; \gamma_i[n])\,, \end{aligned}$$

where $w_{a_i}[n]$, $w_{\gamma_i}[n]$, $w_{f_i}[n]$ (model noise processes) are again zero mean, unit variance AWGN processes. The initial values for the components of the state estimates and error covariances are obtained from [36]

$$\begin{aligned} a_i[0] \;\approx\; N(0 \;,\; q_{ai}^2/(1-\alpha_{ai}^2)) \quad &, \quad \gamma_i[0] \;\approx\; N(0 \;,\; q_{\gamma_i}^2/(1-\alpha_{\gamma_i}^2)) \\ f_i[0] \;\approx\; N(f_{ci} \;,\; p_{f_i}^2) \quad &, \quad \phi_i[0] \;\approx\; N(0 \;,\; p_{\phi_i}^2). \qquad (2.17) \end{aligned}$$

The EKF with the above state model has been used in formant tracking applications to track the IF and IA signals corresponding to each speech resonance [35, 36], where each resonance is modeled as a monocomponent AM–FM signal.

Alternative definitions of the state model for the EKF as in [36], can be used leading to the realization of the EKF in terms of cross–coupled phase–locked loops with amplitude estimation [24, 23, 3]. In a qualitative sense the nonlinear EKF filter acts as a bank of bandpass filters, where the center frequency of the i^{th} filter tracks the IF of the i^{th} component and the bandwidth of the i^{th} filter is set to achieve the optimal trade off between passing signal energy and rejecting noise based on the statistical state model [2]. The EKF differs from the MESA approach [7] in that the filtering is done through the nonlinear state system of the EKF and not separately via the multiband filters and in that the tradeoff between passing the signal energy and rejecting noise is achieved in the process of minimizing the trace of the error covariance matrix in the state model rather than separately designing the multiband filters to meet this purpose.

2.7 Maximum Likelihood Estimation

Multicomponent AM–FM demodulation can also be achieved through maximum likelihood estimation of the parameters of the components of the signal. The procedure in the case of signals corrupted with AWGN becomes equivalent to maximizing the loglikelihood function or minimizing a second–order objective function [14, 15]. The maximum likelihood estimation problem is separable in the amplitudes and the phases/frequency parameters. The optimization procedure for the phase is complicated by the fact that the objective function is a nonlinear function of the phase or frequency parameters and therefore the likelihood function will have multiple local maxima or minima. Iterative algorithms for the optimization of these parameters need to be used [14, 15]. These algorithms, however, need to be initialized close to the global minimum so that they don't converge to local minima. Suboptimum procedures that give reasonable results for high SNR's can be used to initialize the algorithm. The objective function being a linear function of the amplitudes, the amplitudes can then be obtained through linear least–squares optimization.

The optimization algorithm can be initialized close to the global minimum through the use of the *discrete polynomial–phase transform* (DPT) described in [48]. The application of the DPT of order M on a constant amplitude polynomial phase signal of the same order transforms the broadband signal into a single tone whose frequency is related to the highest–order polynomial coefficient [48]. The DPT then estimates the polynomial coefficient of the highest order. The coefficient estimate is then used to remove the highest order polynomial term to obtain a polynomial of one order less. All the other coefficients are estimated by sequentially removing the higher order terms. This DPT provides suboptimal phase estimates for sufficiently high SNR's without the need for phase unwrapping [48]. The SNR required for proper operation of the algorithm increases as the order of the polynomial increases. This phase estimate is then refined through an iterative numerical minimization of the loglikelihood function [15, 48].

Alternatively the HRR algorithm [13] can also be used in conjunction with the maximum likelihood technique for the estimation of the parameters of multicomponent chirp signals that arise in radar target tracking problems involving multiple moving targets [33]. The maximum likelihood problem requires nonlinear optimization of the parameters due to the multimodal nature of the likelihood function. HRR algorithm frequency estimates are used to initialize the optimization procedure which are refined by the Gauss–Newton algorithm [33] to obtain maximum likelihood estimates of the parameters [33].

When the components are spectrally well separated (difference between the component IF signals sufficiently large relative to the bandwidth of the components) the *Fisher information matrix* (FIM) approaches a block diagonal structure where the amplitude and phase parameters of each component appear in blocks. As the difference between the component IF signals decreases, the FIM approaches a singular matrix [15].

CHAPTER 3

ENERGY DEMODULATION OF MIXTURES FOR TWO–COMPONENT AM–FM SIGNAL DEMODULATION

3.1 Introduction

If $x(t)$ is a multicomponent AM–FM signal, then bandpass filtering is needed in the multiband–ESA [7] to isolate each component before applying the ESA. The bandpass filtering causes problems when the components have overlapping spectra. In this chapter, the *energy demodulation of mixtures* (EDM) algorithm for the demodulation of two-component AM–FM signals of the form

$$x(t) \;=\; A_1(t)\cos\left[\int_0^t \omega_1(\tau)d\tau + \theta_1\right] \;+\; A_2(t)\cos\left[\int_0^t \omega_2(\tau)d\tau + \theta_2\right] \tag{3.1}$$

is presented. The EDM algorithm uses nonlinear differential energy operators and the generating differential or difference equations pertaining to the composite signal to accomplish this task. The envisioned applications are in the areas of co–channel signal separation and demodulation and speech formant separation and demodulation. First, we exploit the structural properties of a mixture of two sinusoidal signals by treating the mixture signal as a solution to a generating differential or difference equation (GDE) [68]. The coefficients of the GDE are then expressed in terms of generalizations of the energy operator Ψ to higher orders [40], to achieve both component separation and demodulation of the components into IF and IA information signals.

The EDM algorithm is extended to the case where the composite signal is a complex two–component AM–FM signal and is then compared with the *instantaneous Toeplitz determinant* (ITD) algorithm developed in [29, 30] and with adaptive linear prediction implemented via the LMS as described in [17]. The EDM algorithm is finally applied to the problem of separating and demodulating two–component voice–modulated FM signals.

3.2 Continuous–Time Algorithm

The two–component AM–FM signal is modeled instantaneously by the two–component sinusoidal signal

$$x(t) = a_1 \cos(\omega_1 t + \theta_1) + a_2 \cos(\omega_2 t + \theta_2).$$

This mixture signal satisfies the following fourth-order GDE:

$$x^{(4)} + c_1 \ddot{x} + c_2 x = 0, \tag{3.2}$$

where

$$x^{(n)} = d^n x / dt^n$$

and

$$c_1 = (\omega_1^2 + \omega_2^2) \quad , \quad c_2 = \omega_1^2 \omega_2^2. \tag{3.3}$$

The k^{th}-order differential energy operator is defined as [40]

$$\Upsilon_k(x) \quad \triangleq \quad \dot{x} x^{(k-1)} - x x^{(k)}.$$

As a special case for $k = 2$, we obtain the Teager-Kaiser energy operator $\Upsilon_2 \equiv \Psi$. Second–order operators have dimensions of energy (per unit mass), third–order operators have dimensions of energy velocity, while fourth–order operators have dimensions of energy acceleration.

Using the GDE and its derivative and solving the resultant 2×2 linear system of equations yields the following expressions for the coefficients:

$$c_1 = -\frac{\Upsilon_5(x)}{\Upsilon_3(x)} \quad , \quad c_2 = \frac{\Upsilon_3(\ddot{x})}{\Upsilon_3(x)}. \tag{3.4}$$

Then, the EDM estimates for the frequencies ω_1 and ω_2 are computed as

$$\omega_{1,2} = \sqrt{\frac{c_1 \ \pm \ \sqrt{c_1^2 - 4c_2}}{2}}. \tag{3.5}$$

These frequency estimates are then used in conjunction with second–order energy operators to develop the EDM estimates for the amplitude as follows:

$$\Psi(x^{(3)}) - \omega_1^2\omega_2^2\Psi(\dot{x}) = (a_1^2\omega_1^6 - a_2^2\omega_2^6)(\omega_1^2 - \omega_2^2) \tag{3.6}$$

$$\Psi(\ddot{x}) - \omega_1^2\omega_2^2\Psi(x) = (a_1^2\omega_1^4 - a_2^2\omega_2^4)(\omega_1^2 - \omega_2^2) \tag{3.7}$$

$$a_{1,2}^2 = \frac{\omega_{2,1}^4(\Psi(x^{(3)}) - \omega_1^2\omega_2^2\Psi(\dot{x}))}{\omega_1^4\omega_2^4(\omega_1^2 - \omega_2^2)^2} - \frac{\omega_{2,1}^6(\Psi(\ddot{x}) - \omega_1^2\omega_2^2\Psi(x))}{\omega_1^4\omega_2^4(\omega_1^2 - \omega_2^2)^2}. \tag{3.8}$$

The GDE coefficients and hence the frequencies and amplitudes are time-invariant quantities for sinusoidal signals, but become slowly time-varying (lowpass) quantities for AM–FM signals.

3.3 Discrete–Time Algorithm

Discrete–time two–component AM–FM signals are modeled instantaneously as two–cosine signals:

$$x[n] = a_1 \cos(\Omega_1 n + \theta_1) + a_2 \cos(\Omega_2 n + \theta_2).$$

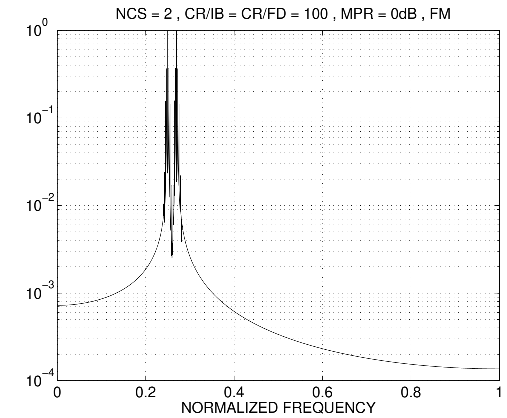

(a)

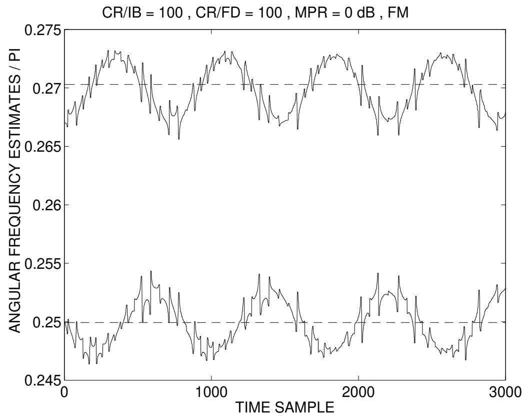

(b)

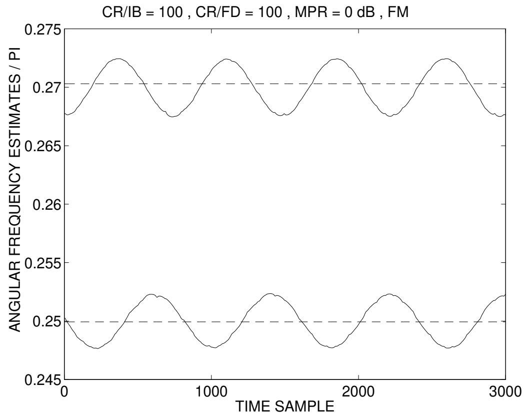

(c)

Figure 3.1: (a) Fourier spectral magnitude of mixture signal. (b) Angular frequency estimates of the EDM as fractions of π. (c) Frequency estimates of the SEDM, i.e. the estimates in (b) after post–smoothing. Solid lines correspond to estimates and the dashed–dotted lines are the carrier frequency estimates.

The mixture satisfies the following fourth-order generating difference equation

$$c_1(x[n-1]+x[n-3])+c_2x[n-2] \;=\; -(x[n]+x[n-4]), \tag{3.9}$$

where

$$c_1 \;=\; -2(\cos\Omega_1+\cos\Omega_2)\;\;,\;\; c_2 \;=\; 4\cos\Omega_1\cos\Omega_2+2. \tag{3.10}$$

By evaluating the GDE at time instants n and $n+1$ and solving the 2×2 linear system of equations, we obtain:

$$c_1 \;=\; \frac{\Upsilon_3(x[n-3])-\Upsilon_3(x[n-1])}{\Psi(x[n-1])-\Psi(x[n-2])} \tag{3.11}$$

$$c_2 \;=\; \frac{\Psi(x[n])-\Psi(x[n-3])}{\Psi(x[n-1])-\Psi(x[n-2])} \;+\; \frac{\Upsilon_4(x[n-2])-\Upsilon_4(x[n-3])}{\Psi(x[n-1])-\Psi(x[n-2])}, \tag{3.12}$$

where Υ_k is the k^{th}-order discrete-time energy operator defined in [40] as

$$\Upsilon_k(x[n]) \;\triangleq\; x[n]x[n+k-2]-x[n-1]x[n+k-1],$$

and Ψ is the discrete-time Teager-Kaiser energy operator [26, 27]:

$$\Psi(x[n]) = (x[n])^2 - x[n+1]x[n-1].$$

Note that for $k=2$ the discrete Υ_k becomes identical to the discrete Ψ. The discrete-time EDM frequency estimation algorithm is then given by

$$\Omega_{1,2} = \cos^{-1}\left(\frac{-c_1}{4} \;\pm\; \frac{\sqrt{c_1^2-4c_2+8}}{4}\right). \tag{3.13}$$

The corresponding EDM amplitude estimation algorithm involves the use of symmetric differences and second–order energy operators:

$$a_{1,2}^2 \;=\; \frac{S_{2,1}^4(\Psi({\Delta_s}^3x)-S_1^2S_2^2\Psi(\Delta_s x))}{S_1^4S_2^4(S_2^2-S_1^2)^2} \;-\; \frac{S_{2,1}^6(\Psi({\Delta_s}^2x)-S_1^2S_2^2\Psi(x))}{S_1^4S_2^4(S_2^2-S_1^2)^2}, \tag{3.14}$$

where $S_{1,2} = \sin(\Omega_{1,2})$, and

$$\Delta_s x = \frac{x[n+1] - x[n-1]}{2} \quad , \quad {\Delta_s}^m x = \Delta_s({\Delta_s}^{m-1} x).$$

Similar results for discrete frequency estimation have been obtained in [32] for two–component sinusoidal signals in the context of AR signal modeling. The novelties of the EDM estimation procedure in the discrete case are:

1) its application to demodulating two–component AM–FM signals;

2) the use of energy operators which give a physically meaningful interpretation to the solution; and

3) amplitude estimation via energy equations instead of estimation via the least–sqaures system in Eq. (2.4).

Finally, note that estimates of the two carrier frequencies and mean amplitudes can be obtained as the time averages of the estimated component IF and IA signals over the duration of the original signal.

As an example, consider a discrete-time mixture signal of two sinusoidally modulated and spectrally close FM signals:

$$\begin{aligned} x[n] &= \sum_{i=1}^{2} a_i \cos\left(\int_0^n \Omega_i[m] dm\right) \\ \Omega_i[n] &= \Omega_{ci} + \Omega_{mi} \cos(\Omega_{fi} n + \theta_i) \quad , \quad i = 1, 2 \quad , \end{aligned}$$

with parameters $\Omega_{ci} = \frac{\pi}{4}, \frac{\pi}{4} + \frac{\pi}{50}, \ \ \theta_i = 0, \pi, \ \ \Omega_{mi} = \Omega_{fi} = \frac{\Omega_{ci}}{100}$. Despite the significant amount of spectral overlap between the two components, as shown in Fig. 3.1(a), the EDM can recover important parts of the original frequency signals, as shown in Fig. 3.1(b), although with some error whose magnitude increases with the amount of spectral overlap. Post–smoothing after the EDM yields the *smoothed EDM* (SEDM) algorithm, which can suppress a significant amount of demodulation error as shown in Fig. 3.1(c). Post–smoothing involves moving-average filtering to remove beating at the carrier difference frequency, while 9-point median filtering is employed to remove spikes in the GDE coefficients.

3.4 Complex Version of the EDM

The complex version of the continuous EDM can be obtained in a manner similar to that of the real case by considering the complex form of the two–component sinusoidal signal

$$x(t) \;=\; a_1 \exp\left[j(\omega_1 t + \theta_1)\right] \;+\; a_2 \exp\left[j(\omega_2 t + \theta_2)\right].$$

the difference being that only a second–order GDE of the form

$$\ddot{x} \;+\; c_1 \dot{x} \;+\; c_2 x \;=\; 0 \;,\; \text{where}$$

$$c_1 \;=\; -j\left(\omega_1 + \omega_2\right) \;,\; c_2 \;=\; -\omega_1 \omega_2, \tag{3.15}$$

is needed to generate the complex two–component sinusoidal signal. Consequently only smaller order derivatives are needed which provides more immunity towards noise. The GDE coefficients of the signal are obtained as ratios of higher–order energy measurements on the signal and its first derivative

$$c_1 \;=\; -\frac{\Upsilon_3(\dot{x})}{\Upsilon_2(x)} \;\;,\;\; c_2 \;=\; \frac{\Upsilon_2(\dot{x})}{\Upsilon_2(x)}. \tag{3.16}$$

The frequencies in the stationary sinusoidal case and the IF information signals of the components in the AM–FM signal case are then computed from the GDE coefficients as

$$\omega_{1,2} \;=\; \frac{1}{2j}\left(-c_1 \;\pm\; \sqrt{c_1^2 - 4c_2}\right). \tag{3.17}$$

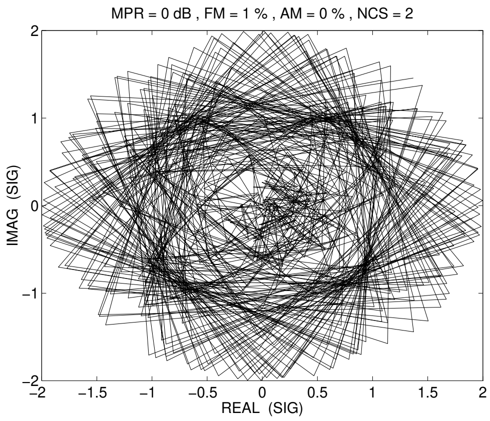

(a)

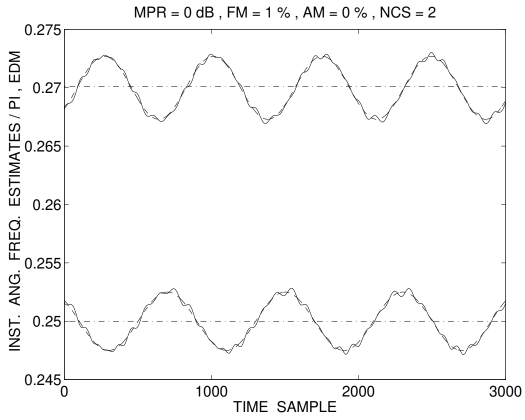

(b)

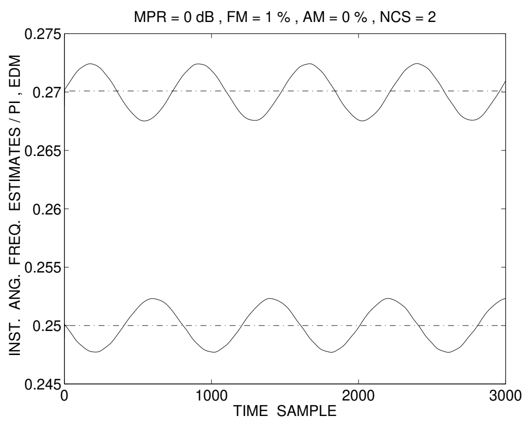

(c)

Figure 3.2: Complex EDM: (a) composite signal, (b) angular IF estimates of the complex EDM (as fractions of π) and (c) IF estimates after post–smoothing. Sinusoidal modulation parameters of the composite signal are identical to those in the real example. Solid lines are estimates, dashed lines are the actual quantities and the dashed-dotted lines are the carrier frequency estimates.

As in the continuous–time case, the discrete–time two–component complex sinusoidal signal only needs a second–order GDE of the form:

$$x[n] \;+\; c_1 x[n-1] \;+\; c_2 x[n-2] \;=\; 0. \tag{3.18}$$

The expressions for the GDE coefficients in this case involve the use of discrete–time higher–order energy operators applied on shifted versions of the signal

$$c_1 \;=\; -\frac{\Upsilon_3(x[n-2])}{\Upsilon_2(x[n-2])} \;\;,\;\; c_2 \;=\; \frac{\Upsilon_2(x[n-1])}{\Upsilon_2(x[n-2])}. \tag{3.19}$$

The component IF signals are then evaluated from the GDE coefficients as

$$\Omega_{1,2} \;=\; \mathrm{Arg}\left(\frac{-c_1 \;\pm\; \sqrt{c_1^2 - 4c_2}}{2}\right). \tag{3.20}$$

As an example, consider the complex version of the FM signal from the real example shown in Fig. 3.2(a). The angular frequency estimates of the complex EDM are shown in Fig. 3.2(b) and the estimates after post–smoothing with median and moving–average filters are shown in Fig. 3.2(c). Despite the significant spectral overlap between the components, the EDM algorithm is able to accomplish simultaneous component separation and demodulation.

3.5 Performance of the EDM

When (the NCS parameter decreases and) the spectral overlap between the components increases beyond a limit (NCS $<$ 1), the energy equations of the EDM become ill-conditioned and finally singular (NCS $=$ 0). This is described in the case of the unmodulated sine mixture by

$$\Upsilon_3(x) = 0 \quad , \quad \Psi(x[n-1]) - \Psi(x[n-2]) = 0, \tag{3.21}$$

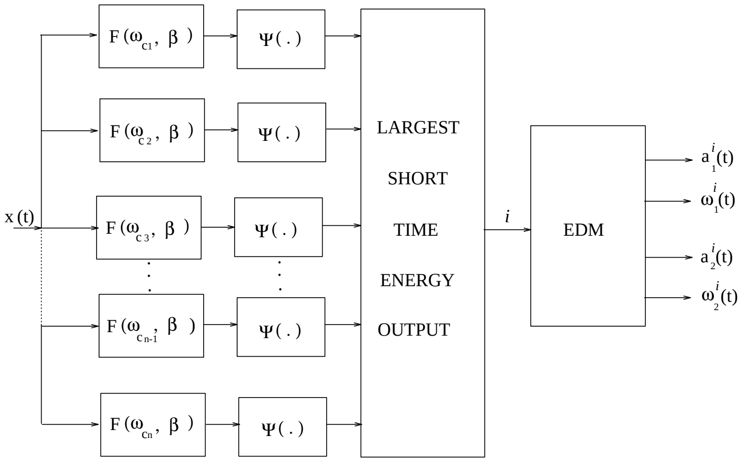

Figure 3.3: Block diagram of the multiband–EDM algorithm

---

resulting in an increase in the demodulation error. As the CR/IB parameter increases, the FM mixture approaches a stationary sinusoidal mixture, resulting in a decrease in the demodulation error as shown in Fig. 3.4(a). The CR/FD parameter measures the strength of signal modulations. As the CR/FD parameter increases, the strengths of the modulations in the components decrease. As the MPR increases, the strength of the first component in the mixture increases and that of the second component decreases. For large MPR parameters, the stronger component dominates the mixture, resulting in a decrease in the amplitude demodulation error of the stronger component, while that of the weaker one rapidly increases as described in Fig. 3.4(c). The EDM frequency estimator on the other hand is derived from the GDE of the composite signal invariant to amplitudes [68], and, consequently, frequency demodulation is independent of MPR as shown by Fig. 3.4(b).

In situations where the signal of interest is corrupted with *additive white Gaussian noise* (AWGN), the EDM is used in conjunction with the multiband filtering scheme proposed in [7]. Namely, in what is called the *multiband–EDM* (MEDM) shown in Fig. 3.3, the mixture signal is first filtered through a bank of Gabor or

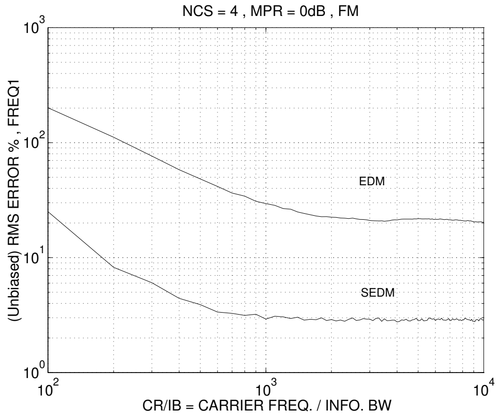

(a)

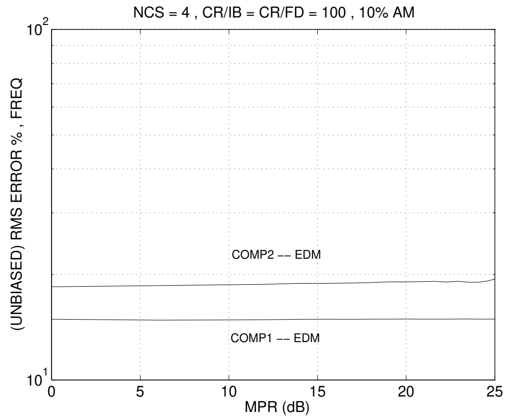

(b)

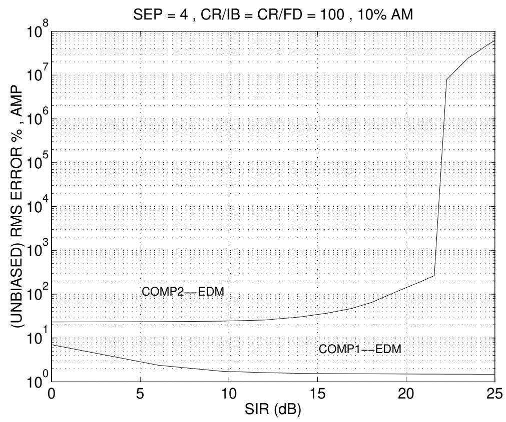

(c)

Figure 3.4: (a) Effect of CR/IB on EDM frequency demodulation obtained by averaging over FM modulation indices $\in \{0.1 - 1\}\%$. (b,c) Effect of MPR on EDM frequency and amplitude demodulation.

linear–phase FIR filters (designed using the Kaiser window design method or the Parks–McClellan algorithm [46]) that sample the frequency domain densely. The multiband filters are designed to achieve the optimal tradeoff between the tasks of minimizing the distortion to the composite signal and noise suppression. An energy detector [7] determines the channel that is most active, i.e., the channel that has the largest mean short-time energy operator output. The output of this channel is then used for demodulation via the EDM, while the outputs of all the other less active channels are discarded. Unlike the multiband ESA [7] where multiband filtering for both component separation and noise rejection purposes, in the MEDM case multiband filtering is used just for the purpose of noise suppression.

3.6 Comparisons

Although the EDM, the modified ITD [30], and the LMS [17] algorithms have a common goal of demodulating two–component AM–FM signals, they differ in terms of their nature, their complexity, their time resolution, and noise suppression capabilities. The EDM, the ITD, and (4th–order) adaptive linear prediction via the LMS are all based on estimating the coefficients of the GDE of the composite signal. The EDM algorithm uses higher-order energy operators to instantaneously estimate the coefficients, the ITD uses instantaneous operators obtained as determinants of 4×4 Toeplitz matrices to perform this task, while the LMS uses signal correlations to estimate the coefficients in a least squares and adaptive sense.

The ITD and the LMS algorithms as implemented in [17, 30] require the computation of 4 or more GDE coefficients. The LMS algorithm also requires extensive optimization of several parameters such as the step size μ and filter order P. The

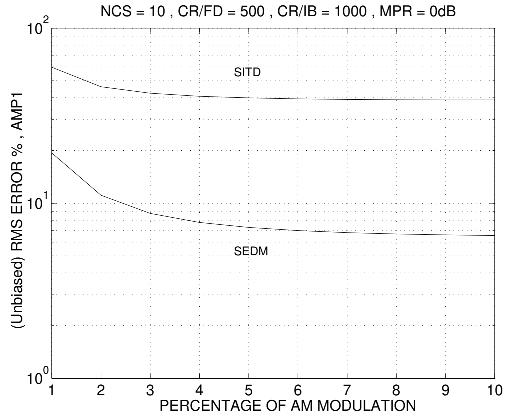

(a)

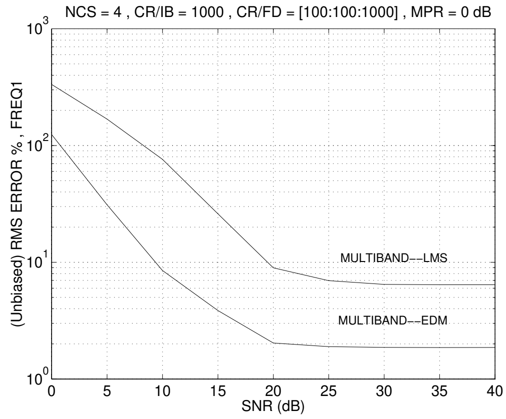

(b)

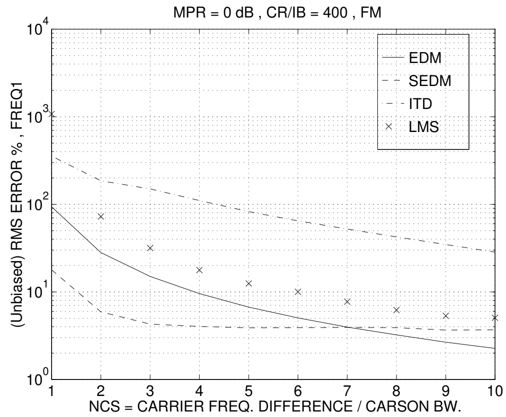

(c)

Figure 3.5: (a) Comparison of amplitude demodulation between the SEDM and the SITD for different AM percentages. (b) Effect of SNR on the performance of the multiband–EDM (MEDM) and the multiband–LMS (MLMS) (averaged over various CR/FD). (c) Effect of spectral separation on the performance of the EDM, the ITD and the LMS (averaged over FM modulation indices $\in \{0.1 - 1\}\%$).

EDM algorithm exploits the inherent symmetry of the problem requiring computation of only two GDE coefficients and does not require extensive optimization of parameters.

The time resolution of the ITD is governed by the assumption that the GDE coefficients are stationary over four time–steps. The time resolution and the length of the transients in the LMS estimates are governed by the order of the predictor and the step size parameter. The EDM algorithm is nonadaptive, does not exhibit transients in the estimates and requires the GDE coefficients stationary over two time–steps, thereby enabling better tracking of the instantaneous frequencies and amplitudes of two–component AM–FM signals.

The amplitude estimation section of both the ITD and the LMS algorithm involves the integration of the component IF estimates and the least–squares solution to a system of linear equations in terms of the amplitudes and phase offsets to smooth out the noise accumulated during the integration of the IF signals. These factors coupled with non-ideal linear filtering of the FM signal in the ITD[5] contribute to a larger amplitude estimation error in the ITD and the LMS algorithms as compared to the EDM algorithm as evident in Fig. 3.5(a) for different AM percentages.

The MEDM is used for demodulation of noisy signals, where the filters are optimized for minimum harmonic distortion. For small SNR parameters, filters with small bandwidths are needed, while for large SNR parameters, filters with larger bandwidths are more appropriate. Noise suppression in the multiband–EDM is achieved by picking the most energetic of the channels and discarding all the other less active channels. The comparison of MEDM with the MLMS) (LMS in conjunction with

[5]Energy equations applied to the output of a linear filter hold approximately only if the frequency response is narrow and flat in its passband [7].

multiband filtering) for different SNR parameters is depicted in Fig. 3.5(b).

As the NCS parameter decreases, the EDM and the ITD develop singularities which manifest as beating in the estimates, while the LMS coefficients develop convergence problems. For smaller separations, the beating in the EDM and the ITD intensifies and swamps the information signals, while the LMS coefficients do not converge even for large step sizes. The comparison of the algorithms for different NCS parameters is shown in Fig. 3.5(c).

3.7 FM–Voice Experiments

An important application of multicomponent AM–FM demodulation is in the area of separation and demodulation of two–component, co–channel and voice–modulated FM signals. In this section, the energy demodulation techniques (EDM, ESA) are applied on two–component voice–modulated FM signals. The results so obtained and the problems encountered are then analyzed in the context of the general co–channel signal separation problem. To obtain two voice–message signals the ESA was first used to extract them from their FM form at a higher sampling rate (400 kHz). With these message signals a two–component FM signal with specified FM modulation index, carrier frequencies, and equal amplitudes was then created.

3.7.1 EDM Applied to FM–Voice Signals

The first set of experiments pertain to the EDM algorithm. The EDM is applied on the equal amplitude two–component voice–modulated FM mixture for different NCS parameters of $\{400, 200, 100, 50, 33, 25, 17\}\%$ respectively. The normalization factor for the computation of the NCS parameter here is, however, not the Carson

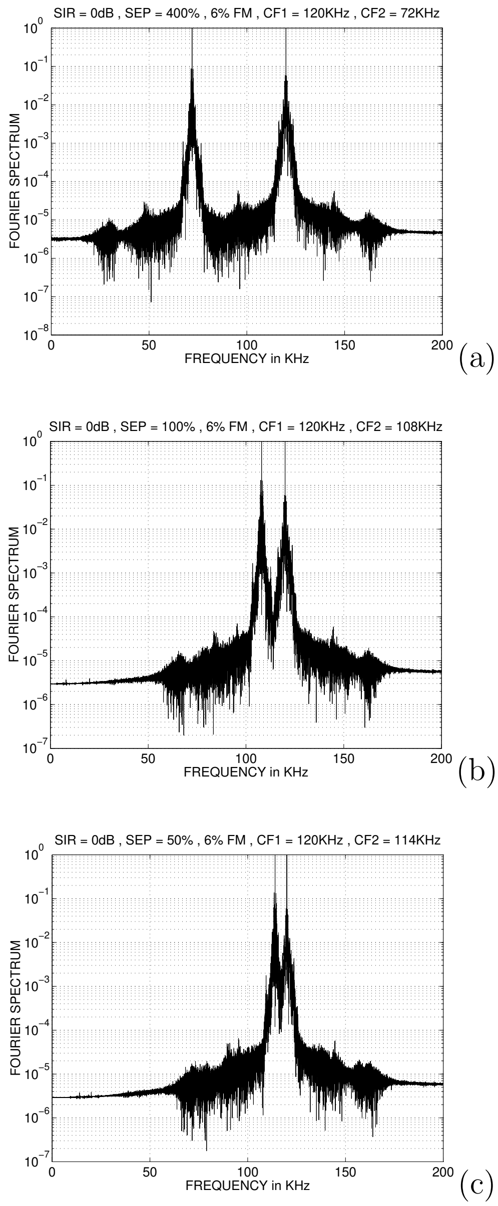

Figure 3.6: Fourier spectrum of the composite signal in the EDM–related voice experiments for carrier separations of $\{400, 100, 50\}\%$.

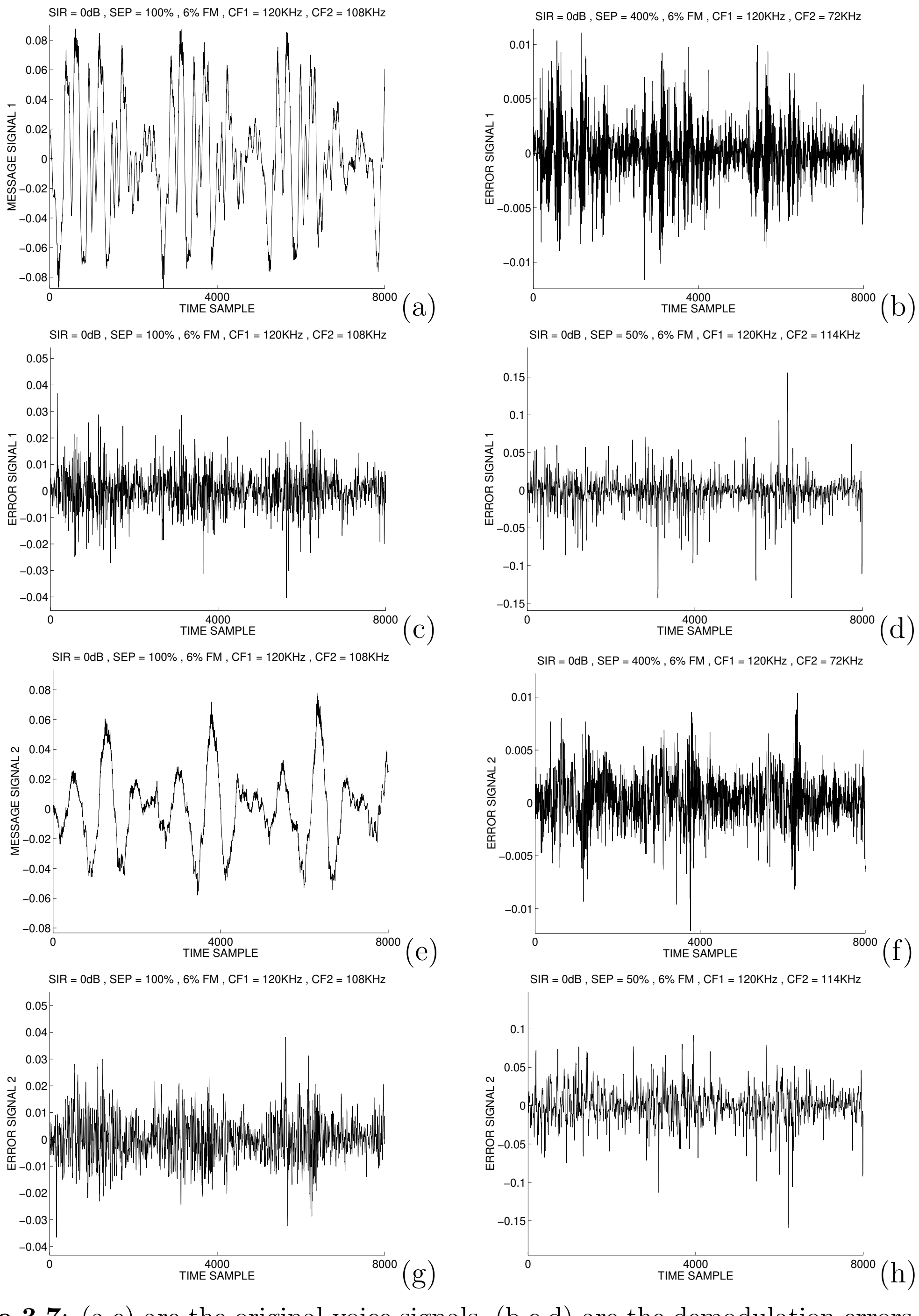

Figure 3.7: (a,e) are the original voice signals, (b,c,d) are the demodulation errors for the first signal component at normalized carrier separations of $\{400, 100, 50\}$ % and (f,g,h) are the estimation errors for the second signal component at normalized carrier separations of $\{400, 100, 50\}$ % for the EDM–related voice experiments.

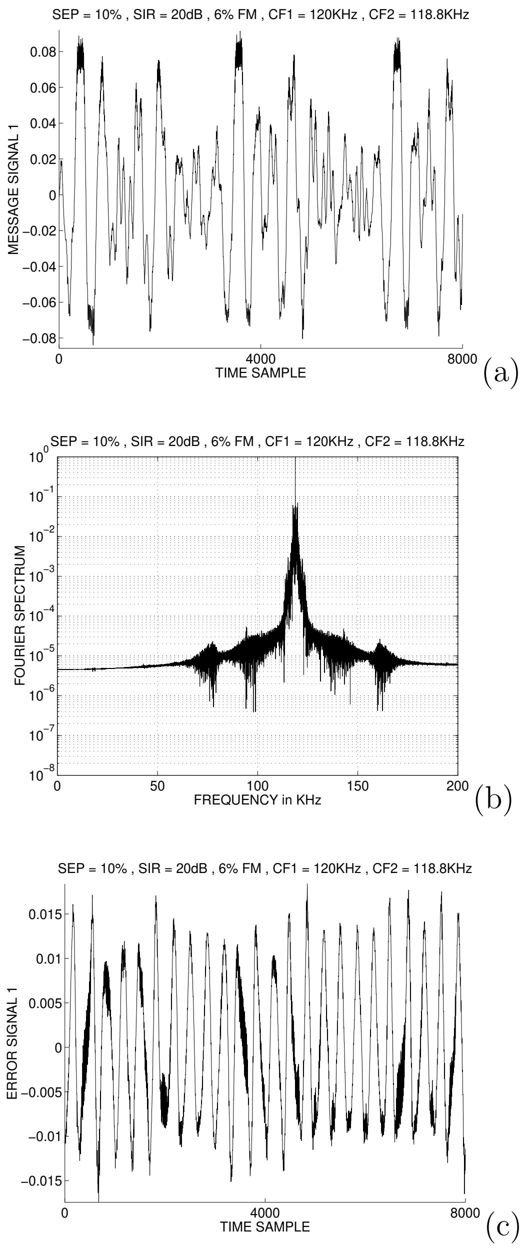

Figure 3.8: (a) Original voice signal (strong component), (b) Fourier spectrum of composite signal and (c) error signal of the FM voice experiment for a normalized carrier separation of 10 % and an MPR of 20 dB, depicting the capability of the ESA to capture the strong component.

bandwidth of the signal but the *radio frequency* (RF) bandwidth of the components which was approximately 12 kHz. The sampling rate used was 400 kHz. The following observations can be made from the experiments:

- For large carrier separations, the EDM produces clean and highly intelligible estimates of the message signals and the interference is not audible. The error signals are much smaller in magnitude as compared with the original message signals.

- For carrier separations larger than 100%, the components do not overlap spectrally. For a separation of 100%, the components are touching each other. For separations smaller than 100%, the signals overlap spectrally.

- For carrier separations of $\{50, 33\}$%, the interference can be heard, but the signals are clearly intelligible and audible. The error signals grow in magnitude as the separation decreases.

- For 25% carrier separation, the interference is audible, while the message signals are still intelligible. For 17% carrier separation, the interference dominates and the message signals are weaker.

Figures 3.6 (a,b,c) are the Fourier spectra of the composite signal for normalized carrier separation of $\{400, 100, 50\}$%. Figures 3.7(a,b,c,d) correspond to the first message signal and demodulation errors for $\{400, 100, 50\}$%. Figures 3.7(e,f,g,h) correspond to the second message signal and demodulation errors for $\{400, 100, 50\}$%. From the FM–voice experiments with the EDM algorithm and from the comparison of the EDM algorithm with the other algorithms using sinusoidally–modeulated two–component AM–FM signals, it becomes clear that when the components are well separated the

EDM algorithm provides a more efficient and simpler alternative to the other demodulation approaches. Although the interference is audible for smaller carrier separations, the EDM algorithm is able to provide intelligible message estimates for both voice signals right down to carrier separations of 25% of the RF bandwidth of the components. For carrier separations separations smaller than this, the interaction between the components overpowers the message signals that are no longer intelligible [4].

3.7.2 ESA Applied to FM–Voice Signals

Consider the specific case where one of the components of this mixture is much stronger than the other, i.e., for MPR $>$ 15 dB. Although the interaction between the component signals is intense when the carriers frequencies are close and the signals are of equal amplitude, for this range of MPR parameters, the two–component mixture starts to resemble a monocomponent signal dominated by the stronger component. In this case, monocomponent demodulation algorithms like the ESA have the capability to capture the stronger component of a co–channel mixture. In this section, the the ESA is applied to the two–component mixture to demonstrate its capability of capturing the stronger signal under co–channel conditions when one component is much stronger than the other. For MPR's greater than 15 dB, the ESA returns an estimate of the message signal corresponding to the stronger component with less than 10% NRMSE. Figure 3.8(a,b,c) describes: (a) the message signal corresponding to the stronger component, (b) the Fourier spectrum of the composite signal, and (c) the demodulation error incurred in estimating the stronger component for a two–component FM signal with a MPR of 20 dB and a NCS of 10 % at 6 % FM.

CHAPTER 4

MULTICOMPONENT AM–FM SIGNAL AND CO–CHANNEL DEMODULATION USING PERIODIC ALGEBRAIC SEPARATION AND ENERGY DEMODULATION

4.1 Introduction

In contrast to the monocomponent case, all the multicomponent AM–FM demodulation algorithms discussed in Chapter 2 and the EDM algorithm discussed in Chapter 3 are still far from a general solution, work only in restricted ranges of spectral separation between components or relative amplitude/power ratios, and cannot deal with cross–over of the component IF tracks. In this chapter, a solution to the general multicomponent AM–FM demodulation problem is presented that greatly improves upon the above mentioned situation.

The new approach presented in this chapter divides the problem into two independent tasks of separation of components and then monocomponent demodulation

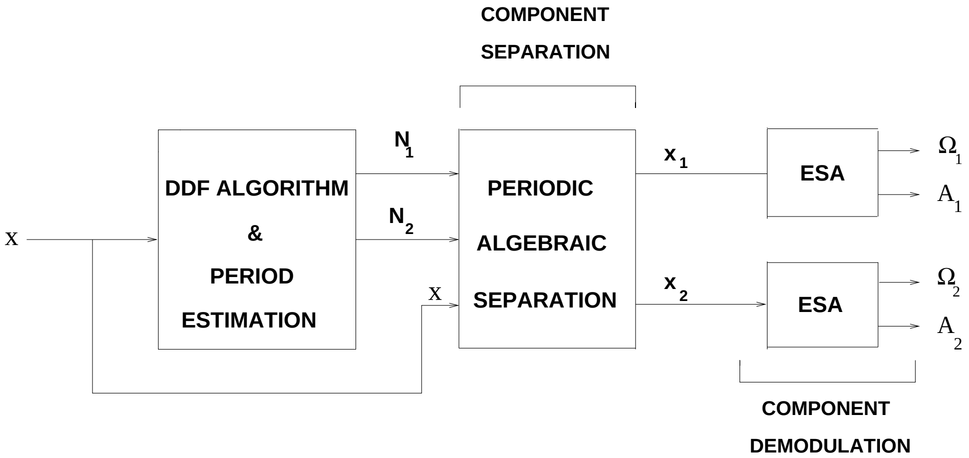

Figure 4.1: Block diagram of the PASED Algorithm

of each component, so that problems in one task do not cascade into the other. For solving the separation task, the algebraic separation technique proposed in [44, 45] is used for the separation of spectrally overlapping periodic signals. Specifically, this algebraic separation technique is extended to multicomponent AM–FM signals with periodic IF and IA information signals. For the monocomponent demodulation, the energy-based method of ESA [38] is used due to its efficiency, low complexity, and excellent time resolution. This combined new approach called the *periodic algebraic separation energy demodulation* (PASED) algorithm does not have the shortcomings of the other techniques, can deal with extremely small spectral separations and a wide range of relative amplitude/power ratios [5, 58], and is able to handle the extreme case where the component IF tracks cross–over. The performance of the PASED algorithm is then evaluated by applying the algorithm to the FM–voice separation and demodulation problem described in Chapter 3.

4.2 Periodic Algebraic Separation Energy Demodulation (PASED) Algorithm

The operation of the PASED algorithm, whose block diagram is shown in Fig. 4.1, can be divided into two tasks: (a) separation of the two–component AM–FM signal into components using periodicity–based signal modeling and algebraic separation techniques described in [44, 45] and (b) demodulation of the separated components into IF and IA information signals for each component using the energy operator based *energy separation algorithm* (ESA) [37, 38, 39].

4.2.1 Periodicity–Based Modeling and Algebraic Separation of the Components

The *matrix algebraic separation* (MAS) algorithm for the separation of periodic signals that overlap both in the time and frequency domain has recently been investigated in [44, 45]. The MAS algorithm distinguishes the components based on a slight difference in their periodicity. Consider a two–component periodic signal

$$x[n] \;=\; x_1[n] \;+\; x_2[n] \;=\; x_1[n+N_1] \;+\; x_2[n+N_2], \qquad (4.1)$$

where the fundamental periods of the components $x_1[n]$ and $x_2[n]$ are N_1 and N_2 respectively. Relating N samples of the composite signal $x[n]$ to the samples of one fundamental period of the components yields the following system of linear equations,

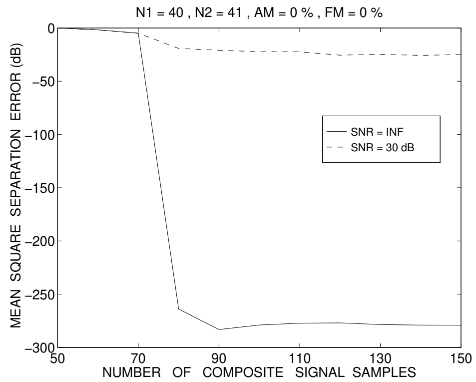

Figure 4.2: (a) Effect of least–squares order in the noise free case and when the SNR is 30 dB.

---

hereafter referred to as the *basic separation system*

$$\underbrace{\begin{pmatrix} x[0] \\ x[1] \\ \vdots \\ x(N-1) \end{pmatrix}}_{\mathbf{x}} = \underbrace{\begin{pmatrix} \mathbf{I}_{N_1} & \mathbf{I}_{N_2} \\ \mathbf{I}_{N_1} & \mathbf{I}_{N_2} \\ \vdots & \vdots \end{pmatrix}}_{\mathbf{S}} \underbrace{\begin{pmatrix} x_1[0] \\ \vdots \\ x_1[N_1-1] \\ x_2[0] \\ \vdots \\ x_2[N_2-1] \end{pmatrix}}_{\mathbf{z}}, \tag{4.2}$$

where $\mathbf{I}_{N_1}$ denotes the identity matrix of order N_1 and the rank of the two–component separation matrix $\mathbf{S}$ is $r(\mathbf{S}) = N_1 + N_2 - \gcd(N_1, N_2)$ [44, 45]. Consequently, the basic separation system requires a minimum of $N_1 + N_2 - 1$ composite signal samples to separate the components. In the absence of noise, least–squares filtering is not required and increasing the number of composite signal samples over this minimum does not help as shown in Fig. 4.2. In the presence of noise however, least–squares smoothing is necessary and increasing the number of samples used decreases the separation error as shown in Fig. 4.2.

The basic separation system is not of full rank and, hence, not invertible. The rank of this system even in the case where the periods are coprime implies that one extra equation is required to complete it [6] which is typically a dc value condition of the form [5, 58]

$$\sum_{n=0}^{N_1-1} x_1[n] \quad = \quad 0. \tag{4.3}$$

The dc value constraint corresponds to the assumption that the signal components are narrowband and bandpass.

The solution to the separation problem when the periods of the components are not coprime involves solving the separation system in partial subgroups. Suppose that the $\gcd(N_1, N_2) = R$, so that $N_1 = RN_1^{'}$, $N_2 = RN_2^{'}$ and $N_{1,2}^{'}$ are mutually prime. The data is taken in subgroups (downsampling by a factor of R). The separation problem is then solvable for each subgroup, since the smaller periods are coprime. The union of the solutions from each group gives the total solution to the separation problem [44, 45]. The R additional constraints that are needed to solve the separation system are obtained as zero dc conditions of the subsampled signals (by a factor of R).

$$\sum_{j=0}^{N_1^{'}-1} x_1[Rj+i] \quad = \quad 0 \quad , \quad i = 0, 1, \ldots, (R-1). \tag{4.4}$$

The solution to the component separation problem is then reformulated as the least–squares solution to the augmented linear system, hereafter referred to as the *augmented separation system*

$$\underbrace{\begin{pmatrix} \mathbf{S} \\ \mathbf{C} \end{pmatrix}}_{\tilde{\mathbf{S}}} \mathbf{z} \quad = \quad \underbrace{\begin{pmatrix} \mathbf{x} \\ \mathbf{0} \end{pmatrix}}_{\tilde{\mathbf{x}}}, \tag{4.5}$$

[6]The solution to the separation system: $\mathbf{S}\,\mathbf{z} \;=\; \mathbf{x}$, is not unique in the sense that if $\{x_1[n]\ ,\ x_2[n]\}$ is a solution to the system then $\{x_1[n] + c\ ,\ x_2[n] - c\}$ is also a solution as observed in [44, 45].

where the dc value constraints (homogeneous) at the scale of R form the constraint matrix $\mathbf{C}$. The equivalent quadratic minimization problem is

$$\min_{\mathbf{z}} \quad ||\mathbf{S}\mathbf{z} - \mathbf{x}||^2 \; + \; ||\mathbf{C}\mathbf{z}||^2.$$

The augmented separation system which is now complete is inverted via the least–squares technique to yield the following solution [5, 58]

$$\hat{\mathbf{z}} \;=\; \tilde{\mathbf{S}}^{\dagger}\tilde{\mathbf{x}} \;=\; \left(\tilde{\mathbf{S}}^T\tilde{\mathbf{S}}\right)^{-1}\left(\tilde{\mathbf{S}}^T\tilde{\mathbf{x}}\right) \;=\; \left(\mathbf{S}^T\mathbf{S} \;+\; \mathbf{C}^T\mathbf{C}\right)^{-1}\left(\mathbf{S}^T\mathbf{x}\right). \tag{4.6}$$

The effective separation system for each of the components can be rewritten as:

$$\begin{aligned} \mathbf{x}_1 &= \left\{[\mathbf{I}_{N_1\times N_1}\;\mathbf{0}_{N_1\times N_2}]\left(\mathbf{S}^T\mathbf{S} \;+\; \mathbf{C}^T\mathbf{C}\right)^{-1}\mathbf{S}^T\right\}(\mathbf{x}) \;=\; \mathbf{S}_1^{\dagger}\,(\mathbf{x}) \\ \mathbf{x}_2 &= \left\{[\mathbf{0}_{N_2\times N_1}\;\mathbf{I}_{N_2\times N_2}]\left(\mathbf{S}^T\mathbf{S} \;+\; \mathbf{C}^T\mathbf{C}\right)^{-1}\mathbf{S}^T\right\}(\mathbf{x}) \;=\; \mathbf{S}_2^{\dagger}\,(\mathbf{x}), \end{aligned} \tag{4.7}$$

where the the notation $\mathbf{S}^T$ stands for the matrix transpose of the matrix $\mathbf{S}$, $\tilde{\mathbf{S}}^{\dagger}$ stands for the least–squares left–inverse of the matrix $\tilde{\mathbf{S}}$ and $\mathbf{S}_1^{\dagger}$, $\mathbf{S}_2^{\dagger}$ are the effective MAS algorithm inverse systems for each component. Note that the ordering of the components and the association of the components with their corresponding periodicities is ambiguous due to the associative property of the superposition. The block nature of the basic separation system allows the MAS algorithm to be easily extendible to the case where there are more than two periodic components [5, 58].

4.2.2 Energy Demodulation of the Components

The separated components are then demodulated into IF and IA information signals using the *discrete energy separation algorithms* (DESA's) [37, 38, 39]. Although in essence other monocomponent demodulation algorithms could have been used for demodulation, the DESA is employed here on account of its simplicity, its efficiency, and its excellent instantaneous–adapting nature [38]. Further, the ESA has many advantages over the classic analytic signal and Hilbert transform approach; detailed comparisons between these algorithms can be found in [51]. Assuming that the separated signal components $x_i[n]$ remain stationary at least over 4-5 consecutive samples, they can be instantaneously modeled as discrete–time monocomponent AM–FM signals of the form

$$x_i[n] \;=\; A_i[n]\cos\left(\int_0^n \Omega_i[k]dk + \theta_i\right)\;,\; i \;=\; 1, 2, \ldots, M.$$

The IF and IA information signals corresponding to each separated component signal is then estimated via the the DESA-1 algorithm [38, 39], where the the discrete–time Teager–Kaiser energy operator

$$\Psi(x[n]) \;=\; x^2[n] \;-\; x[n+1]x[n-1],$$

is applied to the components $x_i[n]$ and their discrete–time derivative
$y_i[n] = x_i[n] - x_i[n-1]$

$$\begin{aligned} \text{Freq} : \hat{\Omega}_i[n] \;&=\; \arccos\left(1 - \frac{\Psi(y_i[n]) + \Psi(y_i[n+1])}{4\Psi(x_i[n])}\right) \\ \text{Env} : |\hat{A}_i[n]| \;&=\; \sqrt{\frac{\Psi[x_i[n]]}{\sin^2(\hat{\Omega}_i)}}. \end{aligned} \tag{4.8}$$

The carrier frequency and mean amplitudes of each component can then be estimated from the mean of IF and IA estimates over the duration of the signal as

$$\begin{aligned} \text{Carrier freq} : \hat{\Omega}_{ci} \;&=\; \frac{1}{N}\sum_{n\,=\,0}^{N-1}\hat{\Omega}_i[n] \\ \text{Mean amp} : \hat{A}_i \;&=\; \frac{1}{N}\sum_{n\,=\,0}^{N-1}|A_i[n]|. \end{aligned} \tag{4.9}$$

In [51] smoothing of the energy signals used in the ESA was recommended before the frequency estimation to reduce the high-frequency component of the error in the time-varying case. The smoothing was done via simple short FIR filters with binomial coefficients. This is called the *smoothed ESA* (SESA), and in its simplest form involves a 3-point 1,2,1 smoothing filter. The SESA can generally provide about 50% reduction in the estimation errors of the ESA when used for AM-FM demodulation [51].

4.3 Two–component AM–FM Signals

In general, for applying the PASED algorithm to two–component AM–FM signals, the components are modeled as quasi-periodic signals. Specifically, when the two IF and IA signals are sinusoidal, the quantities $L_i = \mathrm{lcm}\left(\frac{2\pi}{\Omega_{fi}}, \frac{2\pi}{\Omega_{ai}}\right)$, where the quantities $\left(\frac{\Omega_{ci}}{\Omega_{fi}}\right)$ are constrained to be integers, play the roles of the periods. For the specific case when $\Omega_{fi} = \Omega_{ai}$ (as in all the examples in this chapter), this expression reduces $L_i = \frac{2\pi}{\Omega_{fi}}$. The case where the IF signals are not sinusoidal is addressed later in the section. As an example, consider a two–component sinusoidally modulated AM–FM signal described by the composite signal in Fig. 4.3(a). The demodulation lengths of the two components were $L_1 = 200$ and $L_2 = 201$ samples and these lengths are mutually prime. Since we are dealing with narrowband bandpass components, the dc value of the first component can be approximated as zero. The IF estimates of the PASED algorithm are shown in Fig. 4.3(b), while the IA estimates of the proposed algorithm are shown in Fig. 4.3(c)

If the periods of the components are not coprime then more dc value constraints have to be used to complete the basic separation system. The angular frequency estimates and the IA estimates of the PASED algorithm for the example whose signal environment is described in Fig. 4.4(a) are shown in Fig. 4.4(b,c). The demodulation lengths of the components in this case are $L_1 = 400$ and $L_2 = 402$ samples

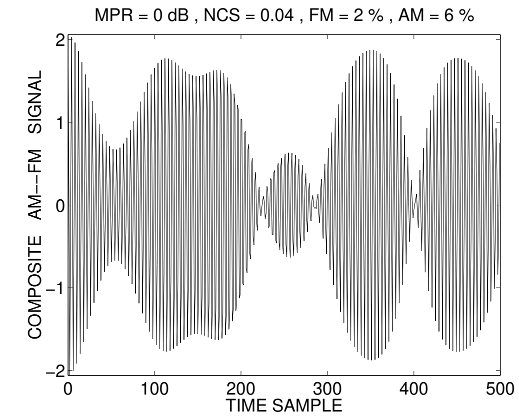

(a)

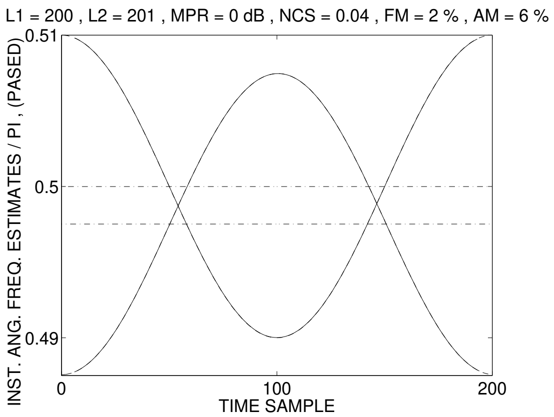

(b)

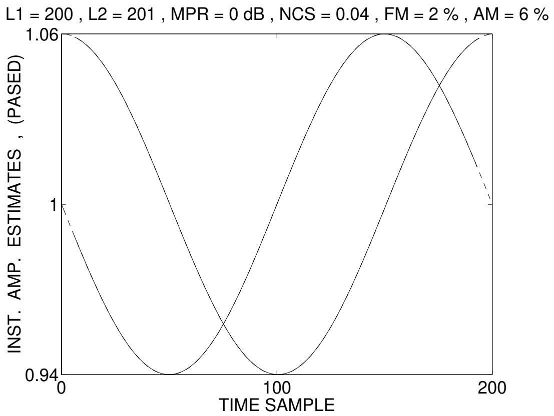

(c)

Figure 4.3: Sinusoidal AM–FM : (a) composite AM–FM signal, (b) IF and carrier estimates (dashed–dotted) of the PASED algorithm (as fractions of π), (c) IA estimates of the PASED algorithm, where solid lines indicate estimates and dashed lines indicate actual quantities. The IF signals are sinusoidal with $\approx 2\%$ FM, 4 % NCS and coprime periods. The IA signals are also sinusoidal with 6% AM and a MPR of 0 dB

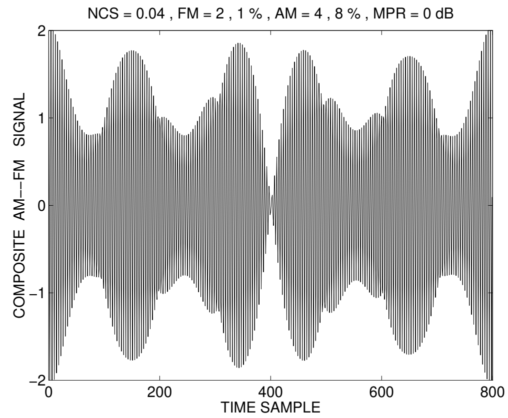

(a)

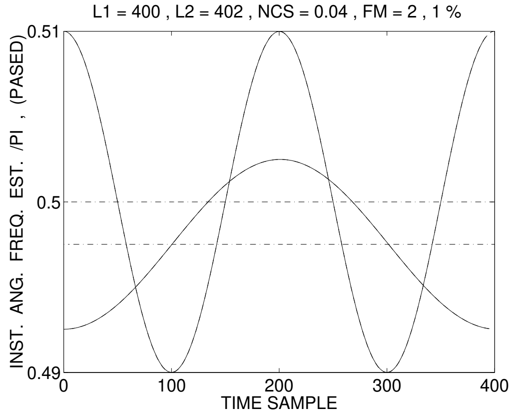

(b)

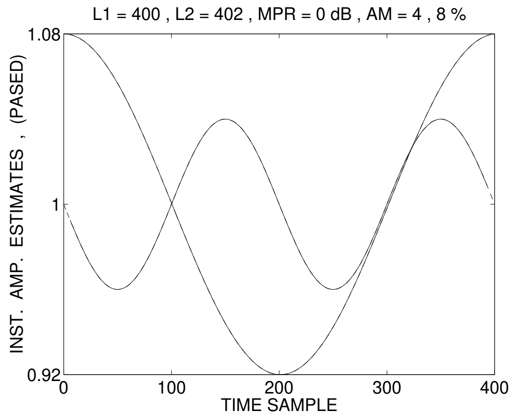

(c)

Figure 4.4: Non–coprime periods: (a) composite AM–FM signal, (b) angular frequency estimates of PASED algorithm (as fractions of π) and (c) IA estimates of the PASED algorithm, where estimates are solid lines, actual quantities are in dashed lines and carrier frequency estimates are in dashed–dotted lines. The IF signals are sinusoidal with 2 , 1 % FM respectively with 4 % NCS and noncoprime periods. The IA signals are also sinusoidal with 4 , 8 % AM and a MPR of 0 dB

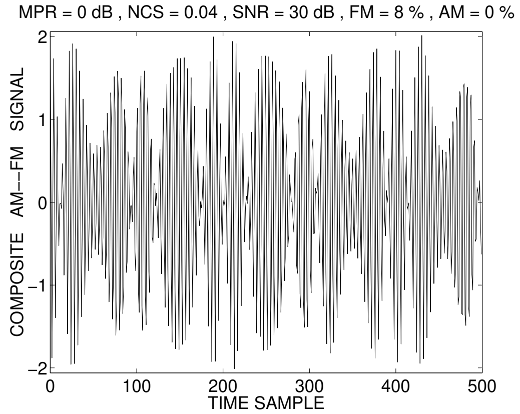

(a)

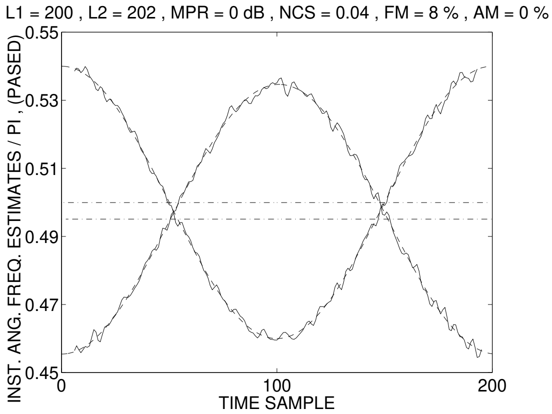

(b)

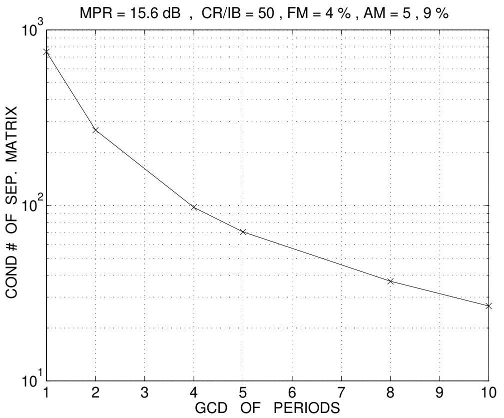

(c)

Figure 4.5: Noisy example: (a) composite signal and the (b) angular frequency estimates (as fractions of π). The SNR of the signal mixture is 30 dB. 4-time binomial smoothing was used for smoothing the energy signals in the ESA. The IF signals are sinusoidal with $\approx$ 8% FM, with 4 % NCS and with periods that have a gcd of 2. (c) Effect of the gcd of the periods on the conditioning of the augmented separation system as measured by its condition number.

respectively. As shown in Figs. 4.3 and 4.4, the frequency and amplitude demodulation errors of PASED algorithm are negligible since the estimated signals are almost indistinguishable from the originals even when the carriers are very close and the frequency tracks cross–over.

For AM–FM signals in noise, the de-noising capability of the least–squares system in Eq. (4.5) enables simultaneous smoothing and component separation. The noisy–FM composite signal (SNR = 30 dB) is shown in Fig. 4.5(a). The energy signals in the ESA are further smoothed using a 4–time application of binomial smoothing. The de-noising capability of the PASED algorithm enables achievement of both component separation and noise suppression simultaneously. The angular frequency estimates of the PASED algorithm (as fractions of π) are shown in Fig. 4.5(b). The conditioning or the condition number (ratio of the maximum nonzero singular value to the minimum nonzero singular value of the augmented separation matrix) of the augmented separation system of the PASED algorithm improves with the increase in the gcd of the demodulation lengths as described in Fig. 4.5(c) and makes the system more robust to the addition of noise. The carrier–unbiased frequency demodulation errors for the two components are 4 & 3.85 %. The strength of the signal modulations can be increased to combat the presence of noise, but increase beyond a certain strength will produce more demodulation error due to loss of stationary behavior.

Since the separation system in the PASED algorithm only assumes periodicity of the components, it is not affected if the signal of interest is complex–valued. The PASED algorithm can therefore be used on complex data without much change. Once the components have been separated using algebraic separation techniques, the real or the imaginary part of the separated components can be used for demodulation via the ESA. Consider for example, sinusoidally modulated complex AM–FM signals of the form

$$x[n] = \exp\left(j\left[\int_0^n \Omega_1[m]dm \ + \ \theta_1\right]\right) + \exp\left(j\left[\int_0^n \Omega_2[m]dm + \theta_2\right]\right).$$

The modulation parameters of the signal are identical to that of the noise–free case the difference being that the signal components are complex. The composite signal is described in Fig. 4.6(a). The angular frequency estimates (as fractions of π) and the IF estimates are described in Fig. 4.6(b,c).

The above ideas also apply when the component AM–FM signals have non-sinusoidal or even aperiodic IF and IA signals. In such cases, following the analysis in [38], knowledge of the AM–FM signal over a finite time interval $[0, N-1]$ is assumed. Assuming periodic extension of the signal outside this finite interval, the IF and the IA signals can be expressed (via the DFT) as a linear combination of discrete–tme cosines. The IF signal in particular is represented by a finite discrete Fourier series of the form

$$\Omega[n] = \Omega_c + \sum_{k=1}^{K} \Omega_{mk} \cos\left(\Omega_{fk} n + \theta_k\right), \tag{4.10}$$

where $K < N/2$, while the carrier frequency is the dc value of the Fourier series:

$$\Omega_c \ = \ \frac{1}{N} \sum_{n\ =\ 0}^{N-1} \Omega[n].$$

In such cases, we set the required demodulation lengths L_i equal to the periods N_i of the extended signal components.

As an example, consider two–component AM–FM signals with linear FM modulation. The instantaneous frequencies of the example are

$$\begin{aligned}
\Omega_1[n] \ &= \ \frac{\pi}{2} + \frac{\pi}{400}\left(\frac{2n}{399} - 1\right) \quad , \quad 0 \le n \le 399 \\
\Omega_2[n] \ &= \ \frac{\pi}{2.005} - \frac{\pi}{400}\left(\frac{2n}{400} - 1\right) \quad , \quad 0 \le n \le 400
\end{aligned}$$

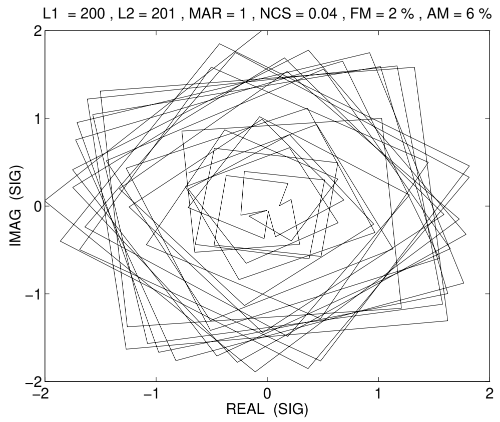

(a)

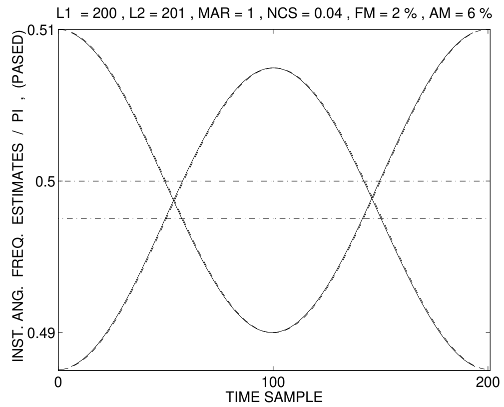

(b)

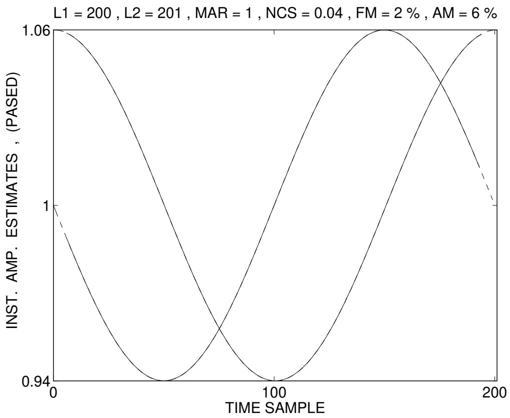

(c)

Figure 4.6: Complex signal example: (a) composite signal, (b) angular frequency estimates of the PASED algorithm (as fractions of π) (c) IA estimates of the PASED algorithm. The signal parameters of the example are identical to the real example, except that the components are complex. The estimates are the solid lines, actual quantities are dashed and the dashed–doted lines are the carrier frequency estimates.

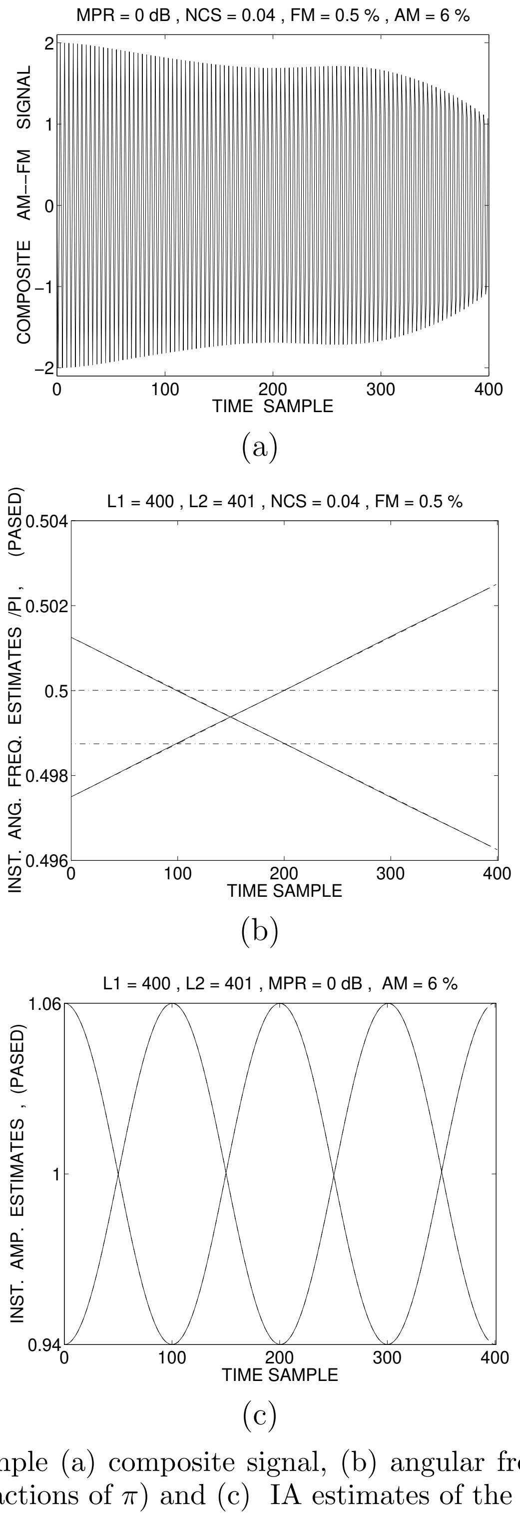

(a) (b) (c)

Figure 4.7: Chirp example (a) composite signal, (b) angular frequency estimates of the PASED algorithm (as fractions of π) and (c) IA estimates of the PASED algorithm. Solid lines indicate estimates, dashed lines indicate actual quantities and dashed-dotted lines are carrier frequency estimates. The component IF signals are linear with 0.5% FM and mutually coprime periods with a NCS of ≈ 4 %, while the IA signals are sinusoidal with a MPR parameter of 0 dB and 6% AM.

The IA signals of the example are sinusoidal with 6% AM , with a CR/IB of 50 and a MPR of 0 dB. The demodulation lengths used in this particular example were $L_1 = 400$ and $L_2 = 401$ samples respectively. The composite signal of the example is shown in Fig. 4.7(a), the angular frequency estimates of the PASED algorithm (as fractions of π) are shown in Fig. 4.7(b), and the IA estimates of the PASED algorithm are shown in Fig. 4.7(c).

4.4 PASED Algorithm: M Components

The M–component PASED algorithm is based on the same philosophy as that of the two–component problem. The separation matrix $\mathbf{S}_M$ has M circulant blocks instead of just two circulant blocks

$$\underbrace{\begin{pmatrix} x[0] \\ x[1] \\ \vdots \\ x(N-1) \end{pmatrix}}_{\mathbf{x}} = \underbrace{\begin{pmatrix} \mathbf{I}_{N_1} & \mathbf{I}_{N_2} & \ldots \mathbf{I}_{N_M} \\ \mathbf{I}_{N_1} & \mathbf{I}_{N_2} & \ldots \mathbf{I}_{N_M} \\ \vdots & \vdots & \vdots \end{pmatrix}}_{\mathbf{S}_M} \underbrace{\begin{pmatrix} \mathbf{x}_1 \\ \mathbf{x}_2 \\ \vdots \\ \mathbf{x}_M \end{pmatrix}}_{\mathbf{z}} . \tag{4.11}$$

The rank of the separation matrix in this case is

$$\begin{aligned} r(\mathbf{S}_M) &= \sum_{i\,=\,1}^{M} N_i - (M-1)\mathrm{gcd}(N_1, N_2, \ldots, N_M) \ , \quad \prod_{i,j\ ,\ i\neq j} \mathrm{gcd}(N_i, N_j)\ = 1 \ \text{ or } \ M = 2 \\ r(\mathbf{S}_M) &\geq \sum_{i\,=\,1}^{M} N_i - \sum_{i,j\ ,\ i<j} \mathrm{gcd}(N_i, N_j) \ , \ \text{otherwise.} \end{aligned} \tag{4.12}$$

The rank of the separation system in the multicomponent case now depends on the pairwise component interactions which are embodied in the form of the product of the pairwise gcd's. For the first case, the extra constraints are obtained as dc value constraints on $(M-1)$ components at their original scale as

$$\sum_{n=0}^{N_i-1} x_i[n] \;=\; 0 \;\;,\;\; i \;=\; 1,2,\ldots,(M-1). \tag{4.13}$$

For the second case, extra constraints are needed and are obtained by considering the two–component interactions in the composite signal. For an M–component signal, there are $\binom{M}{2}$ possible two–component interactions. The constraints in this case are obtained from the dc value constraints applied on the two–component interactions using the information on the pairwise gcd's. For the interaction between the (i,j) pair of components, the constraints take the form

$$\sum_{n=0}^{\left(\frac{N_i}{R_{i,j}}\right)-1} x_i[R_{i,j}n \;+\; p] \;+\; \sum_{n=0}^{\left(\frac{N_j}{R_{i,j}}\right)-1} x_j[R_{i,j}n \;+\; p] \;=\; 0,$$
$$\forall i,j,p \in \; \mathbf{Z}^{+} \ni 1 \leq i < j \leq M \;,\; 0 \leq p \leq R_{i,j}-1. \tag{4.14}$$

The number of constraints and extra information needed goes up with an increase in the number of signal components and the pairwise gcd of the components.

Alternatively, the M–component separation problem can be treated as a sequence of two–component separation problems [44, 45]

$$x[n] = \sum_{i=1}^{M} x_i[n] = x_1[n] + \underbrace{\sum_{i=2}^{M} x_i[n]}_{\tilde{x}_2[n]} \;=\; x_1[n] + x_2[n] + \underbrace{\sum_{i=3}^{M} x_i[n]}_{\tilde{x}_3[n]}.$$

This method, however, requires the use of $N_1 \;+\; \mathrm{lcm}\,(N_2, N_3, \ldots, N_M)$ samples of the composite signal for separation (assuming that there is no spectral cancellation in the sums) while the proposed PASED algorithm requires only $\sum_i N_i$ samples.

As an example consider the case of a five–component sinusoidally modulated AM–FM signal. The composite signal of the example is shown in Fig. 4.8(a). The M–component PASED algorithm developed earlier in this section is applied on this composite signal. The angular frequency estimates of the multicomponent–PASED

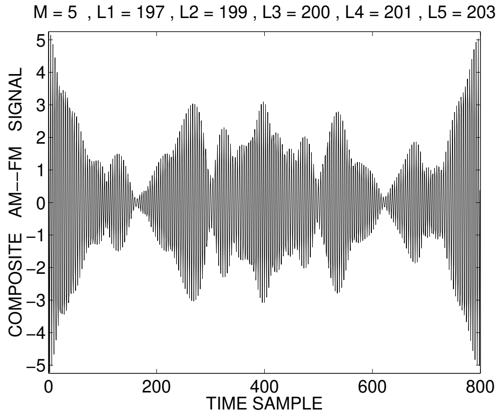

(a)

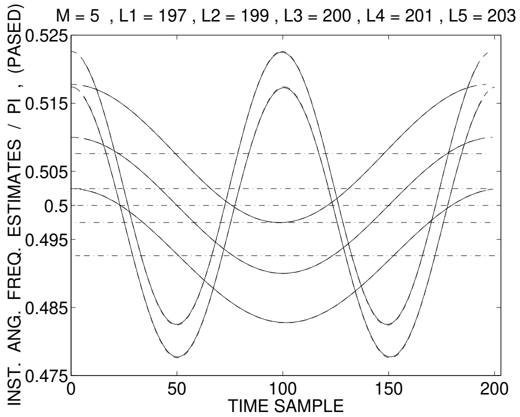

(b)

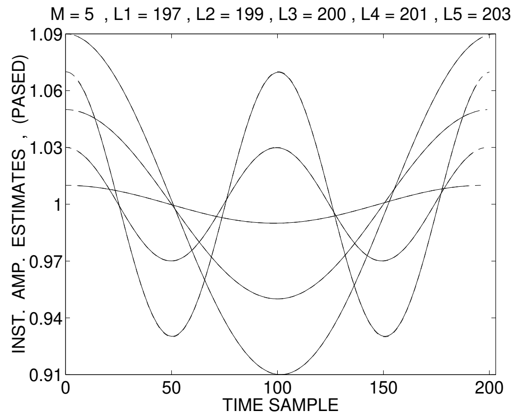

(c)

Figure 4.8: Five–component example: (a) composite AM–FM signal, (b) angular frequency estimates of the multicomponent–PASED algorithm (as fractions of π), (c) IA estimates of the components via the multicomponent–PASED algorithm. Solid lines are estimates, dashed lines are actual quantities and dashed–dotted lines are carrier frequency estimates. The IF signals are sinusoidal with $\approx 0.5\%$ FM and pairwise coprime periods. The IA signals are also sinusoidal with $\kappa_i \in \{1, 3, 5, 7, 9\}\%$ AM.

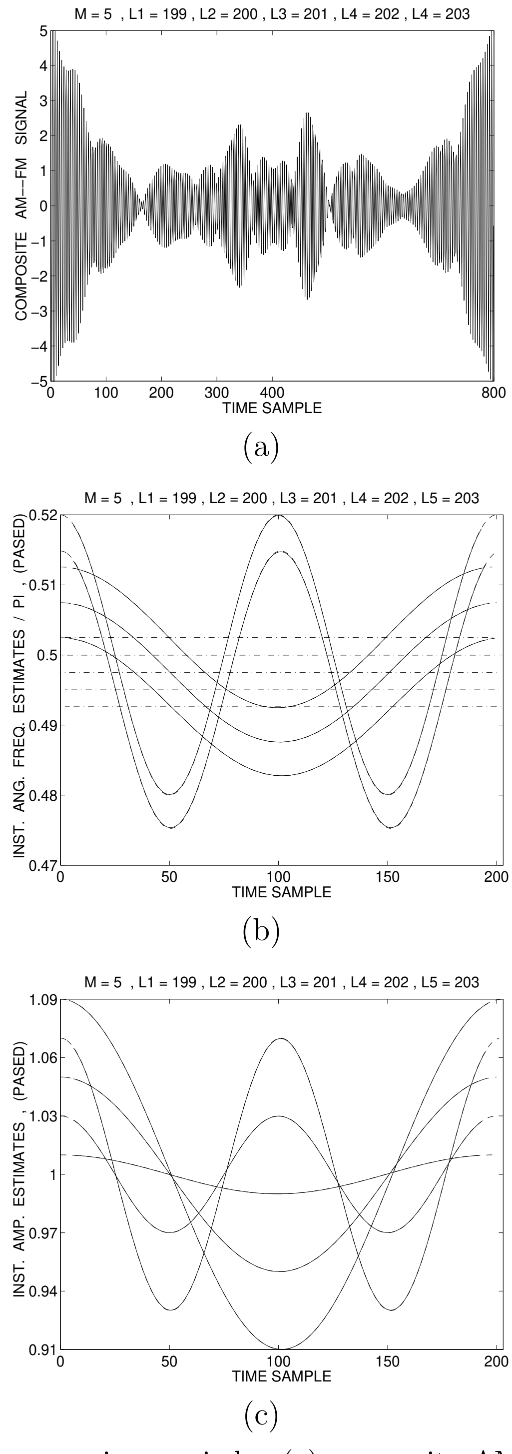

Figure 4.9: Pairwise non–coprime periods: (a) composite AM–FM signal, (b) angular frequency estimates of the multicomponent–PASED algorithm (as fractions of π), (c) IA estimates of the components via the multicomponent–PASED algorithm. Solid lines are estimates and dashed–dotted lines are carrier frequency estimates. The IF signals are sinusoidal with $\approx 0.5\%$ FM and pairwise coprime periods. The IA signals are also sinusoidal with $\kappa_i \in \{1, 3, 5, 7, 9\}\%$ AM.

algorithm as fractions of π are shown in Fig. 4.8(b) and the IA estimates of the multicomponent–PASED algorithm are described in Fig. 4.8(c). The IF's of the components overlap indicating that the components overlap spectrally. As in the case of the two–component example, the demodulation lengths of the PASED algorithm are $L_i = \mathrm{lcm}\left(\frac{2\pi}{\Omega_{fi}}, \frac{2\pi}{\Omega_{ai}}\right)$. The minimum number of composite signal samples needed is $\sum_i L_i$. Fig. 4.9 shows another five–component example where the periods are coprime overall but not pairwise coprime.

4.5 Comparison of the Demodulation Algorithms

Previously investigated techniques for multicomponent AM–FM signal separation and demodulation either assume that the components of the signal are distinct in the time–frequency plane or that the components are separable via linear filtering techniques. For signals in the co–channel range, i.e., when NCS < 0.2, these assumptions of distinctness and separability via linear filtering techniques break down. For the purpose of comparing the algorithms, the effect of the NCS and MPR parameters on demodulation on these algorithms is studied using two–component sinusoidally modulated AM–FM signals.

Separability of the component separation and demodulation tasks is an important factor that distinguishes the PASED algorithm from the others. In the case of the CC–DPLL algorithm, the separation section of the algorithm assumes perfect demodulation from the previous time instant. Demodulation algorithms like the LMS and the EDM perform both of these tasks simultaneously.

Demodulation algorithms like the LMS algorithm, the RLS algorithm, and the CC–DPLL algorithm are highly parameter dependent. The performance, the stability, and the noise suppression capabilities of the LMS and the RLS algorithms are dependent on the choice of the adaptive step size parameter μ or the memory factor ρ, while the performance and the stability of the CC–DPLL algorithm is dependent on the choice of loop filter parameters. The CC–DPLL algorithm in particular is a baseband algorithm while the others are bandpass algorithms. It is more appropriate in this case to compare their performance for a specific case.

Fig. 4.10 describes a two–component sinusoidally modulated AM–FM example where the PASED, the LMS (normalized version of the LMS [22]), the exponentially–weighted RLS, the HRR, the EKF, the MESA, and the CC–DPLL algorithms are compared for a fixed parameter set with NCS = 1 and MPR = 0 dB. Fourth–order predictors ($P = 4$) are used in the case of the adaptive algorithms with a step size parameter of $\mu = 1.25$ for the normalized LMS [22] and a exponential weight parameter of $\rho = 0.945$ for the RLS algorithm [20]. First–order loop filters are used in the design of the CC–DPLL so that the closed loop system is second–order with a damping ratio of 0.707. The components of the signal in this case have significant spectral overlap as described in Fig. 4.10(b). For this spectral separation, the LMS algorithm exhibits severe beating in the estimates as described in Fig. 4.10(d), the RLS estimates in Fig. 4.10(e) also are severely distorted, and post smoothing of the IF estimates does not reduce the frequency demodulation error significantly. The carrier unbiased frequency estimates of the PASED and the other algorithms are shown in Fig. 4.10(a-h). The percentage NRMSEs of the proposed PASED algorithm are two orders less than the other algorithms.

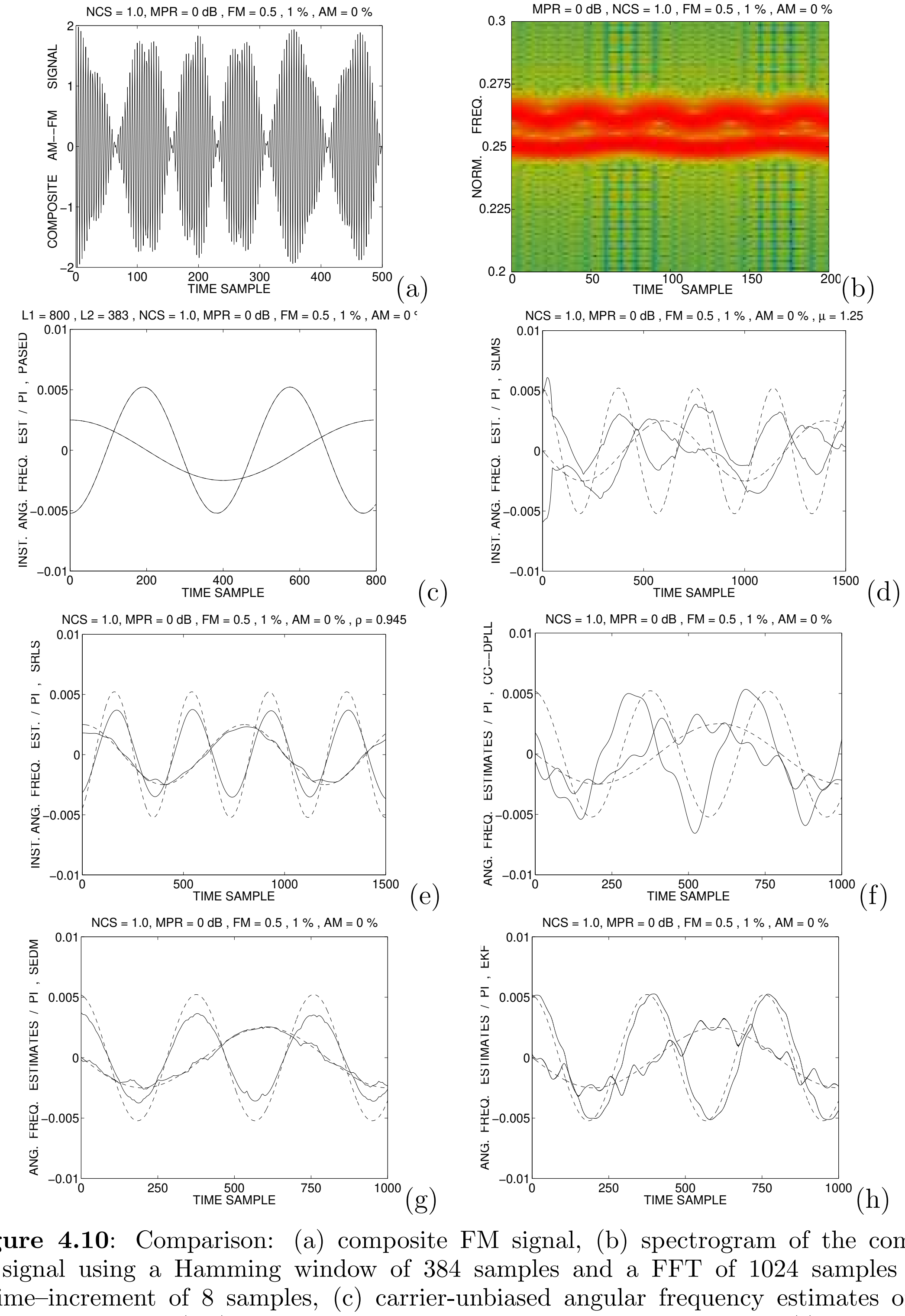

Figure 4.10: Comparison: (a) composite FM signal, (b) spectrogram of the composite signal using a Hamming window of 384 samples and a FFT of 1024 samples with a time–increment of 8 samples, (c) carrier-unbiased angular frequency estimates of the PASED algorithm, (d,e) estimates of the SLMS and the SRLS algorithm, (f) estimates of the CC–DPLL algorithm using a first–order loop filter and (g,h) corresponding estimates of the SEDM and the EKF algorithms. Solid lines are the estimates and the dashed lines are the actual quantities. Post smoothing of the estimates was done by using moving average filtering to remove the beating and 9-pt median filtering to remove spikes.

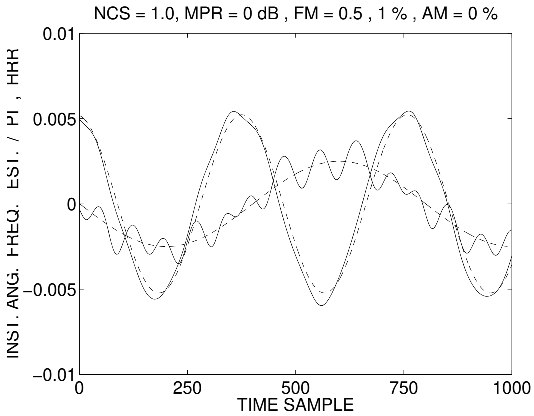

(i)

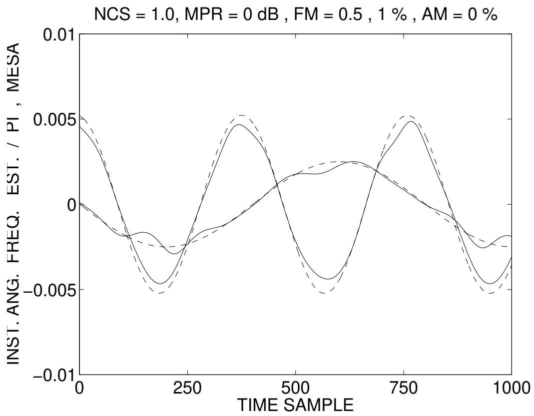

(j)

Algorithm	NRMSE$_1$ (%)	NRMSE$_2$ (%)
PASED	0.01	0.08
MESA , $L = 350$, $\beta = 6.65$	13.96	13.88
HRR , $c = 20$, $L = 20$	38.1	14.93
ALP–SLMS , $\mu = 1.25$, $P = 4$, $L = 20$	73.3	63.25
ALP–SRLS , $\rho = 0.945$, $P = 4$, $L = 20$	56.04	38.77
CC–DPLL	23.9	15.3
SEDM	16.6	31.84

(k)

Figure 4.10: Comparison (continued): (i,j) carrier–unbiased angular frequency estimates of the HRR and the MESA algorithms and (k)NRMSEs of the PASED algorithm as compared to the other multicomponent demodulation algorithms. Long filters and very small passband tolerances are needed in the case of the MESA algorithm. The large errors in the case of the *adaptive linear predictive* (ALP) algorithms are due to the poor conditioning of the autocorrelation matrix $\mathbf{R}_x$ [31].

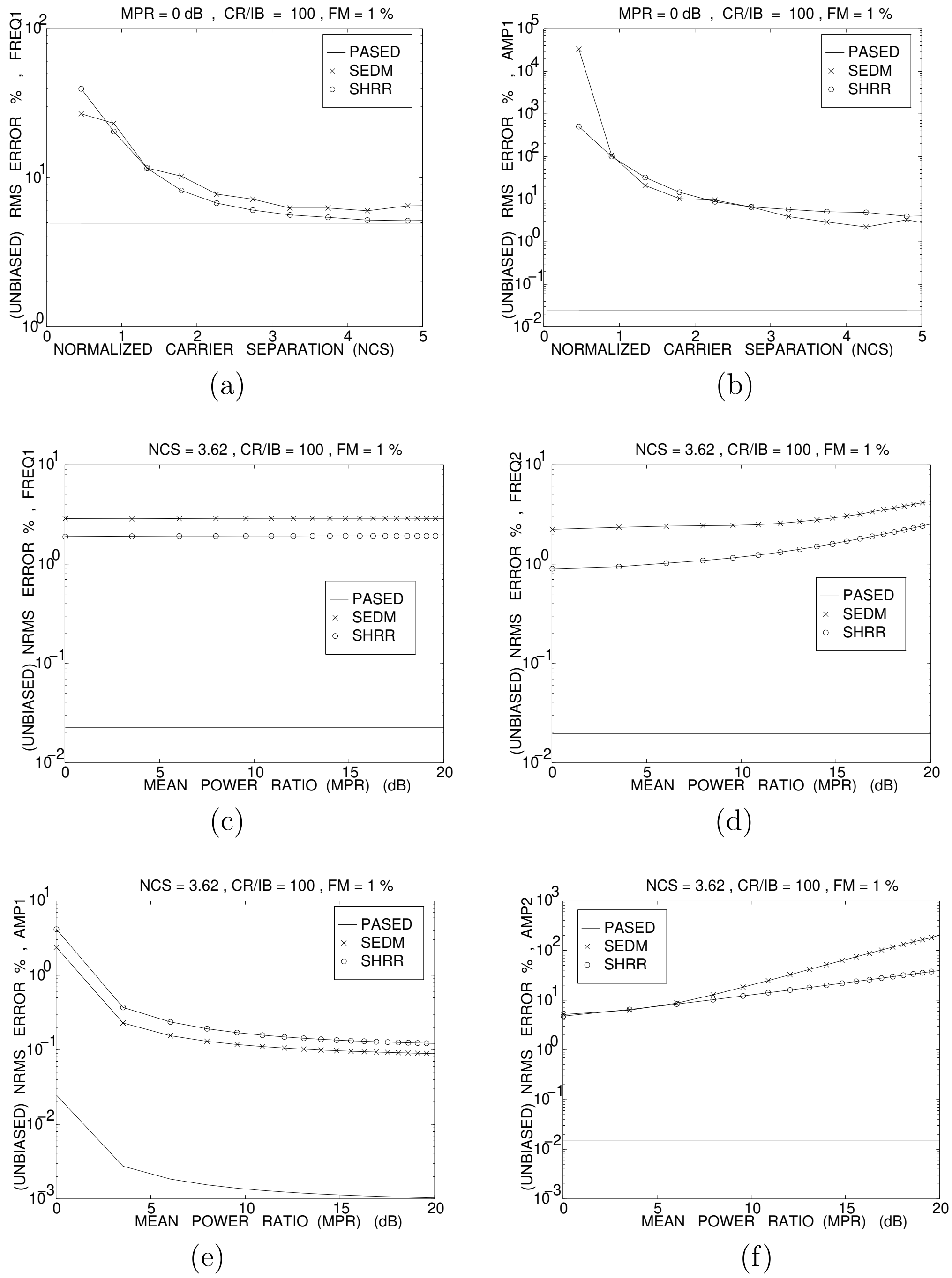

Figure 4.11: (a,b) Effect of NCS on frequency and amplitude demodulation in the PASED , the SEDM, and the SHRR algorithms (the other algorithms developed singularities and broke down for NCS $<$ 0.5) and (c,d,e,f) effect of the MPR parameter on frequency and amplitude demodulation in the PASED, the SEDM, and the SHRR algorithms. Amplitude estimation in the SHRR is accomplished by integrating the IF estimates and solving a least–squares system for the amplitudes. All curves were obtained by averaging over $\kappa_i \in [1-10]\%$ AM. The notation SX refers to the algorithm X with post smoothing.

4.5.1 Effect of Spectral Separation (NCS Parameter)

In the definition of multicomponent AM–FM signal model it has been assumed that the components are distinct in the time–frequency plane. The challenging case, however, is the co–channel case where the components of the signal overlap spectrally. In this case the components are no longer distinct and interact with each other. This interaction for the case of two–component continuous–time sinusoidal signals of the form

$$x(t) \quad = \quad a_1 \cos(\omega_1 t + \theta_1) \quad + \quad a_2 \cos(\omega_2 t + \theta_2)$$

is embodied in the instantaneous envelope and the frequency of the composite signal

$$\begin{aligned} |a(t)| \quad &= \quad \left[a_1^2 \ + \ a_2^2 \ + \ 2a_1 a_2 \cos\left((\omega_2 - \omega_1)t + \theta_1 - \theta_2\right)\right]^{\frac{1}{2}} \\ \omega(t) \quad &= \quad \left(\frac{\omega_1 + \omega_2}{2}\right) \ + \ \left(\frac{\omega_1 - \omega_2}{2}\right)\left(\frac{a_2^2 - a_1^2}{|a(t)|^2}\right). \end{aligned} \tag{4.15}$$

Decrease in the spectral separation between the components (as measured by the NCS parameter) produces singularity problems in these algorithms:

- The energy equations of the EDM algorithm become ill–conditioned [56].
- The covariance matrices used in the LMS algorithm, the RLS algorithm, and the MUSIC algorithm become ill–conditioned [31].
- The Fisher information matrix used in the maximum likelihood approaches [15] becomes ill–conditioned.
- The Toeplitz and the Hankel matrix systems of the ITD and the HRR algorithms become ill-conditioned.
- The observability Gramian of the two–component state model in the CC–DPLL and the EKF algorithms become ill–conditioned [3, 24].

The interaction between the components manifests itself as beating in the estimates. Post smoothing of the estimates can alleviate some of the problems. The demodulation algorithm X with post–smoothing is referred to as SX, i.e., the EDM algorithm with post smoothing is referred to as the SEDM algorithm. Post smoothing of the estimates using 9-pt median filtering and moving average (MA) filtering of the GDE coefficients (lowpass quantities) and the estimates in the EDM removes a significant amount of the beating but in the case of sinusoidal modulation fails for NCS parameters less than 1. The EDM algorithm, particularly for voice modulated FM applications, can provide intelligible estimates for separations down to 25% of the RF bandwidth but fails for further decrease in spectral separation.

The proposed PASED algorithm on the other hand does not make any assumption about the spectral location of the components. This enables the algorithm to handle the case when the components of the signal overlap spectrally, i.e., the co–channel case and the case where the component IF tracks cross-over where all the existing techniques fail. Fig. 4.11(a) illustrates the effect of the spectral separation on the different algorithms. Note that the performance of the PASED algorithm is independent of the spectral separation parameter.

State flipping occurs in the CC–DPLL algorithm (condition where the DPLL's lock onto the wrong signal) as a consequence of unobservability of the states of the state–model which is conditioned on 1) frequency equality (IF tracks cross–over), 2) components completely in phase or out of phase or 3) identical component state transition matrices [3]. The PASED algorithm on the other hand does not exhibit this phenomenon and is capable of handling the case where the IF tracks cross.

4.5.2 Effect of the Mean Power Ratio (MPR) Parameter

The MPR parameter of the signal mixture is a measure of the strength of the desired signal relative to the interference and is also a measure of the strength of the interaction between the components. For large MPR parameters, the stronger component dominates the signal mixture and the interaction between the components is less.

The covariance matrix for the multicomponent demodulation problem when one of the components is stronger than the other becomes singular, and, consequently, demodulation algorithms like the LMS develop singularities as the MPR parameter increases [22]. The performance of the CC–DPLL and the EKF algorithms can be characterized by the observability Gramian of the state–space model corresponding to the composite signal [3]. As one of the components becomes more powerful than the other, the lower–powered component becomes less observable resulting in increased error covariance due to an increase in the coupling between the DPLL's and an increase in the demodulation error corresponding to the weaker component [3, 23].

The frequency estimation section of the EDM algorithm is obtained from the GDE of the composite signal that is invariant to the amplitudes. Consequently, frequency demodulation in the EDM is independent of the MPR parameter. The amplitude demodulation section of the EDM is, however, adversely affected by an increase in the MPR parameter. As the MPR increases, the relative strength of the first component in the mixture increases and the amplitude demodulation error of the first component decreases, while the demodulation error of the second and weaker component increases [56].

The proposed PASED algorithm, however, does not make any assumptions regarding the component interaction, and frequency demodulation in the PASED algorithm is independent of the MPR parameter. An increase in the power of one of the components with respect to the other results in a decrease in the amplitude demodulation error of the stronger component but has no effect on the demodulation error of the weaker one. The effect of the MPR parameter on frequency and amplitude demodulation in the PASED, the SEDM, and the SHRR algorithms is shown in Fig. 4.11(c,d,e,f).

4.5.3 Noise Rejection Capabilities

Multicomponent AM–FM demodulation of noisy signals corrupted with AWGN involves different tradeoff scenarios. The first tradeoff relates to balancing the task of noise rejection with the task of allowing the signal to pass with a minimum amount of harmonic distortion. The second tradeoff scenario is between the strength of signal modulations and loss of stationary behavior. Increasing the strength of the frequency and amplitude modulation results in a initial decrease in demodulation error but will eventually result in increased demodulation errors due to loss of stationary behavior

In the case of the multiband algorithms, noise rejection is accomplished via multiband filtering of the composite signal retaining only the M channels that are most active and rejecting the other less active channels. These multiband algorithms exploit the fact that the components of the AM–FM signal are narrowband bandpass signals. In the case of the exponentially–weighted RLS algorithm, noise rejection is accomplished via the memory factor ρ that performs exponential weighting of the new data and previous data. For low SNR cases, the previous estimates of the matrix $\mathbf{R}_x$ and the vector $\mathbf{p}$ used in the algorithm are more reliable and should be weighted more than the new and current data that is noisy. Larger memory factors are more appropriate for low SNR scenarios while smaller memory factors are more suitable for high SNR and more nonstationary environments.

In the case of the LMS algorithm, this same purpose of noise rejection is accomplished by appropriate choice of the step size and filter order parameters. For low SNR parameter situations, large filter orders (P) and small step size parameters (μ) are needed, while high SNR parameter and more non stationary environments call for smaller filter orders with larger step size parameters. Noise rejection for frequency estimation in the HRR algorithm is accomplished by retaining the significant singular values and rejecting the rest (rank reduction). Low SNR situations call for larger Hankel order while high SNR scenarios call for a smaller filter order. For the amplitudes in the LMS, the RLS, and the HRR algorithms, noise rejection is accomplished through the least–squares solution to the system in Eq. (2.4). This least–squares system has to smooth out the error accumulated in the frequency estimation part and the additive noise.

In the case of the CC–DPLL algorithm, the loop filters in either DPLL need to be designed so as to balance the task of noise and interference rejection with the task of minimizing the harmonic distortion induced. For the case of the EKF, noise rejection is accomplished implicitly via the Kalman gain matrix which adaptively updates the states based on the SNR scenario. When the SNR is low the previous state estimate is weighted more while the new data is weighted more when the SNR is high.

In Fig. 4.12(a,b) the effect of SNR on frequency and amplitude demodulation on the PASED algorithm (least–squares smoothing with mild bandpass filtering), the MEDM algorithm (multiband filtering philosophy), and the HRR algorithm (rank reduction and SVD philosophy) is compared. Hankel matrices of order $c = 20$ were used in the frequency estimation part of the HRR algorithm, while a least–squares order of 20 was used for the amplitude demodulation part to smooth out noise and error accumulated via integration of the IF estimates. FIR linear–phase filters of length $L = 200$ were used in the MEDM algorithm. A least–squares length of $L = 2\,(N_1 \;+\; N_2)$ samples followed by bandpass filtering of the separated components with FIR linear–phase filters of length $L = 20$ samples were used in the case of the PASED algorithm. The curves for each algorithm were obtained by averaging over AM indices $\kappa_i \;\in\; 1 - 10$ %. Results indicate that for both frequency and amplitude demodulation comparable results can be achieved by using any of these noise rejection philosophies but with different and appropriate computational costs.

4.5.4 Computational Complexity

Among the existing multicomponent AM–FM demodulation algorithms, the EDM, the ITD, the LMS, and the exponentially–weighted RLS are all similar in the sense that they are based on instantaneously estimating the GDE coefficients of the signals. The EDM algorithm uses higher–order energy operators for this purpose, the ITD uses instantaneous operators obtained as determinants of Toeplitz matrices, while the LMS algorithm uses instantaneous signal correlations. For an M–component signal the EDM requires the computation of M GDE coefficients; the ITD and the LMS as implemented in [17, 30] require the computation of $2M$ GDE coefficients. The multiband algorithms require optimization of the center frequencies and the bandwidths of the multiband filters so that the tasks of noise rejection and component separation are accomplished with minimum distortion of the components.

Adaptive algorithms like the LMS, the CC–DPLL, and the RLS require extensive optimization of their respective adaptive parameters. The LMS algorithm requires the optimization of the filter order parameter P and the step size parameter μ to match the signal environment. The exponentially–weighted RLS algorithm which is based on rank–one update and adaptive linear prediction, requires optimization of the memory factor ρ to match the parameters of the signal environment. The CC–DPLL algorithm requires the optimization of the loop filter parameters of either DPLL to perform the functions of interference and noise rejection, while keeping the distortion induced by either loop to a minimum. In the notch filter version of the CC–DPLL the loop filter parameters in addition to performing the tasks of interference and noise rejection also have to be optimized for stability of the closed loop [54].

The HRR algorithm requires the computation of the SVD of the global Hankel matrix containing samples of the composite signal, where the Hankel order $c \approx 3M$ and M is the number of components. Component IF signal estimation in the LMS, the RLS, and the HRR algorithms requires optimization of the least–squares order for the system in Eq. (2.4). The EKF algorithm requires requires proper initialization of the model noise covariance and error covariance parameters of the state model for the multicomponent AM–FM signal so that the approximation of linearizing the nonlinear measurement equation about the current state estimate is valid otherwise the filter will diverge.

The log–likelihood function in the maximum likelihood approaches is multimodal, and, consequently, these approaches require nonliear optimization of the phase or frequency parameters. This means that they need proper intialization close to the global solution so that they do not converge to a local minima. This is typically done by using a suboptimum technique to initialize an iterative Newton's algorithm based approach [15].

4.5.5 General Remarks on the PASED Algorithm

The proposed PASED algorithm has the following attractive features:

1. The PASED algorithm does not place any restrictions regarding the spectral location of the components. Hence, its performance is independent of the spectral separation parameter NCS.

2. The PASED algorithm provides separability between the separation and demodulation tasks in multicomponent AM–FM demodulation so that problems in one procedure do not cascade into the other.

3. Increase or decrease in the relative strength parameter MPR does not affect the performance of the PASED algorithm significantly.

4. The least–squares smoothing afforded by the algebraic separation system accomplishes simultaneous component separation and smoothing.

5. The PASED algorithm does not exhibit flipping of estimates when the IF tracks of the components cross.

4.6 Co–Channel and Adjacent Channel Separation

In this section, the performance of the PASED algorithm in regards to the co–channel problem is evaluated by applying the algorithm to the problem of separating and demodulating the components of a mixture of voice–modulated FM signals. The normalized carrier separation (NCS) parameter of the signal mixture is a measure of the spectral overlap between the components of the signal. The denominator of the NCS parameter, however, is the Carson bandwidth of the AM–FM signal which is a conservative estimate of the actual bandwidth of the signal. It is therefore more appropriate in voice–modulated FM applications to use the RF bandwidth of the

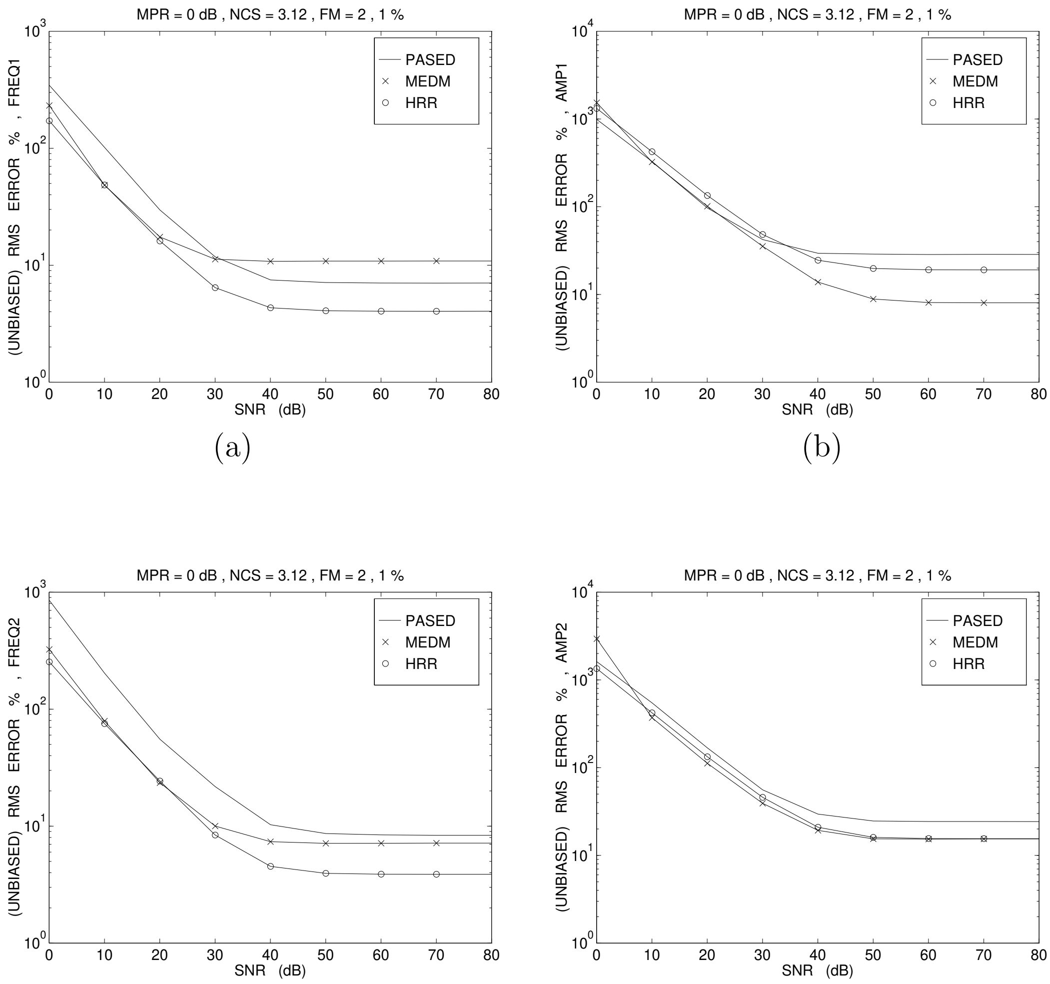

(a) (b)

(c) (d)

Figure 4.12: Effect of SNR on the PASED, the MEDM, and the HRR algorithms: (a,c) frequency demodulation error as function of the SNR and (b,d) amplitude demodulation vs SNR. The number of composite signal samples used in the PASED algorithm was $L = 2\,(N_1\ +\ N_2)$, with bandpass filtering of the separated components with FIR linear–phase filters of length $L = 20$ samples and 3–time binomial smoothing of the energy signals in the ESA. FIR linear–phase filters of length $L = 200$ were used in the implementation of the MEDM algorithm. Hankel matrices of order $c = 20$ were used for frequency demodulation while a least–squares order of 20 was used for amplitude demodulation in the case of the HRR algorithm. The curves for the PASED, the MEDM, and the HRR algorithms were obtained by averaging over AM indices $\kappa_i\ \in\ 1 - 10\ \%$.

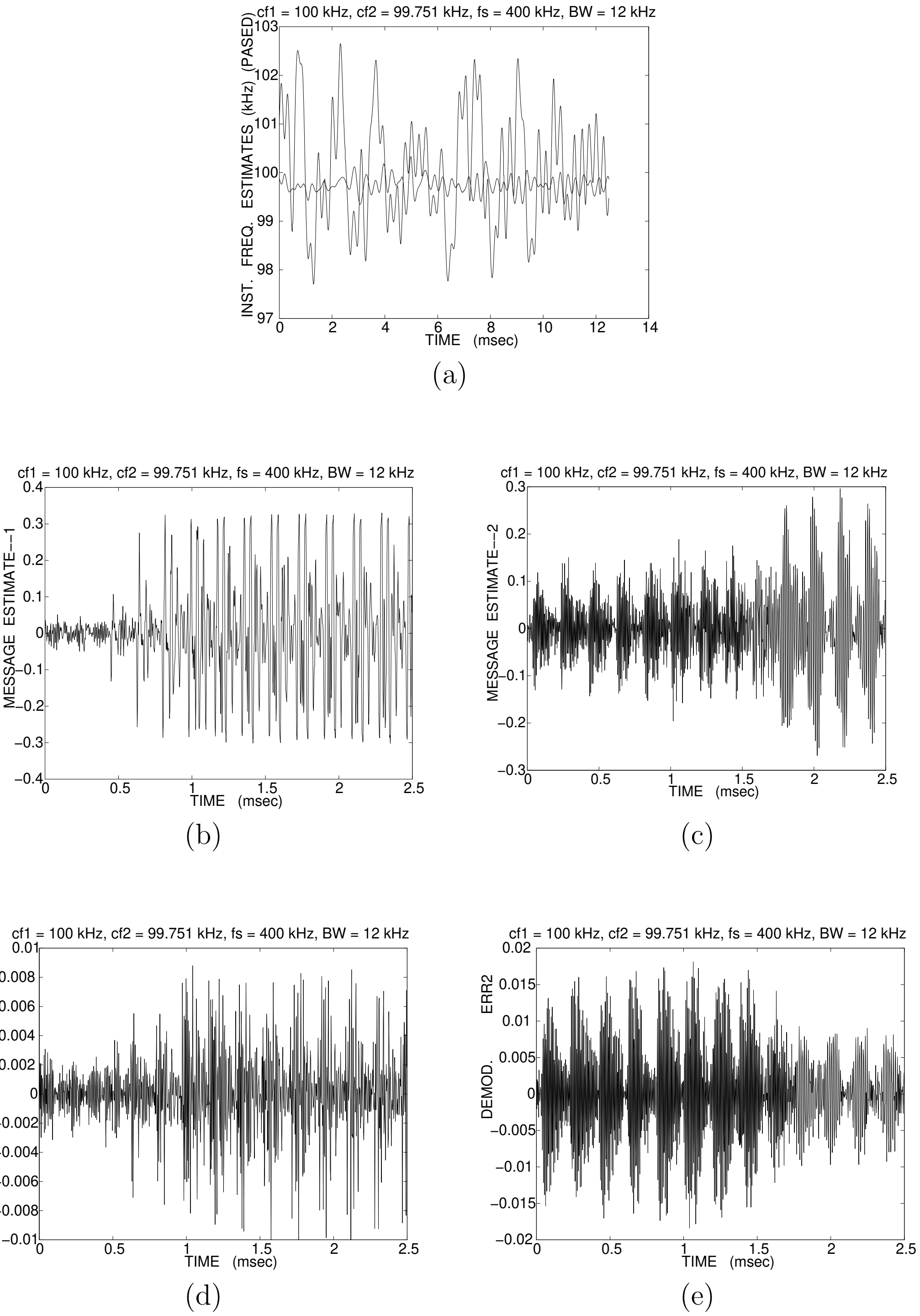

Figure 4.13: FM voice example: (a) instantaneous frequency estimates of the PASED algorithm and (b,c) demodulated message signals of the PASED algorithm and (d,e) associated demodulation errors of the PASED algorithm.

signal to compute the NCS parameter. With the RF bandwidth as the normalization factor: NCS parameters > 1 indicate that the components are well separated and distinct, NCS $= 1$ indicates that components are touching each other, and when the NCS parameter < 1 , the components start to overlap and interact. For spectral separations in the co–channel range (NCS parameter < 0.1), the components completely overlap and they are no longer distinct.

Among the existing multicomponent algorithms, the EDM algorithm has the advantages of computational simplicity and excellent time–resolution while experiencing similar limitations in the spectral separations it can handle as most other existing algorithms [56]. In particular, when applied to the problem of demodulating voice–modulated two-component FM signals, the EDM algorithm has the capability of providing intelligible message estimates for spectral separations up to 25% of the RF–bandwidth but breaks down for further decrease in spectral separation. In the co–channel region all of the existing techniques develop singularity problems. The proposed PASED algorithm, however, does not assume that the components need to be distinct and is not affected by a decrease in spectral separation. Some of the adaptive techniques like the LMS algorithm are also sensitive to the relative power ratio (MPR) of the components and develop singularity problems when the ratio is high. The performance of the proposed PASED algorithm on the other hand is independent of the MPR parameter.

An example of applying the PASED algorithm to the problem of separation and demodulation of two–component voice–modulated FM signals is shown in Fig. 4.13, where the components overlap spectrally, i.e., co–channel range. The sampling period of the message signals is $f_s = 400$ kHz, and the carrier frequencies of the components are $f_{ci} = 100$, 99.75 kHz. The RF bandwidth of each component is 12 kHz and

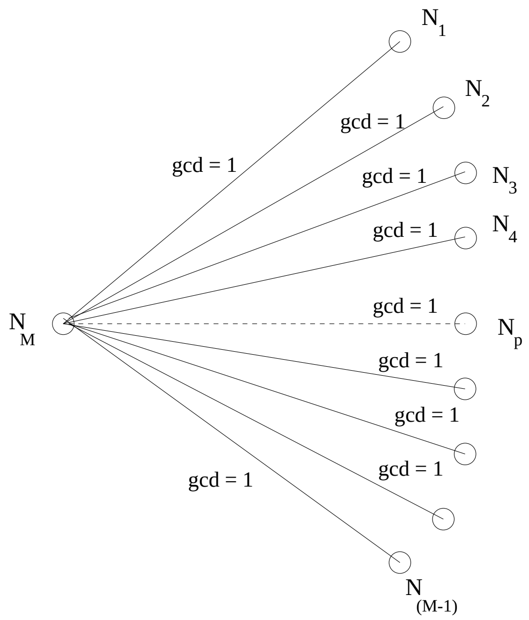

Figure 4.14: Interaction pattern for the case where the periods of the components are pairwise coprime for M components. Each of the components interacts identically with the remaining $(M-1)$ components. The interaction between the components is embodied in the form of the gcd between the periods of the components.

---

the components are modulated with 6 % FM. With these parameters the IF's of the components overlap and cross–over indicating significant spectral overlap. Actually, the carrier separation is 2% of the RF bandwidth (NCS=0.02). The IF estimates of the example are shown in Fig. 4.13(a). The demodulated message signals of the PASED algorithm are shown in Fig. 4.13(b,c) and the corresponding demodulation errors are shown in Fig. 4.13(d,e).

4.7 Proof of Rank Relations

Theorem 1 *The M–component separation matrix $\mathbf{S}_M$ in the case where the component periods $\{N_i \ , \ i = 1, 2, \ldots, M\}$ are pairwise coprime or if there are only two–*

components is of rank

$$r(\mathbf{S}_M) = \sum_{i=1}^{M} N_i - (M-1)\ \gcd(N_1, N_2 \ldots, N_M) \quad , \quad \prod_{i,j\ ,\ i \neq j} \gcd(N_i, N_j)\ = 1 \ \text{ or } \ M = 2.$$

Proof: The M–component separation matrix $\mathbf{S}_M$ has $\left(\sum_{i=1}^{M} N_i\right)$ columns and, hence, a maximum possible column rank of

$$r_{max} = \sum_{i=1}^{M} N_i. \tag{4.16}$$

Exploiting the periodicity of the components we have

$$x_i[n] = x_i[n + N_i]\ ,\ i = 1, 2, \ldots M \quad . \tag{4.17}$$

If $(M-1)$ initial values $x_i[0]$, $i = 2, \ldots M$, are known, using periodicity we can obtain N_1 samples of the first component using

$$x_1[n] = x[n] - (x_2[0] + x_3[0] \ldots + x_M[0]) \tag{4.18}$$

for the indices

$$\begin{aligned} n \ = \ 0\ ,\ R_{N_1}(\text{lcm}(N_2, N_3 \ldots, N_M)) \quad &, \quad R_{N_1}(2\ \text{lcm}(N_2, N_3 \ldots, N_M))\ , \\ & \ldots R_{N_1}((N_1 - 1)\ \text{lcm}(N_2, N_3 \ldots, N_M)), \end{aligned}$$

where the notation $R_i(j)$ denotes the remainder of the integer j modulo i defined by $R_i(j) \equiv r(\text{mod}\ i)$. The next step is to show that these indices are distinct and within the range of 0 and N_1. Let A_1 and A_2 be any two of these indices such that

$$\begin{aligned} A_1 &= M_1\ \text{lcm}(N_2, N_3 \ldots, N_M) \ \equiv \ r_1(\text{mod}\ N_1) \\ A_2 &= M_2\ \text{lcm}(N_2, N_3 \ldots, N_M) \ \equiv \ r_2(\text{mod}\ N_1), \end{aligned} \tag{4.19}$$

where $0 \leq M_1 \neq M_2 \leq N_1 - 1$. If the periods of the components are pairwise coprime then

$$\gcd(N_1, N_2, \ldots N_M) = 1 \quad , \quad \text{lcm}(N_1, N_2, \ldots N_M) = \prod_{i=1}^{M} N_i \tag{4.20}$$

and, hence,

$$\begin{aligned} A_1 &= M_1 \prod_{i=2}^{M} N_i \equiv r_1 (\text{mod } N_1) \\ A_2 &= M_2 \prod_{i=2}^{M} N_i \equiv r_2 (\text{mod } N_1). \end{aligned} \tag{4.21}$$

Subtracting the indices and using the property of the modulo operator we have

$$A_1 - A_2 = (M_1 - M_2) \prod_{i=2}^{M} N_i \equiv (r_1 - r_2)(\text{mod } N_1). \tag{4.22}$$

Since the periods are pairwise coprime and $M_1 - M_2 < N_1$, this implies that the transformation from $A_i \leftrightarrow r_i(\text{mod } N_1)$ is unique and that the indices are within the range of 0 and N_1. This implies that when the periods of the components are pairwise coprime and given that one has knowledge of $(M-1)$ intial values of the components other than the i^{th} component, N_i distinct samples of the i^{th} component can be obtained from the separation system. This inturn implies that the rank of the M–component separation matrix, $\mathbf{S}_M$, which is also the number of linearly independent columns in the matrix $\mathbf{S}_M$, is

$$r(\mathbf{S}_M) = \sum_{i=1}^{M} N_i - (M-1) \quad , \quad \prod_{i,j \ , \ i \neq j} \gcd(N_i, N_j) = 1.$$

For the two–component case, it has been shown [44, 45] that the rank of the two–component separation matrix

$$\begin{aligned} r(\mathbf{S}_2) &= N_1 + N_2 - \gcd(N_1, N_2) \\ r(N(\mathbf{S}_2)) &= \gcd(N_1, N_2). \end{aligned} \tag{4.23}$$

Combining these results we have that

$$r(\mathbf{S}_M) = \sum_{i\ =\ 1}^{M} N_i - (M-1)\gcd(N_1, N_2 \ldots, N_M) \quad , \quad \prod_{i,j \ , \ i \neq j} \gcd(N_i, N_j) = 1 \ \text{ or } \ M = 2.$$

In other words, "the solution to the algebraic separation system of the PASED algorithm in the case where the composite signal contains M components whose periods are coprime is equivalent to the solution to the two–component case where there are $(M-1)$ two–point interactions as opposed to just one". The interaction pattern for the case where the periods are not pairwise coprime is more complex and contains not just the pairwise two–point interactions but also $\binom{M}{k}$ k–point interactions embodied in the form of the appropriate gcd. The next rank result deals with this particular case.

Theorem 2 *The rank of the M–component separation matrix $\mathbf{S}_M$, where the periods of the components are $\{N_i \ , \ i = 1, 2, \ldots, M\}$ in the general case, is given by*

$$\begin{aligned} r(\mathbf{S}_M) &= \sum_{i=1}^{M} N_i - \sum_{i,j \ , \ i<j} \gcd(N_i, N_j) \\ &+ \underbrace{\sum_{i,j,k \ , \ i<j<k} \gcd(N_i, N_j, N_k) + \ldots (-1)^{M-1} \gcd(N_1, N_2, \ldots N_M)}_{Q} \ , \ M \geq 2. \end{aligned}$$

Proof: As in the coprime case the maximum possible rank for the matrix $\mathbf{S}_M$ is the number of columns in the matrix

$$r_{max} = \sum_{i=1}^{M} N_i. \tag{4.24}$$

The n component separation matrix $\mathbf{S}_n$ can be written in block form

$$\mathbf{S}_n = [\mathbf{B}_1 \mid \mathbf{B}_2 \mid \ \ldots \mathbf{B}_n],$$

where the block $\mathbf{B}_i$ corresponds to blocks of identity matrices of order N_i that correspond to the i^{th} component. The rank of the n component separation matrix, $r(\mathbf{S}_n)$, is the number of linearly independent column vectors in $\mathbf{S}_n$ and can be evaluated using subspace addition

$$r(\mathbf{S}_n) = \dim\left(\sum_{i \ = \ 1}^{n} \operatorname{span}(\mathbf{B}_i)\right), \tag{4.25}$$

Within each block $\mathbf{B}_i$ all the column vectors are all linearly independent and are orthogonal, hence

$$\dim(\operatorname{span}(\mathbf{B}_i)) = N_i. \tag{4.26}$$

From the rank of the separation matrix in the two–component case as given by Eq. (4.23), the number of linearly dependent vectors, i.e., the dimension of the null space among the columns of any two blocks that are different put together is

$$\begin{aligned} r_{\max} \quad &- \quad r\left(\mathrm{span}\left(\mathbf{B}_i\right) \; + \; \mathrm{span}\left(\mathbf{B}_j\right)\right) \\ &= \quad \dim\Big(\mathrm{span}\left(\mathbf{B}_i\right) \bigcap \mathrm{span}\left(\mathbf{B}_j\right)\Big) \; = \; \gcd(N_i, N_j) \;\; , \;\; i \neq j. \end{aligned} \tag{4.27}$$

For the case of any two blocks put together, each column in the block $\mathbf{B}_i$ has ones alternating every N_i slots. Similarly each column vector in the block $\mathbf{B}_j$ has ones alternating every N_j slots. The block matrix that corresponds to the intersection of the spans of the two blocks therefore contains column vectors that have ones alternating every $R_{i,j} \; = \; \gcd(N_i, N_j)$ slots and can be written as

$$\Big[\mathrm{span}\left(\mathbf{B}_i\right) \bigcap \mathrm{span}\left(\mathbf{B}_j\right)\Big] \; = \; \begin{pmatrix} \mathbf{I}_{R_{i,j}} \\ \mathbf{I}_{R_{i,j}} \\ \vdots \end{pmatrix}. \tag{4.28}$$

The structure of the block matrix corresponding to the intersection of the spans of the blocks $\mathbf{B}_i$ and $\mathbf{B}_j$ is therefore identical to that of any of the other blocks $[\mathbf{B}_i \; , \; i \; = \; 1, 2, \ldots, n]$ (only the dimension, $R_{i,j}$, of the identity matrices is different). For the case of three arbitrary matrix blocks put together, the dimension of the intersection of the spans of the column of each block, consequently, is given by

$$\begin{aligned} \dim\left(\bigcap_{i\,=\,1}^{3} \mathrm{span}\left(\mathbf{B_i}\right)\right) \quad &= \quad \dim\Big(\Big[\mathrm{span}\left(\mathbf{B}_i\right) \bigcap \mathrm{span}\left(\mathbf{B}_j\right)\Big] \bigcap \mathrm{span}\left(\mathbf{B}_k\right)\Big) \\ &= \quad \gcd\left[\gcd\left(N_i, N_j\right), N_k\right] \\ &= \quad \gcd\left(N_i, N_j, N_k\right) \;\; , \;\; i \neq j \neq k. \end{aligned} \tag{4.29}$$

This relation for the intersection of the spans of the blocks can be generalized to more than three components as

$$\dim\left(\bigcap_{i\,=\,1}^{n} \mathrm{span}\left(\mathbf{B}_i\right)\right) \quad = \quad \gcd\left(N_1, N_2, \ldots, N_n\right). \tag{4.30}$$

If $\{\mathbf{V}_i \ , \ i \ = \ 1, 2, \ldots, n\}$ is a sequence of subspaces in a finite dimensional vector space $\mathbf{V}$ then it can be shown for the case of $n = 2$ that [25]

$$\dim\left(\mathbf{V}_1 \ + \ \mathbf{V}_2\right) \ = \ \dim\left(\mathbf{V}_1\right) \ + \ \dim\left(\mathbf{V}_2\right) \ - \ \dim\left(\mathbf{V}_1 \bigcap \mathbf{V}_2\right). \tag{4.31}$$

This can be frther extended through mathematical induction to the case of n components as

$$\begin{aligned} \dim\left(\sum_{i \ = \ 1}^{n} \mathbf{V}_i\right) \ &= \ \sum_{i=1}^{n} \dim\left(\mathbf{V}_i\right) \ - \ \sum_{i,j \ , \ i<j} \dim\left(\mathbf{V}_i \bigcap \mathbf{V}_j\right) \\ + \ \sum_{i,j,k \ , \ i<j<k} \dim\left(\mathbf{V}_i \bigcap \mathbf{V}_j \bigcap \mathbf{V}_k\right) \ &+ \ \ldots (-1)^{n-1} \dim\left(\bigcap_{i \ =1}^{n} \mathbf{V}_i\right) \ , \ n \geq 2. \end{aligned} \tag{4.32}$$

Equating the spaces $\{\mathbf{V}_i \ , \ i \ = 1, 2, \ldots, n\}$ to $\{\mathrm{span}\left(\mathbf{B}_i\right) \ , \ i \ = 1, 2, \ldots, n\}$ and using the above outlined steps we obtain the required rank result for $n \ = \ M$.

From the rank relation, we see that the sum of pairwise gcd's is the number of linearly dependent vectors in the union of the spans of blocks of the separation matrix $\mathbf{S}_M$ taken a pair at a time. We can also see that the quantity Q in the underbraces is the number of linearly dependent column vectors in the separation matrix $\mathbf{S}_M$ that have been counted multiple times in the sum containing the pairwise gcd's. This quantity Q therefore has to be a positive quantity and, hence, the lower bound in Eq. (4.11) follows.

In the case where the periods are pairwise coprime, all the gcd's are 1 and using the binomial expansion for $(1 \ - \ 1)^M$, we have

$$r\left(\mathbf{S}_M\right) \ = \ \sum_{i \ = \ 1}^{M} N_i \ - \ \sum_{i \ = \ 2}^{M} (-1)^i \binom{M}{i} \ = \ \sum_{i \ = \ 1}^{M} N_i \ - \ (M \ - \ 1), \tag{4.33}$$

which is the result we obtained from the previous theorem

CHAPTER 5

HARMONIC RESTORATION OF SEPARATION METHODS FOR PERIODIC SIGNAL MIXTURES WITH APPLICATION TO VOWEL SEPARATION

5.1 Introduction

The problem of separating an additive mixture of periodic or quasi–periodic signals into its constituent components where one or both of the components may contain useful information is an important signal processing and detection task that one encounters:

(a) when dealing with the problem of recovery of multiple sinusoidal signals in noise [62];

(b) in biomedical signal processing problems such as separating a fetal ECG signal from the composite ECG signal obtained from the abdominal lead of an expectant mother which contains the dominant and omnipresent maternal ECG signal superimposed on a weaker fetal ECG signal [66];

(c) in other ECG applications requiring the removal of periodic interference from powerlines from the recorded ECG signal [66];

(d) when dealing with the problem of interference rejection in communication systems that employ narrowband bandpass signals for transmission [19].

The ability of the human auditory system to selectively attend to one speech signal in a mixture of speech sounds has recently been studied in [1]. In particular, the difference between the pitch frequencies or periods is an important cue used by both human listeners and automatic systems for the task of separating a mixture of vowel sounds. The problem of separating a mixture of discrete-time periodic signals into its constituent components, is hereafter referred to as the *separation of periodic mixtures* (SPM) problem. The relevance of the SPM problem is in its applications in the area of concurrent vowel or other periodic sound separation, in the process of separating a speech signal from an interfering speech signal [1, 64], and in reference to its interference rejection applications [19, 66].

The SPM problem can be approached as a harmonic reassignment problem in the frequency domain [64]. The FFT of the composite signal is dissected and the harmonics in the spectrum of the composite signal are tabulated and tagged as belonging to either of the components. Time–domain waveforms for either component are then obtained by using the inverse FFT [64]. On the other hand, the SPM problem can also be approached as a time-domain filtering problem where separation of the components is accomplished through comb filtering of the composite signal based either on harmonic cancellation or on harmonic enhancement [1]. However, the comb filtering approach used in [1] does not exploit simultaneously both the periodicity of the components and the additive nature of the signal mixture, and has frequency resolution problems when the harmonics of the interfering component and the desired components are close.

Matrix algebraic separation (MAS) of periodic signal mixtures was introduced in [44, 45], where the components of the additive mixture of two periodic signals were separated from the composite signal using their periodicity and samples of the composite signal in a matrix system framework via linear algebra techniques. This MAS method was extended to multicomponent periodic and quasiperiodic AM–FM signals via the PASED algorithm for combined separation and demodulation [5, 58]. As demonstrated in [5, 58], this MAS technique can separate the components of a mixture of two periodic narrowband bandpass signals even in cases when there is significant spectral overlap between the components. Although a matrix-based time-domain analysis of the MAS algorithm was presented in [5, 58], there is a lack of understanding of this technique in the frequency domain.

In this chapter, a harmonic analysis of the general SPM problem is presented. The automated approaches of the MAS algorithm [44, 45] and linear comb filtering [1] are studied in the context of the general SPM problem both in the time and frequency domains. Using the insight gained about these methods in the frequency domain, harmonic restoration methods are proposed for both of the separation methods to improve their performance [57]. These improved methods are then compared in regards to their separation strategies and then applied to four classes of test signals: sines, AM–FM signals, synthetic vowels and periodic portions of real vowels.

5.2 Background on Periodic Mixture Separation

5.2.1 Harmonic Selection via Tabulation

The harmonic selection algorithm proposed in [64] for the separation of speech from interfering speech or more generally, the separation of the constituent components of a mixture of periodic signals is based on harmonic selection, i.e., selection of the harmonics that belong to either component from the composite signal spectrum. The FFT of the composite signal is dissected and based upon knowledge of the periodicities of the components. The spectral peaks in spectrum of the composite signal are then tabulated and tagged as belonging to either component. All maxima in the spectrum of the composite signal are identified as peaks and the estimates of their frequency, amplitude, and phase are entered in the peak tables. The information in these peaks is initially incomplete due to peak overlap. The peak separation procedure in the algorithm tries to resolve overlaps between peaks, and the resolved peak is then added to the peak table. The spectrum of each component is then reconstructed by drawing from the final peak tables only those peaks that belong to the particular component of interest. Time–domain estimates of the components are then obtained via the inverse FFT of the respective spectral impulse trains of either component [64].

5.2.2 Separation based on Linear Comb Filtering

The component separation problem can also be approached purely as a time–domain filtering problem. Linear comb filtering approaches based on either harmonic enhancement or harmonic cancellation philosophies can be used to accomplish this component separation [1]. Component separation in these approaches is accomplished by either enhancing the harmonic content of the desired component or elimination of the harmonic content of the interfering component. The harmonic enhancement approach, however, needs very long comb filters to accomplish the needed improvements in the strength of the desired component via constructive interference of shifted versions of the component with the desired periodicity [1]. On the other hand, harmonic cancellation based linear two–prong FIR comb filters with impulse responses h_i and frequency responses H_i:

$$\begin{aligned} h_i[n] &= \frac{1}{2}\left\{\delta[n] - \delta[n-N_i]\right\} \quad , \quad i = 1 \; , \; 2 \\ H_i\left(\Omega\right) &= j \exp\left(-j\frac{\Omega N_i}{2}\right) \sin\left(\frac{\Omega N_i}{2}\right), \end{aligned} \tag{5.1}$$

can also be used, where N_i the periodicity of the i^{th} component has been exploited to eliminate its spectral content at multiples of the corresponding fundamental frequency, i.e.,

$$H_i\left(\frac{2\pi m}{N_i}\right) = 0 \quad , \quad m = 0, 1, \ldots, (N_i - 1).$$

5.2.3 Matrix Algebraic Separation

The MAS algorithm, which is the separation section of the PASED algorithm described in Chapter 4, has the capability to separate the constituent components of a mixture of discrete periodic signals even in cases where there is significant overlap between the components. The features of this MAS algorithm that are worth repeating are: (a) its noise suppression capability via least–squares smoothing; (b) its performance is independent of the relative power ratio between components and the spectral separation between the components; (c) modular nature that allows easy extension to the case where are more than two periodic components in the mixture.

5.2.4 Estimation of Component Periodicities

The underlying assumption behind all of the three separation algorithms is the exact prior knowledge of the component periodicities. In reality exact prior knowledge of the component periodicities may not be available and robust determination of these periodicities is required. The problem of estimating the periodicities can be solved using the *double difference function* (DDF) algorithm proposed in [1] for the estimation of the pitch periodicities of the components of a mixture of synthetic vowels. If the composite signal is fed through two cascaded comb filters of the form described in Eq. (5.1), with lag parameters equal to the periods, the output is everywhere zero. The two–dimensional lag parameter space of two cascaded comb filters is exhaustively searched for a minimum of the DDF objective function [1] defined by

$$\begin{aligned} \mathrm{DDF}[n, L_1, L_2] \; = \; \sum_{m\,=\,0}^{L\,-\,1} \big| x[n+m] \; &- \; x[n+m+L_1] \\ &- \; x[n+m+L_2] \; + \; x[n+m+L_1+L_2] \big|, \end{aligned} \tag{5.2}$$

where L is the duration of the analysis window, n is the analysis point and L_1 and L_2 are the respective lag parameters of the cascaded comb filters. The coordinates of the minimum of the DDF objective function furnish estimates of the two periodicities sought. The symmetry of the DDF function in the lag parameters can be used to reduce the search space to half a quadrant [1]. It is interesting to note that as is the case in the MAS algorithm, ambiguity regarding the ordering of the periods and association of the components with their corresponding periodicity also exists in the DDF algorithm due to the commutability of two comb filters systems in cascade. If the components of the composite signal are truly periodic then this algorithm is guaranteed to find both the periods unless the periods happen to be equal or multiples of a common subharmonic [1]. Since the estimation of the periods in the DDF algorithm is not based on frequency estimation, problems of limited frequency resolution in frequency estimation part cascading into the period estimation part do not exist. The DDF algorithm can also be easily extended to the case of multicomponent periodic signal mixtures due to its modular nature. The l_2 norm can also be used to define the objective function; however, the l_1 norm is more robust to outliers and to deviations from Gaussian statistics for which the l_2 norm is optimal.

5.3 Harmonic Analysis of the SPM Problem

5.3.1 Common Harmonics

The fundamental step in the comb filtering and the MAS algorithm is the modeling of the components as periodic signals with fundamental period N_i or the assumption that the components satisfy the difference equation

$$x_i[n] \;=\; x_i[n+N_i] \iff x_i[n] - x_i[n-N_i] \;=\; 0. \tag{5.3}$$

Periodicity of each component implies a periodic discrete spectrum with impulses at multiples of its fundamental frequency $2\pi/N_i$:

$$X_i(\Omega) \;=\; 2\pi \sum_{m=-\infty}^{\infty} a_{im}\delta\left(\Omega - \frac{2\pi m}{N_i}\right) \quad , \quad i \;=\; 1,2. \tag{5.4}$$

On the other hand, the composite signal $x[n] = x_1[n] + x_2[n]$ is also periodic with a repetition period $P = \mathrm{lcm}(N_1, N_2)$ and has a discrete spectrum

$$X(\Omega) \;=\; X_1(\Omega) + X_2(\Omega) \;=\; 2\pi \sum_{m=-\infty}^{\infty} b_m\delta\left(\Omega - \frac{2\pi m}{P}\right). \tag{5.5}$$

The inverse problem of separating the components from the composite signal is therefore equivalent to the task of obtaining the sequences $\{a_{im}\}$ from the sequence $\{b_m\}$, i.e., the task of distributing or reassigning the spectral content of the composite signal to that of the components.

If $R = \gcd(N_1, N_2) = 1$, then the fundamental frequencies corresponding to these periods are incommensurate, the harmonics of the fundamental frequencies of the two components are distinct, [7] and hence the spectral reassignment is a relatively easy task. However, if $R > 1$, then the component spectra share harmonics and there will be confusion regarding the reassignment of the spectral content of the R common harmonics at the discrete frequencies

$$\Omega_k = \left(\frac{2\pi}{R}\right) k \quad , \quad k = 0\ ,\ 1\ ,\ \ldots\ ,\ (R-1). \tag{5.6}$$

At these frequencies the spectral impulse amplitudes of the components are superimposed:

$$A_{1k} + A_{2k} = B_k \quad , \quad k = 0, 1, \ldots, (R-1), \tag{5.7}$$

where $\{A_{ik}\}$ and $\{B_k\}$ are the spectral impulse amplitude sequences of the i^{th} component and the sum at the shared frequencies. The superposition of the spectral impulse amplitudes at the common harmonics results in a loss of information at these frequencies. This information deficiency translates into a rank deficiency in the basic separation system (rank deficient by R) of the MAS algorithm. All three of the separation algorithms more or less can recover the distinct harmonics from the composite spectrum, however, they are all confronted with the difficult challenge of recovering the individual impulse amplitudes $\{A_{ik}\}$ from their sum $\{B_k\}$ at the shared harmonics, where information regarding their ratio has been lost.

[7] Note that the frequency $\Omega = 0$ will always be a common harmonic for any R.

5.3.2 Four Basic Options and the Ratio Method

The basic options for the allocation of spectral impulse amplitudes of the composite signal at the shared harmonics are classified as:

OP1: Give it entirely to second component forcing spectral nulls at the common harmonics on the first component, i.e.,

$$A_{2k} \;=\; B_k \;\;,\;\; A_{1k} \;=\; 0 \;\;,\;\; \forall k.$$

OP2: Give it entirely to the first component forcing spectral nulls at the shared harmonics on the second component, i.e.,

$$A_{1k} \;=\; B_k \;\;,\;\; A_{2k} \;=\; 0 \;\;,\;\; \forall k.$$

OP3: Give them to both components in proportion to a ratio

$$\lambda_k \;=\; \frac{A_{1k}}{A_{2k}} \;\;,\;\; \lambda_k \;\in\; \mathbb{C}. \tag{5.8}$$

OP4: Give them to neither component forcing spectral nulls on both components, i.e.,

$$A_{1k} \;=\; A_{2k} \;=\; 0 \iff B_k \;=\; 0 \;,\; \forall k.$$

Note that **OP4** is generally a bad option because it may result in a violation of the known information in Eq. (5.7) when $B_k \;\neq\; 0$. This is actually the option used by the comb filters $H_i\,(\Omega)$. If we allow the parameter λ_k in **OP3** to assume infinite values, i.e., $\lambda_k \;\;\in\;\; \mathbb{C} \,\cup\, \{\infty\}$ then **OP3** includes **OP1** and **OP2** as special cases when λ_k assumes the extremal values of $0\ ,\ \infty$:

$$\begin{aligned}
\mathbf{OP1} : \lambda_k &= 0 \iff A_{1k} = 0\ ,\ A_{2k} = B_k; \\
\mathbf{OP2} : \lambda_k &= \infty \iff A_{1k} = B_k\ ,\ A_{2k} = 0.
\end{aligned} \tag{5.9}$$

In all of the experiments in this paper we will use the same ratio parameter for all of the common harmonics, i.e., $\lambda_k = \lambda\ ,\ \ \forall\, k$.

In general we need additional information to provide a non–arbitrary value of λ. One heuristic approach we have developed to automatically find a satisfactory value of λ is to assume that each component is narrowband and bandpass, i.e., has a narrow effective bandwidth W_i and a spectral peak around the center frequency W_{ci}. Obviously if a common harmonic falls exactly on the center frequency W_{ci} or within the effective bandwidth W_i of either component then there will be a critical loss of information. One specific class of narrowband bandpass periodic signals that we examined are the class of periodic AM–FM signals whose Carson bandwidth is much smaller than their carriers. Assuming for simplicity that the information signals are sinusoidal, the composite signal is the superposition of two narrowband bandpass AM-FM/cosine components:

$$\begin{aligned}
x[n] &= \sum_{i=1}^{2} a_i[n] \cos\left(\int_0^n \Omega_i[m]dm \ +\ \theta_i\right) \\
\Omega_i[n] &= \Omega_{ci} + \Omega_{mi} \cos\left(\Omega_{fi} n \ +\ \alpha_i\right) \\
a_i[n] &= A_i \left[1 + \kappa_i \cos\left(\Omega_{ai} n \ +\ \gamma_i\right)\right],
\end{aligned} \tag{5.10}$$

where $\Omega_i[n]$ and $a_i[n]$ are the instantaneous frequency and amplitude information signals, Ω_{ci} are the carrier frequencies, Ω_{mi} and κ_i are the FM and AM modulation depths and Ω_{fi} and Ω_{ai} are the information bandwidths of the instantaneous frequency and amplitude signals. If the common harmonics do not lie within the passband of either component, then information loss at these points is not critical, [8] i.e., each of the components must satisfy the constraints:

$$\begin{aligned}
\text{Bandwidth constraint:} \quad & \overbrace{2\left(\Omega_{mi}+\Omega_{fi}+\Omega_{ai}\right)}^{\text{Carson Bandwidth}} && \leq && \frac{2\pi}{R} \\
\text{Carrier constraint:} \quad & \min_k \; |\Omega_{ci}-\Omega_k| && \geq && \left(\Omega_{mi}+\Omega_{fi}+\Omega_{ai}\right). \quad (5.11)
\end{aligned}$$

The heuristic rule for the reassignment of the common harmonics via the options **OP1** or **OP2** in the case of mixtures of two AM–FM signals is to force spectral nulls on the component whose spectral peak is further away from the nearest common harmonic, i.e.,

$$\begin{aligned}
\min_k \; |\Omega_{c1}-\Omega_k| \quad &> \quad \min_k \; |\Omega_{c2}-\Omega_k| \quad \Longrightarrow \quad \lambda \; = \; 0 \\
\min_k \; |\Omega_{c2}-\Omega_k| \quad &> \quad \min_k \; |\Omega_{c1}-\Omega_k| \quad \Longrightarrow \quad \lambda \; = \; \infty. \qquad (5.12)
\end{aligned}$$

Although this rule will not settle the reassignment ambiguity in all cases, it will reduce the damage caused by a common harmonic falling on (or close to) the spectral peak of either component.

5.3.3 Spectral Interpolation at the Common Harmonics

Another possibility to restore some of the lost information at the common harmonics Ω_k is to interpolate the corresponding spectral values $\{A_{1k}\}$ of the first (or the second) component from its neighboring spectral values and then to use the information in Eq. (5.7) to fill in the the corresponding values $\{A_{2k}\}$ for the second (or the first) component. This approach is of course valid only if there is considerable amount of spectral correlation or redundancy in either of the component spectra in the local

[8] These constraints place the common harmonics in the tail end of the spectrum of the component signal where there is negligible signal energy. The Carson bandwidth of each AM–FM signal component is a conservative estimate of its effective bandwidth.

neighborhood of the shared harmonics Ω_k and of course require the use of the inverse FFT to obtain the time–domain estimates.

Nearest neighbor interpolation [64], iterative update of the distribution ratio based on minimization of a spectro–temporal cost function [1], spline–based or polynomial interpolation methods that are based upon fitting a spline or polynomial to the spectral magnitudes of the components in the vicinity of the common harmonic or morphological interpolation of the spectral magnitude via the flat morphological closing operator [61, 42] can all be used to fill in or flatten the spectral nulls introduced by the constraints in the options **OP1** or **OP2** to restore some of the information lost. For simplicity sake, we implement just the nearest neighbor interpolation in this paper, i.e., interpolate using the spectral magnitude information from harmonics immediately adjacent to the common harmonics. Its implementation involves linear interpolation of the spectral magnitude of the components with a 3-pt window around the common harmonics and weights of $\{0.5\ ,\ 0\ ,\ 0.5\}$. Time–domain estimates are then obtained via the inverse FFT of the interpolated component spectra.

As the number of common harmonics increases, more of them will fall within the passband of the components and consequently the number of harmonics available for interpolation at the common harmonics decreases and the information loss progressively increases resulting finally in the case where the periods of the components are identical, all the harmonics are shared and N_1 extra constraints, or knowledge of one of the signal components is needed.

5.4 Harmonic Restoration Methods

5.4.1 Restoration for Matrix Algebraic Separation

The MAS algorithm in essence also uses the harmonic reassignment philosophy for accomplishing component separation but differs from the harmonic selection technique in that it involves only time–domain processing. This can be seen clearly by looking at the constraint system in Eq. (4.3) - (4.4) in the time–domain rewritten as matrix constraints

$$\mathbf{C}_1\mathbf{x}_1 \;=\; 0 \quad \text{or} \quad \mathbf{C}_2\mathbf{x}_2 \;=\; 0, \tag{5.13}$$

where the (l, m)–th element of the constraint matrix corresponding to the i^{th} component is

$$\{\mathbf{C}_i\}_{lm} \;=\; \delta[(m-l)_{\text{mod } N_i}], \tag{5.14}$$

where $\delta[n]$ is the discrete-time unit pulse function which has unit amplitude for $n = 0$ and is zero elsewhere. The information relating the composite signal to the components in Eq. (4.1) and the extra constraint information in Eqs. (4.3)-(4.4) essentially perform the harmonic reassignment task in the case of the MAS algorithm. This fact will become evident after multiplying both sides of Eq. (5.13) by the DFT matrix operator $\mathbf{W}_R$ (order R), where

$$\{\mathbf{W}_R\}_{lm} \;=\; \exp\left(-j\frac{2\pi lm}{R}\right). \tag{5.15}$$

Using the structure of the resultant matrix product $\mathbf{W}_R\mathbf{C}_i$, the structure of the matrices $\mathbf{W}_R$ and $\mathbf{C}_i$ and the definition of matrix multiplication we have

$$\begin{aligned}\{\mathbf{W}_R\mathbf{C}_i\}_{lm} &= \sum_{q=0}^{R-1} \exp\left(-j\frac{2\pi lq}{R}\right)\delta[(m-q)_{\text{mod } N_i}] \\ &= \exp\left(-j\frac{2\pi lm}{R}\right).\end{aligned} \tag{5.16}$$

The constraints on the i^{th} component in the frequency domain can then written as

$$\begin{aligned}
\mathbf{W}_R\mathbf{C}_i\mathbf{x}_i &= \sum_{n=0}^{N_i-1} \exp\left(-j\frac{2\pi nk}{R}\right) x_i[n] \\
&= X_i\left(\Omega_k\right) \quad = \quad 0.
\end{aligned} \tag{5.17}$$

So the constraints in Eqs. (4.3)-(4.4) that in the time-domain force the dc value of the subsampled [9] versions of the i^{th} component to zero are equivalent in the frequency domain to forcing the spectral contribution of the i^{th} component at these common harmonics to zero (analogous to options **OP1** and **OP2**). The spectral amplitude of the composite signal at these common harmonics of course can also be divided between the components (analogous to the **OP3**) by using the time-domain matrix constraints or their frequency-domain counterparts:

$$\begin{aligned}
\mathbf{C}_1\mathbf{x}_1 = \lambda\mathbf{C}_2\mathbf{x}_2 \quad &\Longleftrightarrow \quad \mathbf{W}_R\mathbf{C}_1\mathbf{x}_1 = \lambda\mathbf{W}_R\mathbf{C}_2\mathbf{x}_2 \\
&\Longleftrightarrow \quad X_1\left(\Omega_k\right) = \lambda X_2\left(\Omega_k\right).
\end{aligned} \tag{5.18}$$

These constraints, use a single parameter λ to distribute the spectral amplitude of the composite signal identically at all common harmonics corresponding to the option **OP3**. The fourth option corresponds to the case where the constraints are applied on both components

$$\begin{aligned}
\begin{pmatrix} \mathbf{C}_1 & \mathbf{0} \\ \mathbf{0} & \mathbf{C}_2 \end{pmatrix} \begin{pmatrix} \mathbf{x}_1 \\ \mathbf{x}_2 \end{pmatrix} = 0 \quad &\Longleftrightarrow \quad X_1\left(\Omega_k\right) = X_2\left(\Omega_k\right) = 0 \\
&\Longleftrightarrow \quad X\left(\Omega_k\right) = 0.
\end{aligned} \tag{5.19}$$

corresponding to the option **OP4** and in this case the frequency domain equivalent of Eq. (4.1) will not be met at the common harmonics unless the frequency content of the composite signal at these frequencies is already zero.

[9] Downsampling the components by the factor R transforms them into components with periods corresponding to incommensurate fundamental frequencies.

Complete reassignment of the common harmonics and hence complete separation of the components in the MAS algorithm would ideally require matrix constraints of the form

$$\mathbf{W}_R\mathbf{C}_1\mathbf{x}_1 = \mathbf{D}_R\mathbf{W}_R\mathbf{C}_2\mathbf{x}_2 \iff X_1(\Omega_k) = \lambda_k X_2(\Omega_k), \tag{5.20}$$

where the diagonal matrix $\mathbf{D}_R = \operatorname{diag}(\lambda_1, \lambda_2, \ldots \lambda_R)$ contains the spectral distribution ratio of the first component to the second as its diagonal elements.

5.4.2 Restoration for Comb Filter Separation

The comb filters $H_i(\Omega)$ in Eq. (5.1) use directly only the periodicity information regarding the components and do not exploit simultaneously the additive nature of the signal mixture embodied in the information in Eq. (5.7). These filters eliminate the spectral content of both components at the common harmonics corresponding to the option **OP4** and therefore may violate the known information in Eq. (5.7). These filters also do not have the requisite frequency resolution to sufficiently attenuate the harmonics of the interfering component and accentuate the harmonics of the desired component when those harmonics are close and both of them fall within the same cycle of the factor $\sin\left(\frac{\Omega N_i}{2}\right)$ in the frequency response $H_i(\Omega)$.

If, however, we were to use the periodicity information about the components in conjunction with the additive nature of mixture, i.e.,

$$\begin{aligned}
x_1[n] - x_1[n-N_1] &= 0 &\iff&& H_1(\Omega)X_1(\Omega) &= 0\\
x_2[n] - x_2[n-N_2] &= 0 &\iff&& H_2(\Omega)X_2(\Omega) &= 0\\
x_1[n] + x_2[n] &= x[n] &\iff&& X_1(\Omega) + X_2(\Omega) &= X(\Omega),
\end{aligned} \tag{5.21}$$

we obtain the component separation system comprising of the two IIR filters:

$$
\begin{aligned}
T_1(\Omega) &= \frac{\zeta H_2(\Omega)}{H_1(\Omega) + \zeta H_2(\Omega)} \quad , \quad \Omega \neq \Omega_k \\
T_2(\Omega) &= \frac{H_1(\Omega)}{H_1(\Omega) + \zeta H_2(\Omega)} \quad , \quad \Omega \neq \Omega_k \quad , \quad \zeta \in \mathbb{R},
\end{aligned} \tag{5.22}
$$

with $R = \gcd(N_1, N_2)$. At the indeterminate points (common harmonics) the filter frequency responses via the L'Hospital's rule take the values

$$
\begin{aligned}
T_1(\Omega_k) &= \lim_{\Omega \to \frac{2\pi k}{R}} T_1(\Omega) = \frac{\zeta N_2}{N_1 + \zeta N_2} \\
T_2(\Omega_k) &= \lim_{\Omega \to \frac{2\pi k}{R}} T_2(\Omega) = \frac{N_1}{N_1 + \zeta N_2}.
\end{aligned} \tag{5.23}
$$

The spectral amplitude distribution ratio of the first to the second component at all of these indeterminate points is $\lambda_k = \frac{\zeta N_2}{N_1}$ and corresponds to the inclusive option **OP**3 of the general separation problem. A parameter value of $\zeta = 0$ corresponds to the case where spectral nulls are forced on the first component and the entire spectral amplitude of the composite signal goes to the second component, i.e., the option **OP1**, when $\zeta = \frac{N_1}{N_2}$ the amplitudes are divided equally and for $\zeta = \infty$ spectral nulls are forced on the second component at these indeterminate frequencies corresponding to the option **OP2**. Note that $T_1(\Omega) + T_2(\Omega) = 1$ at all frequencies including the indeterminate points thereby satisfying the known information in Eq. (5.7) at these points.

5.5 Experimental Results

5.5.1 Experiments with Sinusoidal Signals

Consider the example of a mixture two sinusoidal signals with carriers at digital frequencies of $\Omega_{ci} = \frac{\pi}{2}$, $\frac{\pi}{2.005}$ and amplitudes of $A_i = 2$, 4. The exact periodicities

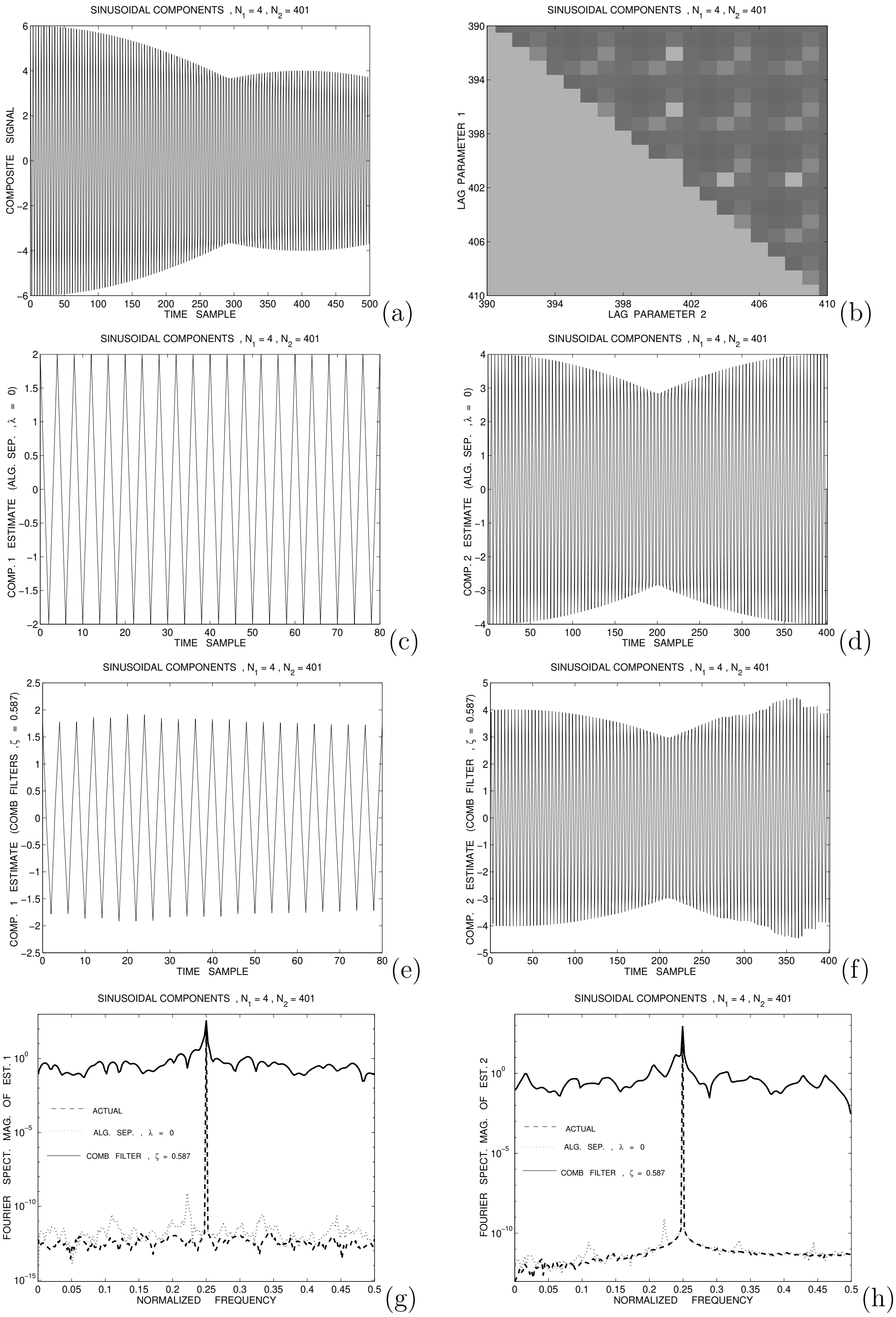

Figure 5.1: Sinusoidal example: (a) composite signal, (b) DDF objective function in the search area shown as the brightness function with dark areas indicating high DDF value and light areas indicating small DDF values, (c,d) MAS algorithm time–domain estimates using the option **OP**1, (e,f) comb filtering time–domain estimates using $\zeta = 0.587$ and (g,h) Fourier spectral magnitude of the estimates of the matrix algebraic separation and the comb filtering techniques depicting the frequency resolution limitations of the latter.

of the components are $N_1 = 4$ and $N_2 = 401$ samples respectively. The periodicity estimates of the components from the DDF algorithm are $\hat{N}_1 = 392$ (first multiple of N_1 that lies within the search area) and $\hat{N}_2 = 401$ samples as described in the Fig. 5.1(b). Note that using the DDF period estimate $\hat{N}_1$ which is a multiple of the actual period N_1 does not affect the results of the MAS algorithm and just adds more rows to the separation system thereby increasing its robustness (least–squares). Although there are multiple minima of the objective function within the search area, the periodicity pattern of the DDF objective function (every 4 samples) within the search area allows the determination of the periods. The estimated component periodicities are coprime which implies that the dc frequency $\Omega = 0$ is the only common harmonic between the two components. The spectral harmonics of the two components at multiples of their respective fundamental frequencies, however, are very close to each other.

The spectral peaks of the two components in particular at their carrier frequencies are extremely close and the comb filters in Eq. (5.22) with $\zeta = 0.587$ implemented using FFT's of ten times the duration of component periods (best possible case) due to the limitations of their numerators do not have the requisite frequency resolution to separate the two components. These comb filters due to their resolution problems are unable to effect both harmonic restoration and simultaneous and satisfactory time–domain separation of the components, thereby producing RMS separation errors of 24.8 , 6.49 % for the first and second component, respectively, which is evident from both the time-domain estimates depicted in Fig. 5.1(e,f) showing attenuation of the first component and the corresponding Fourier spectra depicted in Fig. 5.1(g,h). On the other hand, the MAS algorithm does not have these resolution problems as depicted in the Fourier spectra of the estimates shown in Fig. 5.1(g,h) and the corresponding time–domain estimates with $\lambda = 0$ (**OP**1) shown in Fig. 5.1(c,d) have negligible separation errors.

5.5.2 Experiments with AM–FM Signals

Consider the example with sinusoidally modulated two–component AM–FM signal described in Fig. 5.2(a) with carrier frequencies of $\Omega_{ci} = \frac{\pi}{2}$, $\frac{\pi}{2.20}$, information bandwidths of $\Omega_{fi} = \frac{\pi}{200}$, $\frac{\pi}{220}$, 2 , 4 % FM modulation, 1 , 3 % AM modulation, mean amplitudes of $A_i = 2$, 4 and phase offsets of $\alpha_i = 0$, $\frac{\pi}{2}$ and $\gamma_i = \pi$, 0. The actual periodicities of the components are $N_1 = 200$ and $N_2 = 220$ samples respectively. The component periodicities estimated using the DDF algorithm and the intensity image of the DDF function as depicted in Fig. 5.2(b) are found to be $\hat{N}_1 = 200$ and $\hat{N}_2 = 220$ samples. With this parameter setting the IF and IA signals of the components overlap and consequently there is a significant amount of spectral overlap between the components and in particular there are $R = 20$ common harmonics between the components.

First we separate the components by inverting the basic separation system in Eq. (4.2) that is deficient in rank by R via its pseudoinverse. Due to this lack or loss of information regarding the distribution of spectral information at the R common harmonics the Fourier spectra of the estimates exhibit wide deviations from the actual spectra at these frequencies as evident from Fig. 5.2(q,r) resulting in large RMS separation errors of 36.38 , 18.19 % that are evident from the corresponding time–domain estimates which are depicted in Fig. 5.2(c,d).

Second assuming that we have no knowledge of the carrier locations we apply constraints on the first component, i.e., $\lambda = 0$ (**OP**1). These constraints will force spectral nulls at the common harmonics in the spectrum of the first component

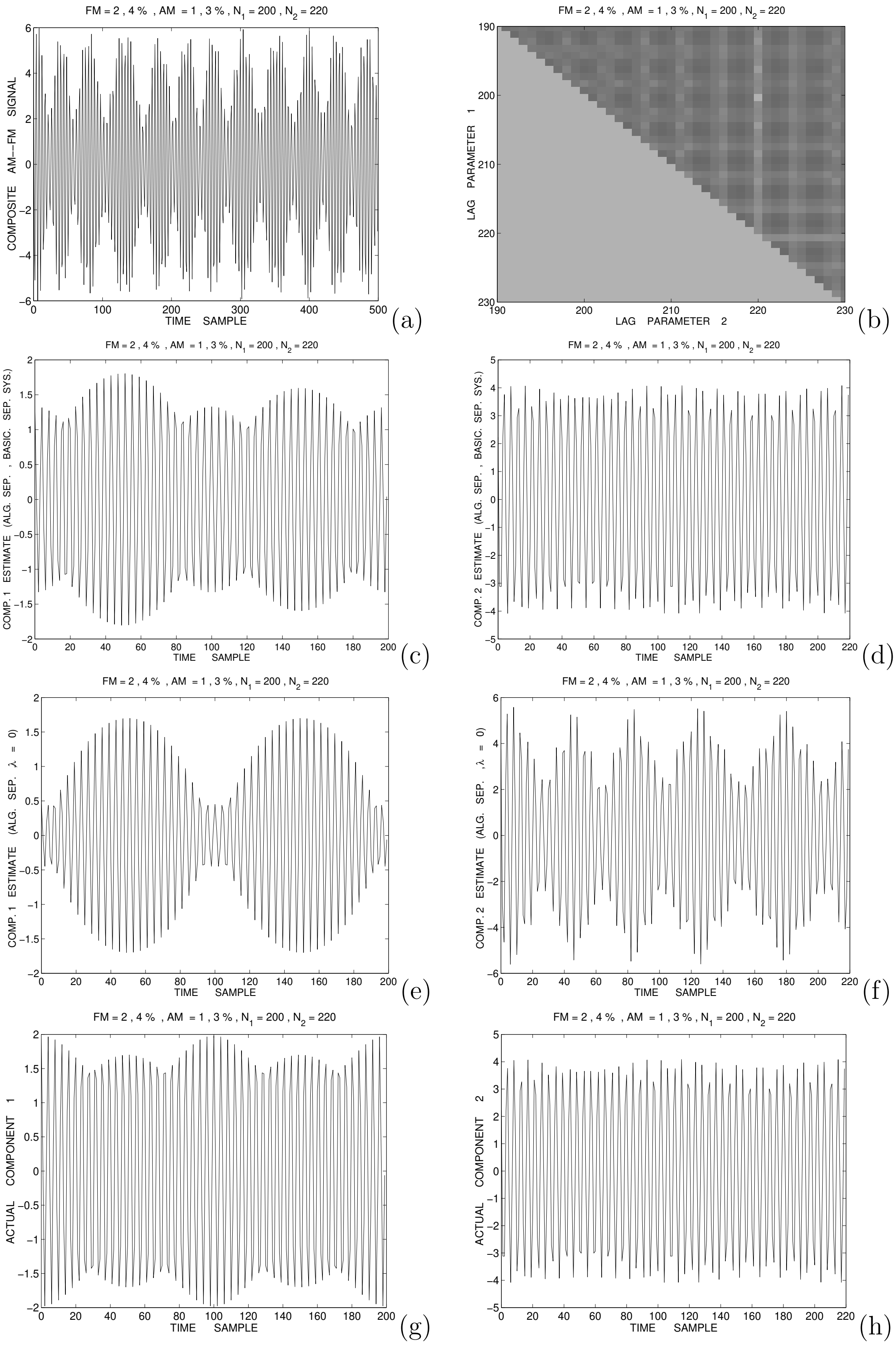

Figure 5.2: Sinusoidal AM–FM Signals: (a) composite two–component AM–FM signal with sinusoidal FM and AM modulation, (b) DDF objective function in the search area shown as the brightness function with dark areas indicating high DDF value and light ones indicating low DDF values, (c,d) time–domain estimates of the MAS algorithm via the pseudoinverse of the basic separation system in Eq. (4.2), (e,f) MAS algorithm time–domain estimates with option **OP**1 and (g,h) actual time–domain quantities.

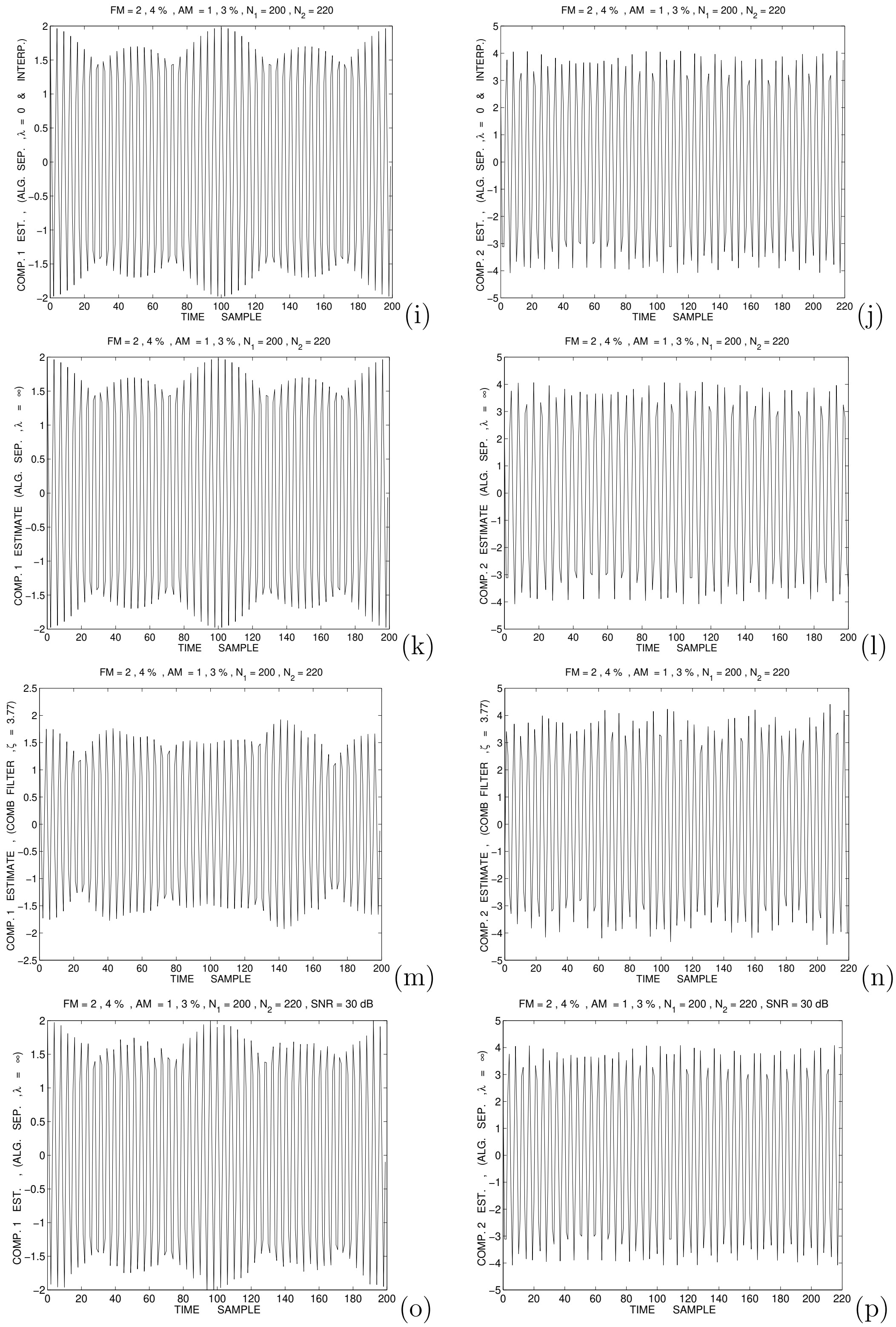

Figure 5.2: Sinusoidal AM–FM Signals (continued): (i,j) MAS algorithm time–domain estimates with **OP**1 after nearest neighbor spectral interpolation on the second component with a window of 3–samples and weights of $\{0.5\ ,\ 0\ ,\ 0.5\}$, (k,l) MAS algorithm time–domain estimates after the use of the heuristic rule in Eq. (5.12) with the option **OP**2, (m,n) time–domain estimates after spectral cancellation via the comb filters in Eq. (5.22) with $\zeta\ =\ 3.77$ and (o,p) MAS algorithm estimates using **OP**2 and $N = 2\,(N_1 + N_2) = 840$ composite signal samples

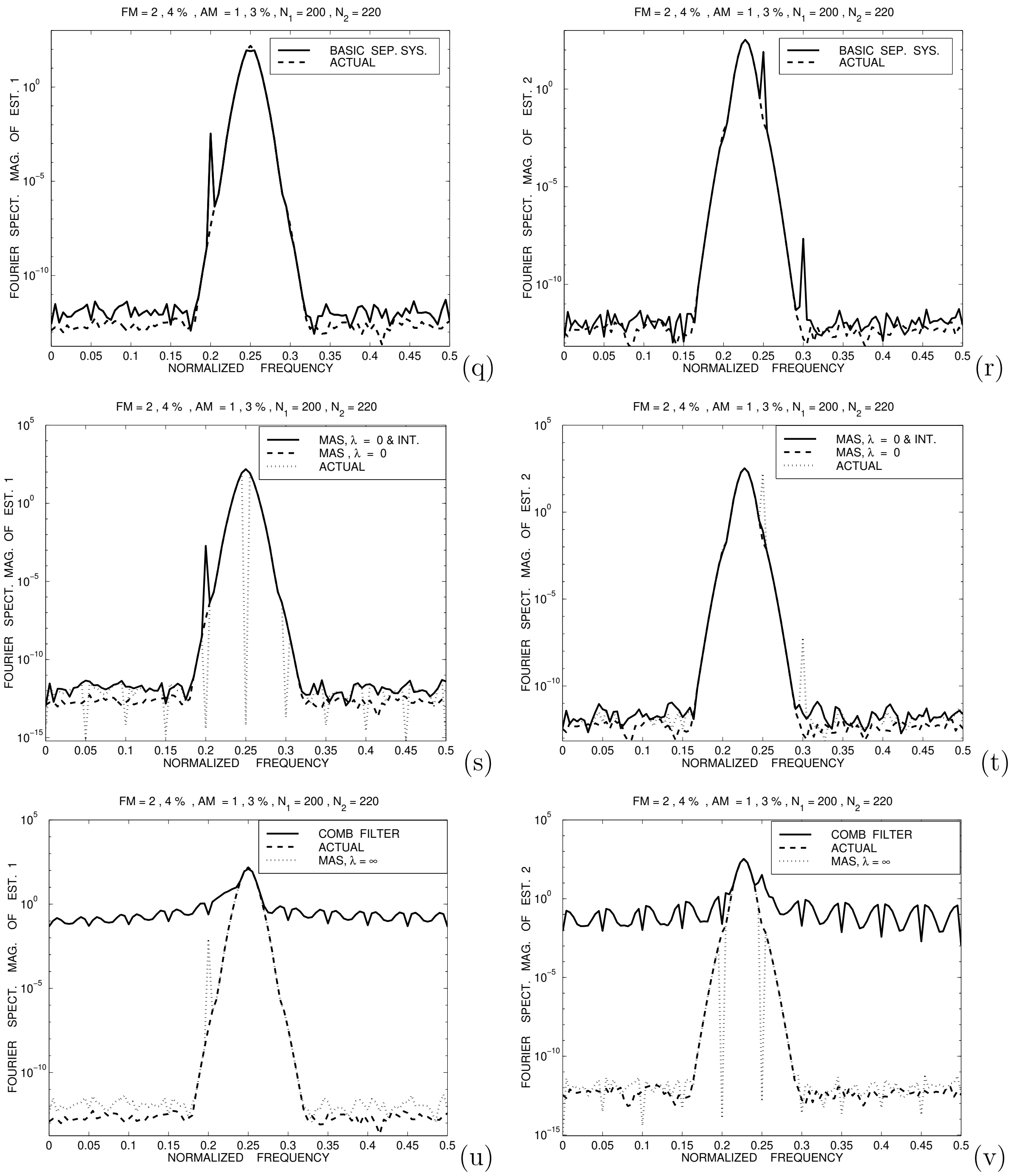

Figure 5.2: Sinusoidal AM–FM Signals (continued): (q,r) Fourier spectra of the estimates from the pseudoinverse of the rank deficient basic separation system, (s,t) Fourier spectra of the MAS algorithm estimates with option **OP**1 before and after harmonic restoration via interpolation of the second component, (u,v) Fourier spectrum of the MAS algorithm using the heuristic rule with **OP**2 and linear comb filtering depicting frequency resolution limitations,

and the 11^{th} common harmonic ($k = 10$) at the digital frequency $\Omega = \frac{\pi}{2}$ falls exactly on the first carrier (critical loss of information) as depicted in Fig. 5.2(s,t) producing very large RMS separation errors of 76.4 , 38.19 % as described by the time–domain estimates in Fig. 5.2(e,f). Note that the spectral nulls forced by **OP**1 produce attenuation of the first component time–domain estimate and amplification of the corresponding time–domain estimate of the second component.

Under the assumption that there is spectral correlation in the local neighborhood of the common harmonics, some of the lost spectral information can be filled in using interpolation from adjacent harmonics in conjunction with the heuristic rule proposed. From the estimated component periodicities, we determine the location of the common harmonics and apply nearest neighbor interpolation to the spectral magnitude of the second component (carrier is further away from Ω_{10}). Eq. (5.7) is then used to determine the spectral impulse amplitudes of the first component at the common harmonics as depicted by the Fourier spectral magnitudes in Fig. 5.2(s,t) resulting in a reduction of the RMS separation error to 0.04 , 0.02 % as described by the corresponding time–domain estimates in Fig. 5.2(i,j). Of course the nearest interpolation can also be applied to the first component to restore some of the information lost. This approach , however, produces larger RMS separation errors of 54.5 , 27.25 % due to loss of critical and non recoverable information at the first carrier. Other types of interpolation methods were also implemented and tried but only the nearest neighbor type is reported here because the other methods performed in a very similar way.

Using the heuristic rule in Eq. (5.12), however, the 11^{th} common harmonic at the digital frequency $\Omega = \frac{\pi}{2}$ which falls exactly on the first carrier is closer to first component so the constraints are applied on the second component, i.e., $\lambda = \infty$

(**OP**2). This option produces spectral nulls at the common harmonic locations for the second component as depicted in Fig. 5.2(u,v), while the corresponding MAS algorithm time–domain estimates are depicted in Fig. 5.2(k,l) with very small RMS separation errors of 0.009 , 0.005 %. Comb filtering was performed using the filters in Eq. (5.22) with $\zeta = 3.77$ using FFT's of ten times the duration of the component periods to avoid aliasing. These comb filters, however, do not possess the requisite frequency resolution to sufficiently attenuate the interfering component and accentuate the desired component as evident from the Fourier spectral magnitude of the estimates described in Fig. 5.2(u,v) resulting in a large RMS separation error of 17.2 % for the first component (critical loss of information at the carrier) and 7.98 % for the second component that are evident from the corresponding time–domain estimates depicted in Fig. 5.2(m,n).

Finally, we apply the MAS algorithm to the noisy version of the composite signal which has been contaminated with *additive white Gaussian noise* (AWGN) with a SNR of 30 dB via **OP**2. It has been observed in [5, 58] that the conditioning of the augmented separation system improves with increase in R thereby making the system more robust to the addition of noise. The large value of $R = 20$ coupled with increase in the number of rows in the basic separation system to $N = 840$ samples (twice the minimum) provides robustness towards addition of noise resulting in small RMS separation errors of 4.10 , 2.07 % as depicted in Fig. 5.2(o,p).

5.5.3 Experiments with Two Synthetic Vowels

In this section, the MAS algorithm is applied to the problem of separating the components of a mixture of two synthetic vowels (/a/ and /i/). The formant frequencies and bandwidths of the synthetic vowels are obtained from [1]. The formants are then

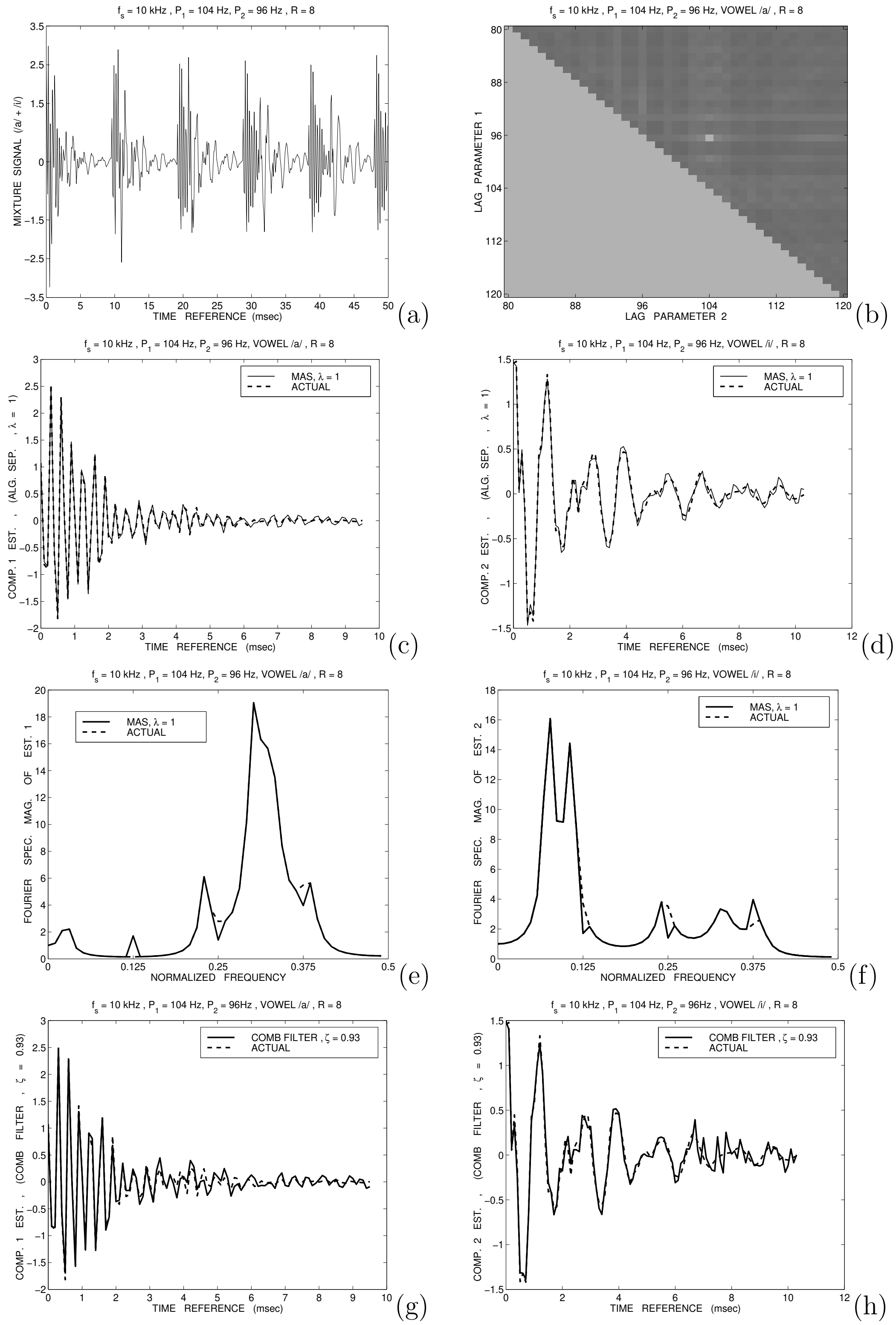

Figure 5.3: Two synthetic vowels: (a) Composite signal is a mixture of two synthetic vowels /a/ and /i/. Both the vowels are synthesized using a sampling frequency of 10 kHz with pitch frequencies of $P_1 = 104$ Hz and $P_2 = 96$ Hz and (b) DDF function in the search area shown as the brightness function with bright areas indicating low DDF value and dark areas indicating large DDF values, (c,d) MAS algorithm estimates using a redistribution parameter of $\lambda = 1$ (**OP**3), (e,f) corresponding Fourier spectra of the component estimates and (g,h) time–domain estimates of the comb filtering procedure with $\zeta = \left(\frac{N_1}{N_2}\right) = 0.93$.

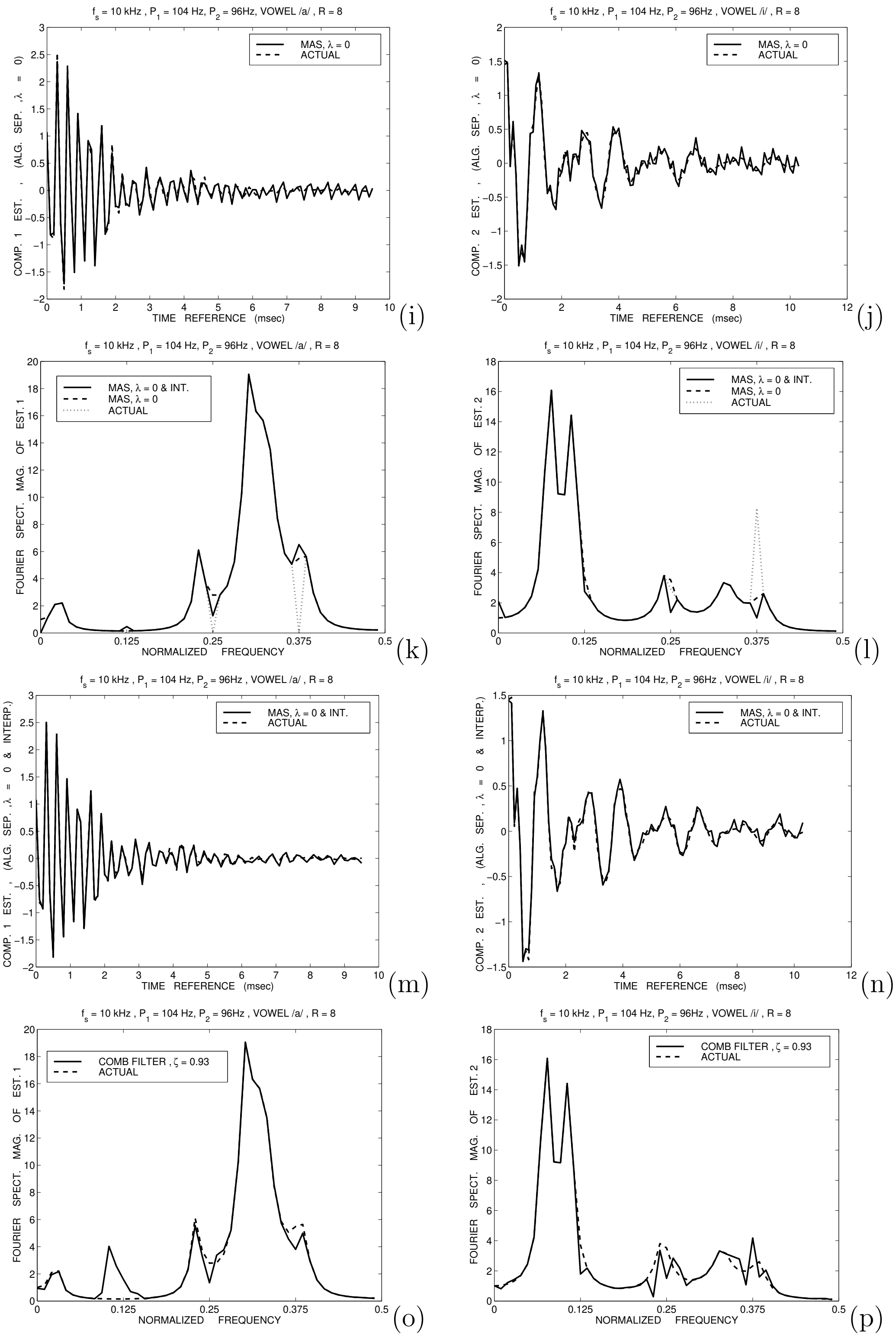

Figure 5.3: Two synthetic vowels (continued): (i,j) time–domain estimates of the MAS algorithm for a redistribution parameter of $\lambda = 0$ (**OP**1), (k,l) corresponding Fourier magnitude spectra of the component estimates before and after nearest neighbor interpolation at the common harmonics for the first component using a 3-pt window with weights $\{0.5\ ,\ 0\ ,\ 0.5\}$, (m,n) corresponding time–domain estimates obtained from the inverse FFT of the interpolated spectra and (o,p) Fourier magnitude spectra of the comb filter estimates with $\zeta = \left(\frac{N_1}{N_2}\right) = 0.93$.

synthesized using the linear source model described in [53] in the cascade form realization. The first couple of pitch periods from both vowels are then removed to avoid transients from the linear source model. Both the vowels are synthesized using a sampling frequency of 10 kHz with pitch frequencies of $P_1 = 104$ Hz and $P_2 = 96$ Hz and the information regarding the formants. The periodicities of the vowels are estimated using the DDF algorithm where the symmetry of the DDF function in the comb filter lag parameters is used to reduce the search area. The pitch periods of the two vowels from the image intensity plot of the DDF function shown in Fig. 5.3(b) are found to be $\hat{N}_1 = 96$ samples and $\hat{N}_2 = 104$ samples. Consequently there are $R = 8$ harmonics common between the components where information has been lost in the superposition of the components and harmonic reassignment is ambiguous.

Fig. 5.3(c,d) are the time–domain estimates of the MAS algorithm using a redistribution parameter of $\lambda = 1$ (**OP**3). Fig. 5.3(e,f) are the corresponding Fourier spectra of the estimated components. Fig. 5.3(i,j) are the time–domain estimates of the MAS algorithm using a redistribution factor of $\lambda = 0$ (**OP**1). The RMS component separation errors for the MAS algorithm with $\lambda = 1$ (**OP**3) are 9.4 , 12 % respectively. The corresponding errors with $\lambda = 0$ (**OP**1) are 16 , 20.5 %. Forcing spectral nulls at the common harmonics on the first component produces more separation error because the entire spectral strength of the composite signal at the common harmonics goes to the second component while the small yet non zero spectral content of the first component at these frequencies that gets eliminated due to the constraints.

Fig. 5.3(k,l) are the Fourier spectra of the components before and after nearest neighbor linear interpolation of the spectra from the case with $\lambda = 0$ (**OP**1) at the common harmonics. Fig. 5.3(m,n) are the corresponding time–domain estimates after applying the inverse FFT to the interpolated spectral estimates while the corresponding RMS separation errors for the estimates after nearest neighbor interpolation on the first component are 7.59 , 11.34 %. The reduction in the separation error is because the spectral correlation in the local neighborhood around the common harmonics of either component has been exploited to partially fill up the lost information at the common harmonics. When the IIR filters in Eq. (5.22) with $\zeta = \frac{\hat{N}_1}{\hat{N}_2} = 0.93$ and FFT's of 10 times the duration of the component periods are used for the same synthetic vowel separation experiment, we obtain the time–domain estimates in Fig. 5.3(g,h) with corresponding RMS separation errors of 16.57 , 17.28 %. The corresponding Fourier spectral magnitudes of the estimates are shown in Fig. 5.3(o,p) depicting the inability of the comb filters to resolve all the spectral peaks in the component spectra and effect simultaneous and satisfactory separation of both components. Alternatively the flat morphological closing operator (flat structuring element) [61, 42] can also used to flatten the valleys from the spectral nulls.

As the number of common harmonics increases, the task of harmonic restoration using interpolation becomes increasingly complicated because the number of spectral harmonics that can be used to interpolate the missing values decreases. In the case where the components of the mixture of the real vowels due to the variation of the pitch periods from frame to frame the component periodicities need to be estimated using the DDF algorithm over every frame before the application of the MAS algorithm where the size of the frame would have to be chosen to balance the task of tracking changes in pitch period with the task of noise suppression.

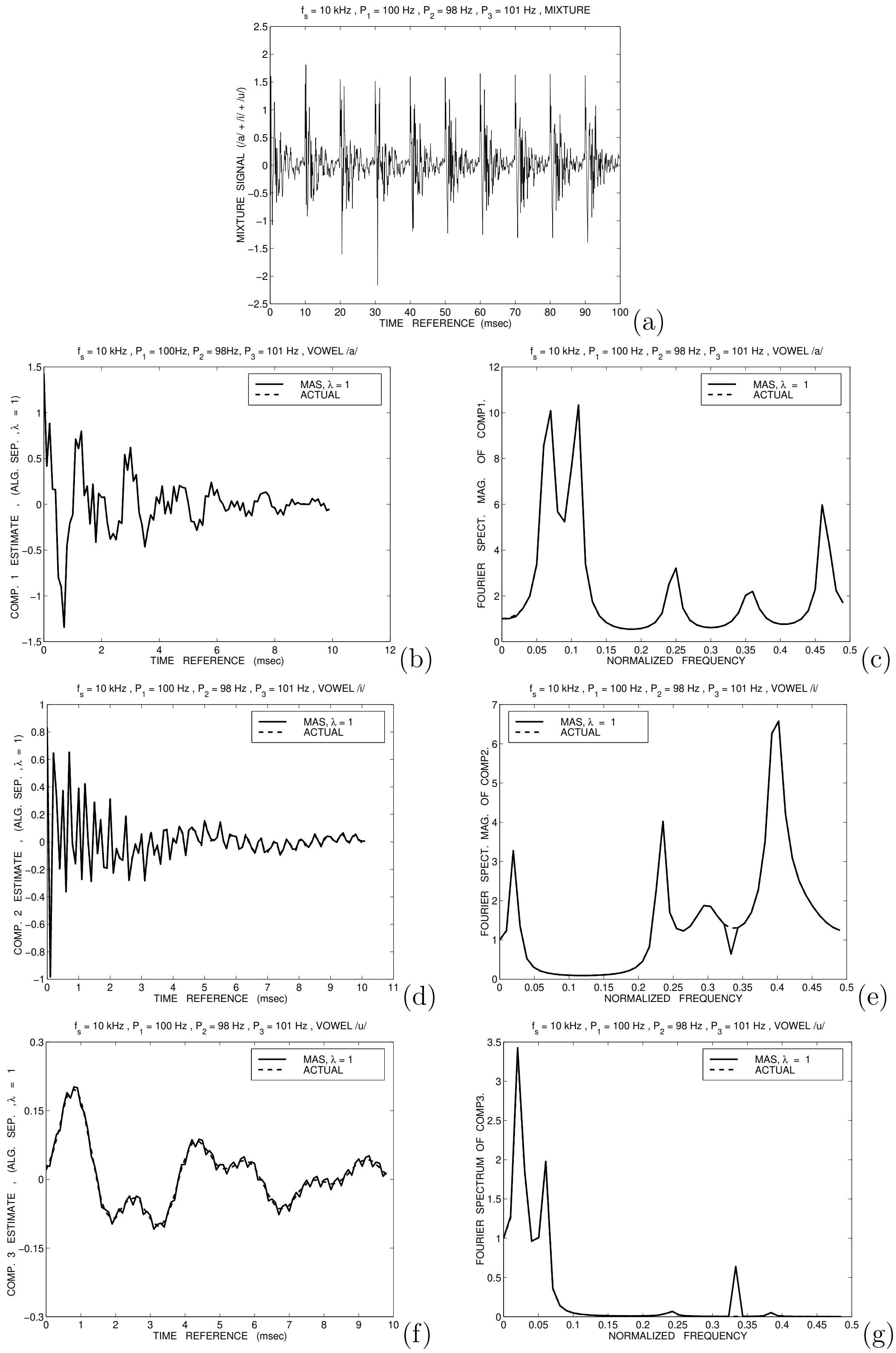

Figure 5.4: Three synthetic Vowels: (a) mixture signal containing the synthetic vowels /a/, /i/ and /u/, (b,d,f) MAS algorithm time–domain estimates for the components over a single pitch period using **OP**3 distribution parameters of {1 , 1 , 1} for the three components and (c,e,g) Fourier spectral magnitude of the MAS algorithm estimates over corresponding pitch period.

5.5.4 Experiment with Three Synthetic Vowels

In this section, the multicomponent matrix algebraic separation technique [5, 58] developed in Chapter 4 is applied to the problem of separating a mixture of three synthetic vowels /a/,/i/ and /u/ into its constituent components. In the three–component case in particular there are three two–component interactions embodied in the form of the pairwise gcd's $R_{i,j}$ between the periods and there is one three–component interaction embodied in the form of the 3-pt point gcd $R_{i,j,k}$ between the periods. The constraints needed to augment and complete the basic separation system are obtained from applying dc value constraints on the the two–component interactions instead of the components [5, 58].

The vowels were generated at a sampling frequency of $f_s = 10$ kHz with pitch frequencies of $P_1 = 100$ Hz, $P_2 = 98$ Hz and $P_3 = 101$ Hz using the information on the formant frequencies and bandwidths and the linear source model both obtained from [53] and as before the first couple of pitch periods are discarded from each formant to avoid transients from the linear source model. The corresponding periods of the components are $N_1 = 100$, $N_2 = 102$ and $N_3 = 99$ samples respectively. With these parameters there are $R_{1,2} = 2$ common harmonics between the first and the second components at digital frequencies of $\Omega = 0\ ,\ \pi$, there are $R_{2,3} = 3$ common harmonics between the second and the third component at digital frequencies of $\Omega = 0\ ,\ \frac{\pi}{3}\ ,\ \frac{2\pi}{3}$, there is $R_{1,3} = 1$ common harmonic between the first and the third component at $\Omega = 0$ and the dc frequency is common to all three of the components ($R_{1,2,3} = 1$).

Fig. 5.4(a) describes the composite signal that is a mixture of the three synthetic vowels. The multicomponent matrix algebraic separation algorithm developed in Chapter 4 is applied on this three–component composite signal with equal distribution of spectral amplitudes at the harmonics common between the pairs of components i.e., $\lambda_1 = 1$, $\lambda_2 = 1$ and $\lambda_3 = 1$, where λ_i are the **OP**3 parameters described in Eq. (5.18) associated with each two–component interaction. The time–domain estimates of the algorithm are depicted in Fig. 5.4(b,d,f) and the corresponding Fourier spectra of the estimates are depicted in Fig. 5.4(c,e,g). The RMS separation for each of the vowels are 0.5 , 4.5 , and 13.4 % respectively.

5.6 Experiments with Real Vowels

In this section, the MAS algorithm developed for the purpose of separating a mixture of periodic signals is applied to the problem of separating a quasi–periodic mixture of real vowel segments. The data for the real vowel experiments was obtained from the M.I.T. Lincoln labs stressed speech database. The first component of the mixture is the vowel /ee/ obtained after segmentation from the normal speech file steer.pcm containing the speech utterance "steer". The second component of the mixture is the vowel /oh/ obtained from the file oh1.pcm. The sampling frequency of the both vowels is $f_s = 12$ kHz. For the first part of the experiment, a single period of either vowel is periodically extended using periods of $N_1 = 94$ and $N_2 = 100$ samples respectively. The extended signals are then added together to obtain a two–component periodic mixture signal described in Fig. 5.5(a). The DDF algorithm is applied to this signal and the period estimates obtained after mapping the DDF intensity values to the jet colormap in matlab as described in Fig. 5.5(b) were $\hat{N}_1 = 94$ and $\hat{N}_2 = 100$. With these periodicity estimates, the MAS algorithm using **OP**3 with $\lambda = 1$ is applied to the mixture. The MAS algorithm time–domain estimates are described in Fig. 5.5(c,d) with very small RMS separation errors of 0.2 , 0.1 %.

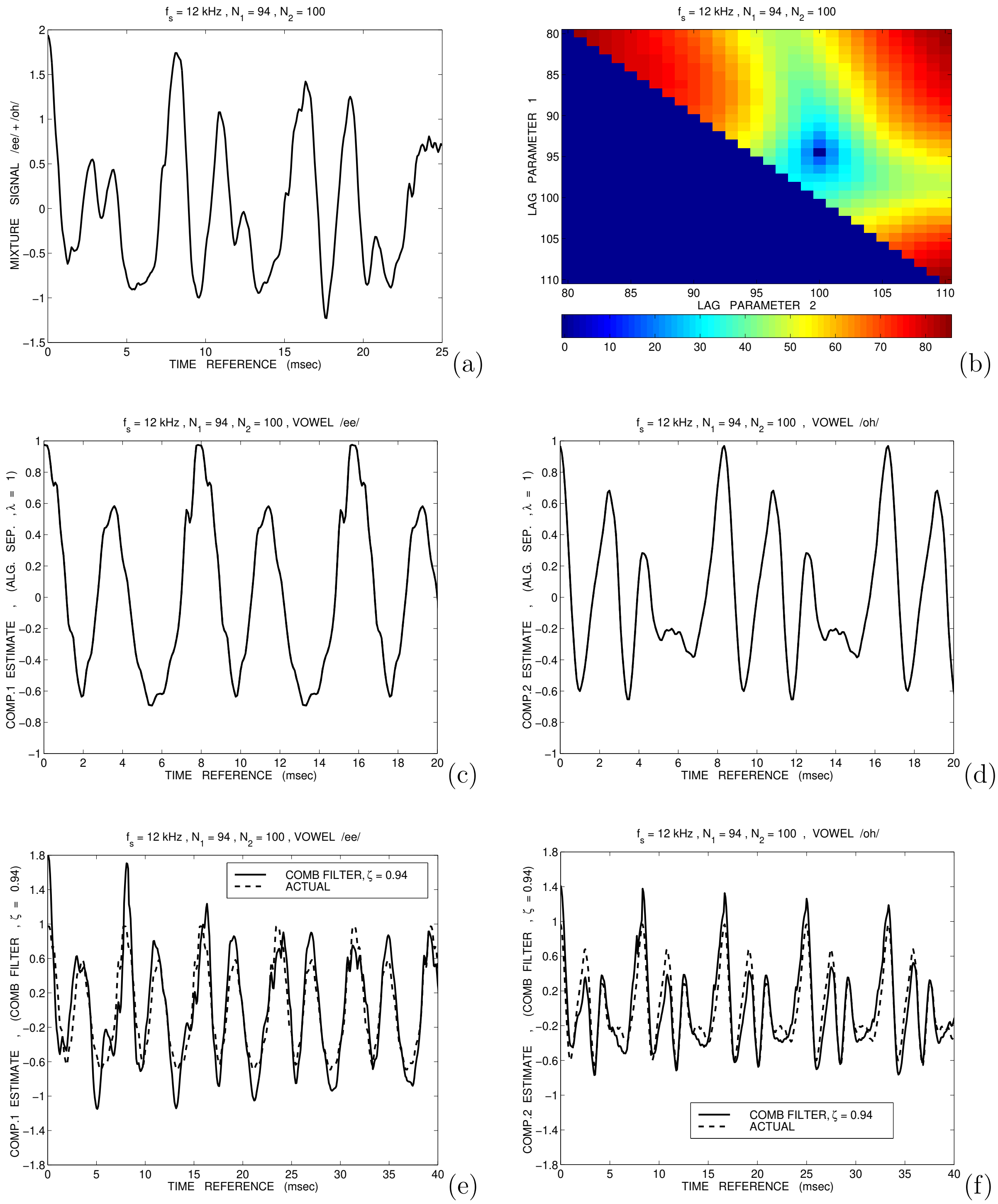

Figure 5.5: Real vowel experiments: (a) composite signal after periodic extension and superposition, (b) DDF function in the search area of the DDF algorithm and (c,d) MAS algorithm time–domain estimates using **OP3** with $\lambda = 1$, where the difference between the actual and the estimated quantities is very small so the actual components are not displayed and (e,f) corresponding comb filter estimates using $\zeta = 0.94$.

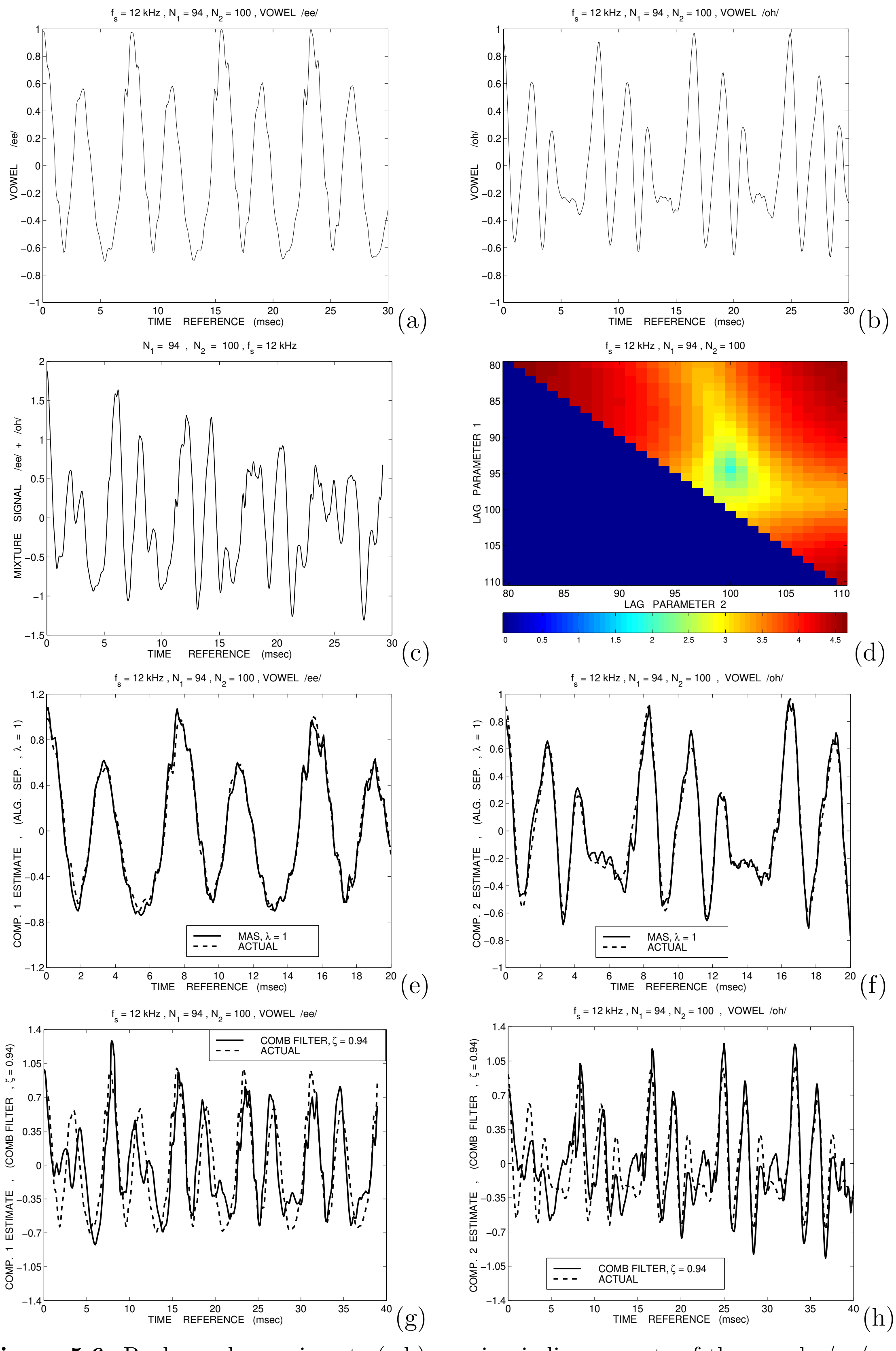

Figure 5.6: Real vowel experiment: (a,b) quasiperiodic segments of the vowels /ee/ and /oh/, (c) mixture of periodic segments of real vowels /oh/ and /ee/, (d) DDF function in the search area of the DDF algorithm and (e,f) MAS algorithm estimates for the components using **OP**3 with $\lambda = 1$ and (g,h) comb filter estimates using $\zeta = 0.94$.

For the second part, sections of the vowels that are approximately periodic with periods of $N_1 = 94$ and $N_2 = 100$ samples corresponding to pitch frequencies of $P_1 = 120$ Hz and $P_2 = 127$ Hz are extracted from the vowels as described in Fig. 5.6(a,b) and are added together to obtain a two–component quasi–periodic mixture that is shown in Fig. 5.6(c). The MAS algorithm is then applied to this quasi–periodic mixture. The period estimates of the DDF algorithm for this signal mixture are $\hat{N}_1 = 94$ and $\hat{N}_2 = 100$ samples respectively as shown in Fig. 5.6(d), where the DDF intensity values are mapped to the jet colormap in matlab. The MAS algorithm estimates for the components with these period estimates using **OP**3 and $\lambda = 1$ are shown in Fig. 5.6(e,f) with corresponding RMS separation errors of 10.33 , 13.55 %. A significant portion of these errors can be attributed to the approximate periodicity of the components.

5.7 Comparison and Discussion

The common theme behind all three of these separation techniques is the reallocation of spectral information in the composite signal to that of the individual components. The harmonic selection technique performs this task by tabulation of the harmonics of the composite signal that belong to the component of interest purely in the frequency domain. Component separation via linear comb filtering uses either the harmonic cancellation philosophy to accomplish the component separation purely in the time–domain via the difference equation of the filter. The MAS algorithm uses a mixture of the two to perform the reassignment of the spectral information at the common harmonics to either or both of the components but does so entirely in the time–domain.

The time invariant comb filters $H_i(\Omega)$ are obviously deficient both in terms of utilization of the known information in Eq. (5.7) regarding the spectrally additive nature of the mixture and in terms of their frequency resolution limitations. When linear comb filters in Eq. (5.22) are used to separate the components these filters unlike the filters $H_i(\Omega)$ do not violate the known information in Eq. (5.7). Analogous to the λ parameters described in the general separation problem and the MAS algorithm, these filters distribute the spectral amplitude of the composite signal to the components identically at all the common harmonics via the parameter $\lambda = \zeta \frac{N_2}{N_1}$. The comb filters in Eq. (5.22), however, require the use of the FFT and the IFFT to enforce the spectral impulse values for the responses in Eq. (5.23) at the indeterminate points. Component separation here is still accomplished by the numerators of the system functions of the filters $T_i(\Omega)$ and these numerators do not have the requisite frequency resolution to adequately reject the harmonics of the interference and accentuate the harmonics of the desired component as in the case of the filters $H_i(\Omega)$. On the other hand, the MAS algorithm due to the inherent time varying nature of its matrix system is not plagued by the frequency resolution problems found in the comb filters when the spectral harmonics of the components are close to each other. The MAS algorithm can also have both harmonic restoration via appropriate choice of the options and immunity to noise via the use of a large number of rows in the basic separation system which is not possible in the case of the comb filters.

With prior knowledge or estimation of the component periodicities via the DDF algorithm all three separation algorithms are more or less able to perform this reallocation task when the spectral harmonics of the components do not coincide (comb filters have resolution problems when the harmonics are close). However, all of them are faced with the challenging task of reallocation of the shared harmonics where information has been lost in the superposition of the components. The information missing in particular is the ratio of the spectral impulse amplitudes of the components.

With the knowledge of the periodicities and hence the locations of the common harmonics, nearest neighbor interpolation of the spectral magnitude of the component estimates in the vicinity of the common harmonics is able to fill in some of the information lost when using the option **OP**1 or **OP**2. Some of the interpolation techniques that were tried relate to the fitting of a spline or a polynomial to the spectral magnitude of the components in the vicinity of the common harmonics. Alternatively, morphological interpolation of the spectral magnitude was also tried using the flat closing operator to fill in the the spectral nulls that are introduced in the options of the general SPM problem where the common harmonics are allocated to either component. Of course the underlying assumption behind all these interpolation methods is that spectral redundancy or correlation is existent in the local neighborhood of the common harmonics.

Another restoration method that was tried in relation to the estimation of a single spectral amplitude ratio λ parameter for all the common harmonics was to initially choose a ratio. This ratio is then iteratively updated using the ratio of the local l_2 norms (l_2 norm of the component spectral values around the spectral peak) of the estimated components until convergence. However, the ratio of the l_2 norms does not carry phase information, i.e., the ratio parameter is assumed to be purely real while the information lost at the common harmonics also has phase information associated with it.

The loss of information at the common harmonics in the case of narrowband bandpass signals becomes critical when it falls at or close to the spectral peak of either component. The proposed heuristic rule can be used to reduce the damage caused in these cases when the carrier locations are known and to decide whether the critical common harmonic should be assigned to first or the second component. The proposed heuristic rule can also used in conjunction with the interpolation techniques whereby the component whose spectral peak is further away from the nearest common harmonic is interpolated and the spectral impulse amplitudes of the other component are obtained by subtraction of the interpolated values from the composite signal spectrum. Speech vowels, however, are multiband signals that contain multiple spectral peaks one for each formant and in this case the options of assigning the common harmonics to either component will result in loss of valid information. In this case, the option distributing the spectral amplitude equally to both components at the common harmonics produces better results. In general the MAS algorithm with harmonic restoration either through the use of spectral interpolation methods or the heuristic rule produces superior separation results over the comb filtering method. This technique can also provide some immunity to noise via the use of a larger number of rows in the basic separation system.

CHAPTER 6

CONCLUSIONS

6.1 Contributions of the Thesis

The signal processing task of interest in this thesis is that of multicomponent AM–FM signal demodulation. The thesis goal of multicomponent AM–FM demodulation is actually a two part task that involves: (a) the separation of the components from the composite signal and (b) the extraction of the information bearing IF and IA signals from the separated components. Towards this goal, the existing multicomponent AM–FM demodulation approaches were briefly discussed and simulated in Chapter 2. The limitations of these existing demodulation algorithms in being able to work only in a restricted range of normalized carrier separations (NCS) and mean power ratios (MPR) were pointed out.

For the two–component AM–FM signal case, in this restricted range, the EDM algorithm discussed in Chapter 3 provides a computationally simple and physically meaningful alternative to the existing methods. The EDM algorithm, performs simultaneous component separation and demodulation via the use of the GDE of the composite signal and the Teager–Kaiser energy operator and its higher–order extensions. The EDM algorithm, when applied to the problem of separating and demodulating a mixture of voice–modulated FM signals, is able to provide intelligible messages for carrier separations as small as 25 % of the radio frequency bandwidth of either component. In the co–channel range (NCS $<$ 0.2), as in the case of the other existing demodulation algorithms, the EDM algorithm develops singularity problems and break down.

The PASED algorithm developed in Chapter 4 divides the multicomponent AM–FM signal demodulation task into two separate parts. The component separation task is accomplished via the use of the *matrix algebraic separation* (MAS) algorithm that is based on modeling the components as periodic signals. The component demodulation task is accomplished via the use of the *energy separation algorithm* (ESA). By separating the two tasks, the situation where a failure in one task causes a failure in the other is averted. This new approach does not make any of the assumptions that the previous approaches make, does not have the shortcomings of the existing methods, its performance is independent of the NCS and MPR parameters, and it is even able to handle the extreme case where the component IF signals overlap or cross over. The least–squares smoothing afforded by the MAS algorithm also provides some immunity to noise. Due to these attractive features, the PASED algorithm has superior performance and is able to separate and demodulate the components of a mixture of voice–modulated co–channel FM signals as demonstrated in Chapter 4.

The first part of the PASED algorithm involves the signal processing task of separating the components of a mixture of periodic signals, i.e., the *separation of periodic mixtures* (SPM) problem that was separately discussed in Chapter 5. The task of separating the components of a periodic mixture is equivalent to the task of spectral reallocation from the composite signal to either, both or neither of the components. Existing approaches to solving this problem include: (a) frequency–domain harmonic selection or (b) time–domain comb filtering. Via either prior knowledge of the component periodicities or through periodicity estimation via the DDF algorithm, this task of harmonic reallocation is a relatively simple task when the spectral harmonics of either component do not coincide. The task of spectral reallocation at common harmonics, however, is very challenging because at these harmonics critical information information regarding the distribution of the spectral information in the composite signal to that of the components has been lost. The insight gained through the harmonic analysis of the SPM problem and frequency–domain analysis of the MAS and linear comb filtering techniques can be used to perform harmonic restoration in both techniques to improve their performance. This improved MAS algorithm is able to separate the components of a periodic mixture of synthetic vowels and periodic or quasi–periodic sections of real vowels as demonstrated in Chapter 5.

6.2 Suggestions for Future Work

The experimental and theoretical results presented in this thesis in regards to the problem of separation and demodulation of multicomponent AM–FM signals, specifically in the case where the components overlap spectrally, are encouraging given the fact that none of the existing methods are able to handle the spectral overlap of the components or the cross over of the component frequency tracks. This, however, does not imply that there is no scope for improvement or further development of these results. There are numerous possibilities for future research in the topic of this thesis that include:

- The constraint system of the MAS algorithm involves the use of zero dc value conditions on either the component signals themselves or the subsampled versions of these components. The estimates of MAS algorithm, therefore, have zero dc value and when implemented in block form this produces a bias problem that comes up in the FM–voice applications when the actual message signals are not zero mean over each block.

- Extension of the basic separation system of the MAS algorithm to the cases where the component periodicities can vary slowly, which is the case in real vowels and in the ECG problem involving the separation of quasiperiodic waveforms corresponding to the maternal and fetal ECG signals.

- Extension of the PASED model to the problem of separating and demodulating the formants of a short–time segment of speech. The present PASED model requires a difference in the pitch periodicities of the different formants.

- Development of a fast algorithm for the inversion of the augmented separation system of the MAS algorithm possibly utilizing the sparsity of the basic separation system to reduce the computational burden.

APPENDIX A

PHASE–LOCKED LOOPS (PLL)

A.1 Analog Phase–Locked Loop

The analog phase–locked loop (APLL) is a closed loop system that estimates the instantaneous phase of its input signal. APLLs have been studied extensively in [18, 34] after finding applications in phase tracking, synchronization, and the demodulation of narrowband bandpass FM/PM signals of the form

$$x(t) = A_c \cos\left(\omega_c t + 2\pi k_c \int_0^t m(\tau) d\tau\right), \tag{A.1}$$

where A_c is the amplitude of the input signal, ω_c is the carrier frequency of the input signal, and k_c is the frequency sensitivity of the input signal in Hz per volt. The APLL displayed in Fig. A.1 has three major components (1) phase detector (modulator), (2) *voltage–controlled oscillator* (VCO), and (3) loop filter with transfer function $H(s)$. The phase detector modulates the input signal $x(t)$ with the output of the VCO of the form

$$r(t) = A_v \sin\left(\omega_c t + 2\pi k_v \int_0^t v(\tau) d\tau\right), \tag{A.2}$$

where A_v and k_v are the corresponding amplitude and frequency sensitivity parameters of the VCO output signal. The loop filter removes high frequency modulation

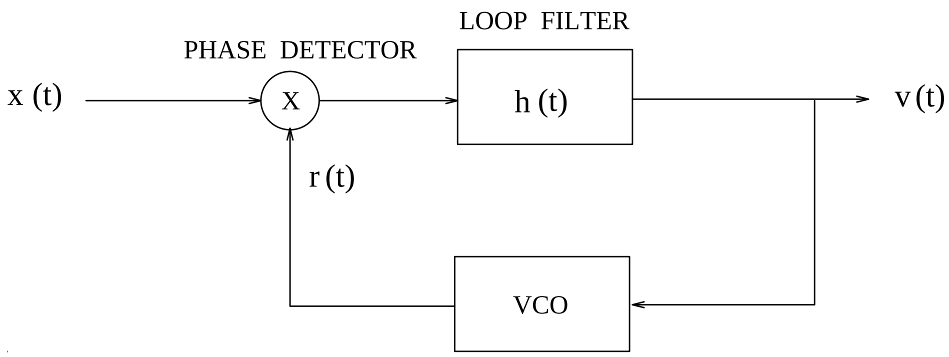

Figure A.1: Block diagram of the PLL

products produced by the phase detector. The output of the loop filter, which contains information on the phase estimation error, controls the VCO output.

Nonlinear Model of APLL

The nonlinear model of the APLL is described in Fig. A.2 and contains a sine nonlinearity. The nonlinear integro–differential equation that governs the behavior of the APLL after the high frequency modulation products from the phase detector have been removed via the lowpass filter is given by

$$\frac{d\theta_e(t)}{dt} = \frac{d\theta_1(t)}{dt} - 2\pi k_0 \int_{-\infty}^{\infty} \sin\left(\theta_e(\tau)\right) h(t-\tau) d\tau, \tag{A.3}$$

where $\theta_1(t)$ is the phase of the input signal, $\theta_2(t)$ is the phase estimate of the APLL and $k_0 = A_c A_v k_m k_v$, where k_m is the multiplier gain [21].

Linear Approximation to APLL

Under the assumption that the APLL is in the linear region of its phase characteristic curve (phase error is small in magnitude), the nonlinear model can be simplified to a linear model as shown in Fig. A.3. The linearized differential equation describing

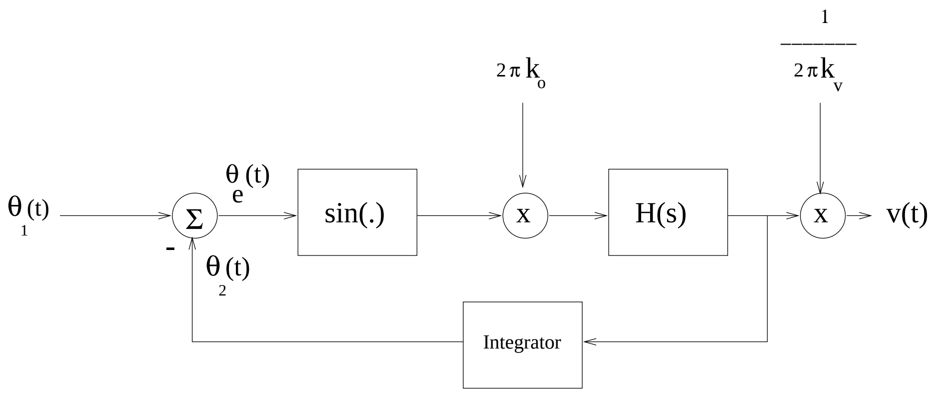

Figure A.2: Nonlinear model of the APLL

the approximation is of the form

$$\frac{d\theta_e(t)}{dt} = \frac{d\theta_1(t)}{dt} - 2\pi k_0 \int_{-\infty}^{\infty} \theta_e(\tau)h(t-\tau)d\tau. \tag{A.4}$$

As described in [34], the linearized loop acts as a bandpass filter, whose bandwidth and damping factor depend on the APLL phase transfer function. The order of the loop is the highest power of **s** in the closed loop transfer function of the linearized APLL. Second–order loops are the most common and are used for phase tracking under narrow bandwidth specifications. First–order loops have limited lock range and third–order loops could become unstable if not controlled properly. The APLL needs to be designed so that it is in the linear mode of operation. It is typically designed so that the damping ratio of the resultant second–order closed loop transfer function is 0.707. The loop filter in the APLL is designed so that the high frequency modulation products produced by the modulator and out of band noise are rejected, while minimizing the harmonic distortion introduced. A detailed discussion of the APLL and the method of design can be found in [16]. Nonlinear analysis of the pertinent Fokker–Plank differential equations involved using phase plane techniques have been carried out in [65].

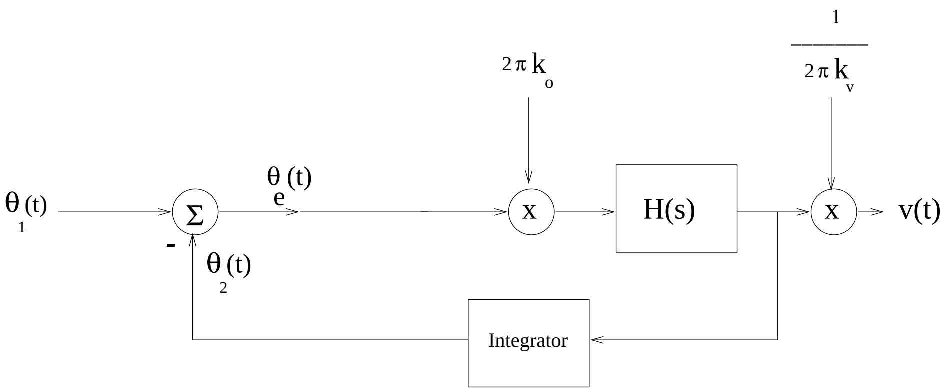

Figure A.3: Linear approximation of the APLL

A.2 Digital Phase–Locked Loops (DPLL)

The *discrete–time PLL* (DPLL) is similar in structure to the APLL and has been investigated in [34]. The *baseband* version of the DPLL (BB–DPLL) proposed in [55] is obtained by using both the inphase and quadrature versions of the input signal. The narrowband bandpass input signal is first modulated with the inphase and quadrature versions of the carrier signal and lowpass filtered

$$c_i[n] = \cos(\Omega_c n) \quad , \quad c_q[n] = \sin(\Omega_c n) \, ,$$

to yield the baseband version of the input signal. The inphase and quadrature components of the resultant baseband signal

$$x_i[n] = a\cos(\phi[n]) \quad , \quad x_q[n] = a\sin(\phi[n])$$

are then modulated with the corresponding quadrature versions of the baseband VCO output . The modulation products are then removed by subtraction rather than filtering. The BB–DPLL is an adaptive and iterative algorithm which can be summarized as

$$e[n] \;\; = \;\; \phi[n] - \hat{\phi}[n] \;\; , \;\; \hat{\phi}[n+1] \;\; = \;\; \hat{\phi}[n] + \sin(e[n]) * f[n]$$

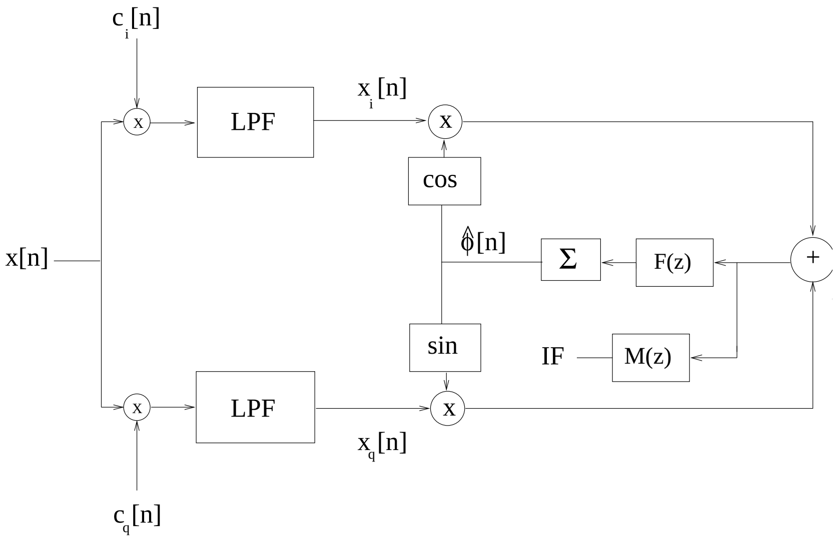

Figure A.4: Block diagram of the BB–DPLL

$$\hat{\Omega}_i[n] \quad = \quad \frac{\hat{\phi}[n+1] - \hat{\phi}[n-1]}{2} \quad , \quad a[n] \quad = \quad \sqrt{x_i^2 + x_q^2}, \tag{A.5}$$

where $\hat{\phi}[n]$ is the phase estimate of the BB–DPLL, $\phi[n]$ is the phase of the baseband version of the input signal, $\Omega_i[n]$ denotes the instantaneous frequency of the input signal, $f[n]$ is the impulse response of the loop filter and $*$ denotes the convolution operation. The DPLL phase transfer function and phase error transfer function are given by

$$T(z) \quad = \quad \frac{F(z)}{z - 1 + F(z)} \quad , \quad \Phi_e(z) \quad = \quad (1 - T(z))\,\Phi_1(z), \tag{A.6}$$

where $F(z)$ is the transfer function of the loop filter. The noise bandwidth of the DPLL is then determined as

$$\mathrm{B_w} = \frac{1}{2\pi j} \oint_{|z|=1} T(z)T(z^{-1})z^{-1}dz. \tag{A.7}$$

BIBLIOGRAPHY

[1] Alain de Cheveigne. Separation of Concurrent Harmonic Sounds: Fundamental Frequency Estimation and a Time–Domain Cancellation Model of Auditory Processing. *J. Acoust. Soc. of Am.*, 93(6):3271 – 3290, June 1993.

[2] B. D. O. Anderson and J. B. Moore. *Optimal Filtering*. Prentice Hall, Englewood Cliffs, New Jersey, 1979.

[3] B. A. Hedstrom and R. L. Kirlin. Co–Channel Signal Separation Using Cross–coupled Digital Phase–Locked Loops. *IEEE Trans. Commun.*, 44(10):1373 – 1384, Oct 1996.

[4] Balasubramaniam Santhanam and Petros Maragos. Energy Demodulation of Two–Component AM–FM Signals with Application to Speaker Separation. In *Proc. ICASSP–96*, volume 6, pages 3517 – 3520, May 1996.

[5] Balasubramaniam Santhanam and Petros Maragos. Demodulation of Discrete Multicomponent AM–FM Signals Using Periodic Algebraic Separation And Demodulation. In *Proc. ICASSP–97*, volume 3, pages 2409 – 2412, Munich , Germany, April 1997.

[6] Y. Bar-ness, F. A. Cassara, H. Schachter, and R. Difazio. Cross–Coupled Phase–Locked Loop with Closed Loop Amplitude Control. *IEEE Trans. Commun.*, 32(2):195 – 198, Feb 1984.

[7] A. C. Bovik, P. Maragos, and T. F. Quatieri. AM–FM Energy Detection and Separation in Noise Using Multiband Energy Operator. *IEEE Trans. Sig. Process.*, 41(12):3245 – 3265, Dec 1993.

[8] J. N. Bradley and R. L. Kirlin. Phase–Locked Loop Cancellation of Interfering Tones. *IEEE Trans. Sig. Process.*, 41(1):391 – 394, Jan 1993.

[9] Jonathan N. Bradley. Suppression of Adjacent–Channel and Cochannel FM interference Via Extended Kalman Filtering. In *Proc. ICASSP–92*, volume 4, pages 693 – 696, San Francisco, CA, U.S.A, March 1992.

[10] Leon Cohen. What is a Multicomponent Signal? In *Proc. ICASSP–92*, volume 5, pages 113 – 116, San Francisco, CA, U.S.A., March 1992.

[11] R. D. Degroat and R. A. Roberts. Efficient, Numerically Stabilized Rank–One Eigenstructure Updating. *IEEE Trans. ASSP*, 38(2):301 – 316, Feb 1990.

[12] R. D. Degroat and R. A. Roberts. Tracking Non–Stationary, Narrow–Band Signals with Reduced Rank Updating. In *Proc. 21st Asilomar Conference on Signals, Systems and Computers*, pages 447 – 451, Pacific Grove, California, Nov 87.

[13] C. L. Dimonte and K. S. Arun. Tracking the Frequencies of Superimposed Time–varying Harmonics. In *Proc. ICASSP–90*, volume 2, pages 2539 – 2542, 1990.

[14] Meir Feder and Ehud Weinstein. Parameter Estimation of Superimposed Signals Using the EM algorithm. *IEEE Trans. Sig. Process.*, 36(4):477 – 489, April 1988.

[15] B. Friedlander and J. M. Francos. Estimation of Amplitude and Phase Parameters of Multicomponent Signals. *IEEE Trans. Sig. Process.*, 43(4):917 – 926, 1995.

[16] F. M. Gardner. *Phaselock Techniques.* John Wiley & Sons Inc., New York, Second edition, 1979.

[17] L. J. Griffiths. Rapid Measurement of Digital Instantaneous Frequency. *IEEE Trans. ASSP.*, 23:207 – 222, April 1975.

[18] S. C. Gupta. Phase–Locked Loops. *Proc. IEEE*, 63(2):291 – 306, Feb 1975.

[19] H. W. Hawkes. Study of Adjacent and Co–Channel FM interference. *Proc. IEE*, 138(4), Aug 1991.

[20] Monson H. Hayes. *Statistical Digital Signal Processing and Modeling.* John Wiley & Sons Inc., New York, 1996.

[21] Simon Haykin. *Communication Systems.* John Wiley & Sons Inc., Second edition, 1983.

[22] Simon Haykin. *Adaptive Filter Theory.* Prentice Hall, Englewood Cliffs, New Jersey, 1991.

[23] B. A. Hedstrom and R. L. Kirlin. Detection, Enumeration and Estimation of Multiple Co–Channel Signals. In *Proc.* 6^{th} *SP Workshop on Statistical Signal and Array Processing*, Victoria, BC, Canada, Oct 1992.

[24] B. A. Hedstrom and R. L. Kirlin. Performance Measures for Coupled Digital Phase–Locked Loops for the Separation of Co-Channel Signals. In *Advanced Algorithms and Architectures for Signal Processing*, pages 188 – 197, 1992.

[25] I. N. Herstein. *Topics in Algebra.* John Wiley & Sons Inc., New York, Second edition, 1975.

[26] J. F. Kaiser. On a Simple Algorithm to Calculate the Energy of a Signal. In *Proc. ICASSP–90*, Albuquerque, New Mexico, April 1990.

[27] J. F. Kaiser. On Teager's Energy Algorithm and its Generalization to Continuous signals. In *Proc. IEEE DSP Workshop*, New Paltz, NY, Sep 1990.

[28] J. F. Kaiser. Some Useful Properties of Teager's Energy Operators. In *Proc. ICASSP–93*, volume 3, pages 149 – 152, Minneapolis, MN, April 1993.

[29] R. Kumaresan and A. G. Sadasiv. An Invariance Property of the Determinant of a Matrix Whose Elements are a Sum of Sinusoids and Its Application. *Archiv fur Electronik und Ubertragungstechnik (Int'l J. Electronics and Communication)*, 47(2):119 – 122, 1993.

[30] R. Kumaresan, A. G. Sadasiv, C. S. Ramalingam, and J. F. Kaiser. Instantaneous Nonlinear Operators For Tracking Multicomponent Signal Parameters. In *Proc. 6^{th} SP Workshop on Statistical Signal and Array Processing*, pages 404 – 407, Victoria, BC, Canada, Oct 1992.

[31] H. B. Lee. Eigenvalues and Eigenvectors of Covariance Matrices for Signals Closely Spaced in Frequency. *IEEE Trans. Sig. Process.*, 40(10):2518 – 2535, Oct 1992.

[32] Ta-Hsin Li and B. Kedem. Iterative Filtering for Multiple Frequency Estimation. *IEEE Trans. Sig. Process.*, 42(5):1120 – 1132, May 1994.

[33] R. M. Liang and K. S. Arun. Parameter Estimation For Superimposed Chirp Signals. In *Proc. ICASSP–92*, volume 5, pages 273 – 276, San Francisco, CA, U.S.A, March 1992.

[34] W. C. Lindsey and Chak Ming Chie. A Survey of Digital Phase–Locked Loops. In *Proc. IEEE*, pages 410 – 431, April 1981.

[35] Shan Lu and P. C. Doerschuk. Modelling and Processing Speech With Sums of AM–FM Formant Models. In *Proc. ICASSP–95*, pages 764 – 767, Detroit, Michigan, May 1995.

[36] Shan Lu and P. C. Doerschuk. Nonlinear Modeling and Processing of Speech Based on Sums of AM–FM Formant Models. *IEEE Trans. Sig. Process.*, 44(4):773 – 782, April 1996.

[37] P. Maragos, J. F. Kaiser, and T. F. Quatieri. On Separating Amplitude from Frequency Modulations Using Energy Operators. In *Proc. ICASSP–92*, volume 2, pages 1 – 4, 1992.

[38] P. Maragos, J. F. Kaiser, and T. F. Quatieri. Energy Separations in Signal Modulations with Application to Speech Analysis. *IEEE Trans. Sig. Process.*, 41:3024 – 3051, Oct 1993.

[39] P. Maragos, J. F. Kaiser, and T. F. Quatieri. On Amplitude and Frequency Demodulation Using Energy Operators. *IEEE Trans. Sig. Process.*, 41:1532 – 1550, April 1993.

[40] P. Maragos and A. Potamianos. Higher Order Differential Energy Operators. *IEEE Sig. Process. Letters*, 2(8), Aug 1995.

[41] P. Maragos, T. F. Quatieri, and J. F. Kaiser. Detecting Nonlinearities in Speech using an Energy Operator. In *Proc. 4th IEEE Digital Signal Processing Workshop*, Mohonk (New Paltz), NY, Sep 1990.

[42] Petros Maragos and Ronald W. Schafer. Morphological systems for multidimensional signal processing. *Proc. IEEE*, 78(4):690 – 710, April 1990.

[43] S. C. Martin. Some Results of Experiments in Co–Channel Signal Separation. In *Proc. IEEE Military Communications Conference* (MILCOM), pages 38.3.1 – 38.3.4, 1984.

[44] Mou-yan Zou and R. Unbehauen. An Algebraic Theory for Separation of Periodic Signals. *Archiv fur Elektronik und Ubertragungstechnik*, 45(6):351 – 358, Nov - Dec 1991.

[45] Mou-yan Zou and Chai Zhenming and R. Unbehauen. Separation of Periodic Signals by Using an Algebraic Method. In *Proc. ISCAS–91*, volume 5, pages 2427 – 2430, 1991.

[46] A. V. Oppenheim and R. W. Schafer. *Discrete-Time Signal Processing*. Prentice Hall, Englewood Cliffs, New Jersey, 1989.

[47] P. Maragos and A. Bovik. Image Demodulation Using Multidimensional Energy Separation. *J. Opt. Soc. of Am.*, 12(9):1867 – 1876, Sept 1995.

[48] S. Peleg and B. Friedlander. The Discrete Polynomial–Phase Transform. *IEEE Trans. Sig. Process.*, 43(8):1901 – 1914, Aug 1995.

[49] M. W. Y. Poon, R. H. Khan, and Son Le-Ngoc. A Singular Value Decomposition (SVD) Based Method for Supressing Ocean Clutter in High Frequency Radar. *IEEE Trans. Sig. Process.*, 41(3):1421 – 1425, March 1993.

[50] A. Potamianos. *Speech Processing Applications Using an AM–FM Modulation Model*. PhD thesis, Harvard University, Division of Applied Sciences, Cambridge, Massachusetts, 1995.

[51] A. Potamianos and P. Maragos. A Comparison of the Energy Operator and Hilbert Transform Approaches for Signal and Speech Demodulation. *Signal Processing*, 37(1):95–120, May 1994.

[52] A. Potamianos and P. Maragos. Speech Formant Frequency and Bandwidth Tracking Using Multiband Energy Demodulation. *J. Acoust. Soc. Am.*, 99(6):3795 – 3806, 1996.

[53] L. R. Rabiner and R. W. Schafer. *Digital Processing of Speech Signals*. Prentice Hall, Englewood Cliffs, New Jersey, 1978.

[54] D. A. Rich, Steven Bo, and F. A. Cassara. Co–Channel FM Interference Suppression Using Adaptive Notch Filters. *IEEE Trans. Commun.*, 42(7):2384–2389, July 1994.

[55] W. Rosenkranz. Design and Optimization of a Digital FM Receiver Using DPLL Technique. In *Proc. ICASSP–85*, pages 592 – 595, Tampa, Florida, 1985.

[56] Balasubramaniam Santhanam and Petros Maragos. Energy Demodulation of Two–Component AM–FM Signal Mixtures. *IEEE Sig. Process. Letters*, 3(11):294 – 298, Nov 1996.

[57] Balasubramaniam Santhanam and Petros Maragos. Harmonic Analysis and Restoration of Separation Methods for Periodic Signal Mixtures: Algebraic Separation Vs. Comb Filtering. *Submitted to Signal Processing* and *CSIP Technical Report TR–97–06, Georgia Institute of Technology*, October 1997.

[58] Balasubramaniam Santhanam and Petros Maragos. Multicomponent AM–FM Demodulation Via Algebraic Separation and Energy Demodulation. *Submitted to IEEE Trans. Commun.* and *CSIP Technical Report: TR–97–03, Georgia Institute of Technology*, April 1997.

[59] S. Say and F. Cassara. Experimental Results on the Cross–Coupled Phase–Locked Loop Interference Canceller with Closed Loop Amplitude Control. In *Proc. IEEE Military Communications Conference* (MILCOM), pages 47.1.1 – 47.1.5, 1986.

[60] L. L. Scharf. *Statistical Signal Processing : Detection, Estimation and Time Series Analysis*. Addison–Wesley Publishing Company, Inc, New York, 1990.

[61] Jean Serra. *Image Analysis and Mathematical Morphology*. Academic Press, 1985.

[62] Petre Stoica and Arye Nehorai. MUSIC, Maximum Likelihood, and Cramer–Rao Bound. *IEEE Trans. Sig. Process.*, 37(5):720 – 741, May 1989.

[63] T. S. Sundresh, F. A. Cassara, and H. Schachter. Maximum A Posteriori Estimator for Suppression of Interchannel Interference in FM Receiver. *IEEE Trans. Commun.*, 25(12):1480 – 1485, Dec 1977.

[64] Thomas. W. Parsons. Separation of Speech from Interfering Speech by Means of Harmonic Selection. *J. Acoust. Soc. of Am.*, 60(4):911 – 918, Oct. 1976.

[65] A. J. Viterbi. *Principles of Coherent Communication*. McGraw–Hill, New York, 1966.

[66] B. Widrow and S. D. Stearns. *Adaptive Signal Processing*. Prentice-Hall, Englewood Cliffs, New Jersey, 1985.

[67] D. Wulich, E. I. Plotkin, M. N. S. Swamy, and E. Kashi. Separation of Close Sinusoids by Cross–Coupled Phase–Locked Loop. In *Proc. ICASSP–89*, volume 4, pages 2128 – 2131, 1989.

[68] A. Zayezdny and I. Druckmann. A New Method of Signal Description and its Applications to Signal Processing. *Signal Processing*, 22:153 – 178, 1991.

Multicomponent AM–FM Energy Demodulation with Applications to Signal Processing and Communications

Balasubramaniam Santhanam

151 pages

Directed by: Dr. Petros Maragos

The goal of this thesis is to study the problem of energy–based demodulation of multicomponent AM–FM signals (components contain both amplitude and frequency modulation) and its applications to signal processing and communications. Specific attention is given to the case where the component signals have overlapping spectra (co–channel problem). Existing multicomponent AM–FM demodulation approaches either assume that the components are distinct or that they can be separated by linear filtering techniques. These assumptions produce singularity problems in the algorithms when the components overlap spectrally or when one of the components is much stronger than the other. To illustrate these shortcomings the existing approaches are briefly discussed and simulated.

This goal of multicomponent AM–FM demodulation is actually a two part task that first involves component separation followed by demodulation of the separated components into frequency and amplitude information signals. The underlying concepts behind the energy–based demodulation approaches are the tracking of the source energy or higher–order energy measures using the second-order (Teager–Kaiser) energy operator or its higher–order extensions and separation of these energies into amplitude and frequency components via instantaneous nonlinear algorithms. The first algorithm, the *energy demodulation of mixtures* (EDM), uses higher–order energy signatures of the composite signal to perform both tasks simultaneously. The second approach embodied in the *periodic algebraic separation energy demodulation* (PASED) algorithm performs these tasks separately using algebraic separation techniques to separate the components and monocomponent energy demodulation (the *energy separation algorithm*) (ESA) to demodulate each component. This enables the PASED algorithm to deal with the difficult cases where the components overlap spectrally or when the component frequency tracks cross over. Both these algorithms are evaluated by applying them to the problem of separation and demodulation of voice–modulated two–component co–channel FM signals (message signals are human voice signals). The *matrix algebraic separation* (MAS) algorithm which is the separation section of the PASED algorithm is independently analyzed in the frequency domain and the insight obtained from this analysis is used to improve the performance of the MAS algorithm via harmonic restoration techniques. The improved MAS algorithm

is then applied to the problem of separating the components of a mixture of both synthetic and natural vowels.